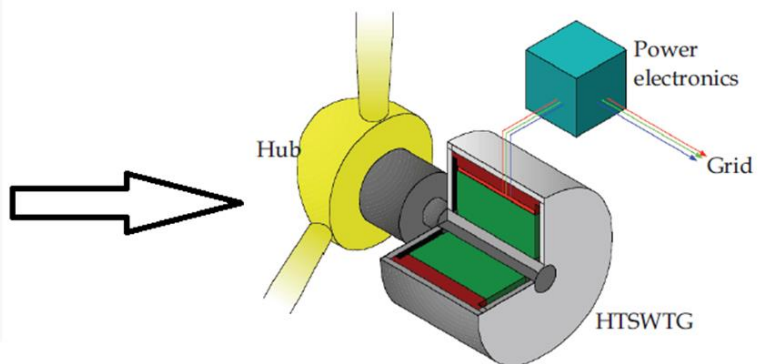
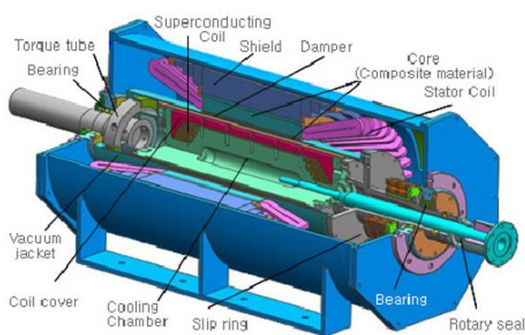


MSc Thesis in Sustainable Energy Technology

Rough design of a 10 MW HTS wind generator



Dimitris Kostopoulos

Supervisor: Dr. Ir. H. Polinder

June 2013

Acknowledgements

Acknowledgements

My most sincere gratitude goes to my supervisor prof. H. Polinder. I would like to thank him for the opportunity he gave me to work on such an interesting argument and for his infinite morale support, scientific guidance and patience throughout this thesis which helped me go over all the obstacles that appeared in my path. I will never forget our very long talks on various matters and I can only say it was a pleasure to receive his scientific and moral teachings. I would like to thank EWT for supporting me in this project. In particular, I would like to thank Mr. Alfred van den Brink for his support and patience. This acknowledgement section would not be complete if I would not thank my father and my mother for their infinite moral and material support. Without them I would never have arrived to write this thesis. In particular I would like to thank my mother that actively assisted me in the last period of conclusion of this thesis after my unfortunate accident.

Abstract

Offshore wind is considered a vital component of the future large scale renewable generation portfolio. Currently the cost of energy of offshore wind farms is still too high. Intense R&D effort is occurring in both technology and the supply chain aiming to cost reduction. Moving to higher power rating turbines is expected to enhance feasibility. The drivetrain of wind turbines is an area of continuous evolution with various configurations currently available at the market. In order to upscale offshore wind turbines in the +10 MW power range and mitigate the observed reliability problems innovation is required. A possible solution is the adoption of superconducting technology. The potential benefits are multiple comprising weight, dimension and cost reduction in both capital and operating costs.

Fully superconducting synchronous machines have been developed in the past with low temperature superconductors for different applications and into a small scale mainly due to their extreme cost and technical difficulties. HTS cuprates suffer AC losses that make their cryogenic heat budget unfeasible. Magnesium diboride (MgB_2) is a newer HTS superconductor and is produced in filamentary round wires that reduce the AC losses and could be feasible with the low rotational speed of direct drive wind turbines.

In this thesis a rough analytical design is presented of an MgB_2 fully superconducting wind generator. The general outline of the proposed generator is a fully superconducting machine with a non-magnetic composite rotor body housed in a single cryostat with an environmental shield that encloses the generator. An analytical current sheet distribution is adopted to calculate the magnetic field of the generator and estimate the steady state performance.

The objective of this thesis is to assess the technical feasibility of the chosen topology and illustrate the main design aspects of superconducting machines. Some tradeoffs are analyzed in an attempt to assess the status of the state of the art and the potential application in wind turbines. Finally possible bottlenecks are identified and recommendations are given for future development.

Table of contents

Table of contents

Abstract	2
Table of contents.....	3
Chapter 1 Introduction.....	5
1.1 Background.....	5
1.2 Problem statement and thesis objective	7
1.3 Thesis outline.....	8
Chapter 2 Why HTS wind turbines?.....	9
2.1 Landscape of the wind industry	9
2.1.1. Market status	9
2.1.2. Drivetrain technological status.....	11
2.2 Bottlenecks in the development	14
2.2.1. Technological limits	14
2.2.2. Material scarcity	15
2.3 Why HTS drive trains	18
Chapter 3 Superconductivity and its application to rotating machinery	22
3.1 Introduction to superconductivity.....	22
3.2 HTS wires	23
3.2.1. Wire properties	24
3.2.2. YBCO	25
3.2.3. BSSCO	26
3.2.4. MgB ₂	27
3.2.5. Stability of HTS wires.....	30
3.2.6. Discussion on wires	32
3.3 HTS generator topologies.....	34
3.4 Cooling systems.....	38
3.4.1. The cryostat	38
3.4.2. Cryogenic fluids	39
3.4.3. Cryocoolers.....	40

Table of contents

3.4.4.	Heat transfer mechanism	42
3.5	Demonstrators.....	44
3.6	Designs of HTS wind turbine generators	52
Chapter 4	Rough Design of a 10 MW HTS wind turbine generator	59
4.1	Introduction.....	59
4.2	A 10 MW wind turbine	60
4.3	HTS generator concept.....	61
4.4	Winding design	64
4.4.1.	Wire adopted.....	64
4.4.2.	Rotor	69
4.4.3.	Stator	70
4.5	Electromagnetic design	71
4.5.1.	Equivalent current sheets.....	71
4.5.2.	Electromagnetic field of the generator	73
4.5.3.	Design parameters	77
4.5.4.	Environmental shield calculation	84
4.6	Losses in the generator	85
4.7	Mechanical and thermal rough design.....	89
4.7.1.	Morphological chart and design choices.....	89
4.7.2.	Heat loads and cooling power estimation.....	94
4.7.3.	Weight estimation	98
4.8	Summary.....	99
Chapter 5	Conclusion	101
References	104

Chapter 1 Introduction

1.1 Background

Increasing environmental awareness is progressively leading to a shift in electrical generation from fossil fuel power plants towards renewable solutions. Wind energy is a vital component of the renewable generation portfolio and is the renewable considered more close to be competitive with fossil fuels. Grid parity is still not a reality. However, the gap with conventional technology is closing making the industry and the European commission to set ambitious targets [1]:

- Make onshore wind the most competitive energy source by 2020 and offshore by 2030
- Supply 20% of EU electricity by 2020, 33% by 2033 and 50% by 2050

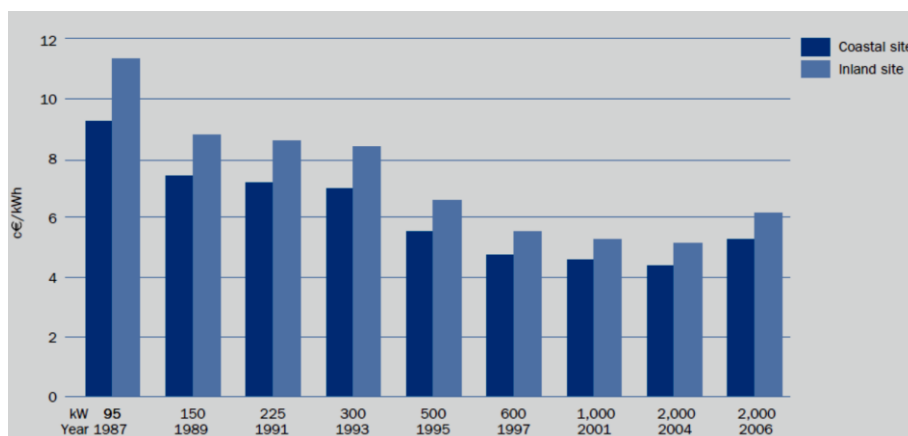


Figure 1 Total wind energy costs per unit of electricity produced, by turbine size (c€/kWh, constant €2006 prices)[2]

In the direction of these targets already a lot has been done. Intense research and development has resulted in increasingly efficient and complex machines. In figure 1 the evolution of the energy production cost from wind is shown as calculated in [2]. Passing from the 9.2 c€ /kWh for the 95 kW turbine of the '80s to 5.3 c€ /kWh for a 2,000 kW machine in 2006 is a remarkable improvement of more than 40%. Cost projections for the near future do not foresee a dramatic breakthrough in the reduction of the cost of energy. However, there is a lot of potential in the mid and long term with estimates of grid parity for the best onshore sites in 2015 and in 2023-25 for offshore wind [3].

Wind energy is a capital intensive business with a lot of cost factors that are site specific and external to the turbine technology itself. For onshore wind the turbine accounts in the total cost share to a range from 65% to 84%, whereas offshore from 30 to 50% [4]. In offshore wind the presence of other important cost factors (foundations, grid connection, installation, maintenance etc.) diminishes the impact of the cost of the turbine itself and therefore potential designs that could lower other cost factors but increment the turbine

Chapter 1 Introduction

cost could still be viable. In this prospect in the offshore wind industry a trend is establishing itself in looking forward to larger turbines in power rating in the +10 MW range. Offshore wind is a much newer business than onshore wind. In order to achieve cost reduction there are multiple paths to walk through. As indicated in [5], there are cost reduction possibilities both in the technology and in the supply chain.

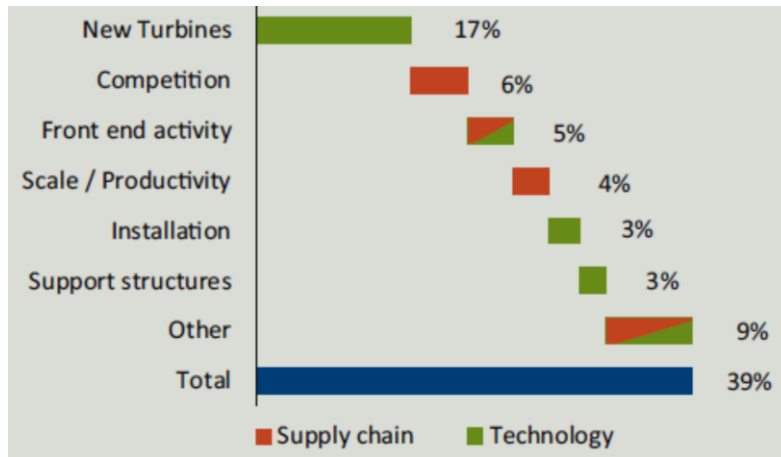


Figure 2 Offshore wind power cost reduction % potential in levelized cost of energy for projects with final investment decision in 2011 and in 2020 [5]

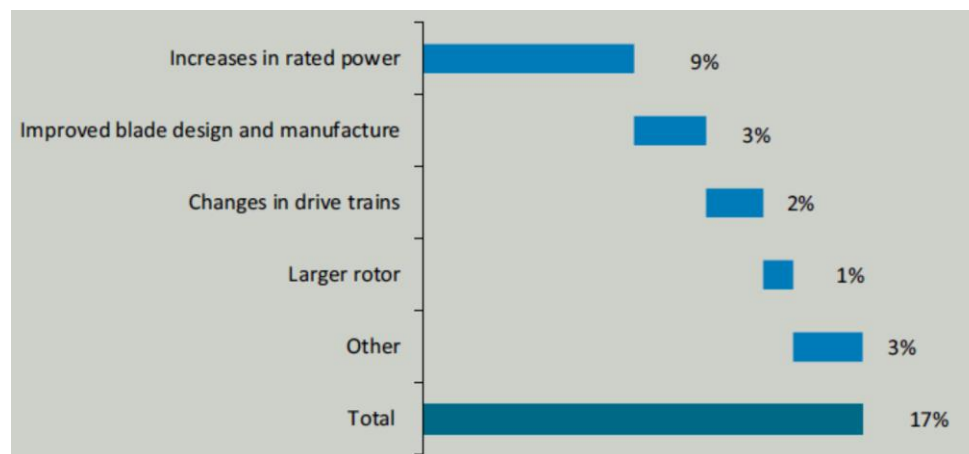


Figure 3 Offshore wind power cost reduction opportunities from changes in turbine [5]

As it emerges from figure 2 there is a considerable amount of possible cost reduction through the introduction of new turbines which ideally would be larger, more reliable, more efficient and would have lower operating costs. From figure 3 it emerges that the area of major room for cost reduction is through upscaling of the power rating. The increase in capital costs with the will be largely offset by the decrease in operating costs and the increase of energy capture.

Reliability is an important aspect in offshore wind since the site location makes maintenance possible in specific periods of time. The first operational data from the UK offshore wind farms has shown that the technical availability is around 80% well below the 93% established by Middelgrunden wind farm [6]. In the future with development further offshore these figures should be considerably improved to ensure a low cost of energy. Reliability studies have been conducted almost exclusively to onshore wind turbines [7], [8].

Chapter 1 Introduction

These studies have shown that the drive train subassembly (meaning the transmitting mechanism of the aerodynamic torque regardless of adopting gearbox or direct drive) is one of the major sources of failures with various downtimes depending on the specific component that fails.

Geared turbines seem to suffer less frequent failures. Operational experience has demonstrated that although the gearbox is not the most frequent source of failures, it is among the ones that provoke the greatest downtime. Moreover, gearbox reliability operational data has demonstrated that gearbox technology in wind turbines has reached equivalent reliability figures as in other industrial applications and therefore significant improvements are probably difficult.

Direct drive solutions have not proved more reliable but they suffer shorter downtime periods. This means that a direct drive could potentially reach higher availability with a suitable maintenance strategy. However, more frequent failures in the offshore wind sector also means a considerable additional amount of effort in the operation and maintenance with subsequent cost impact.

As a consequence from the above discussion it can be concluded that to date there is no definite preferable configuration of the drive train of an offshore wind turbine in terms of reliability. Combining this fact with the trend to upscale the turbine power rating this creates a constant demand for innovation in 2 directions [9]:

- Incremental innovation: cost reduction through economies of scale
- Breakthrough innovation: new products

As stated in the UpWind report even a 20 MW turbine is feasible provided key innovations are developed and integrated.

1.2 Problem statement and thesis objective

One possibility in the breakthrough innovation path of the drive train subassembly is the adoption of superconducting technology. The development of high temperature superconductors (HTS) has occurred since their discovery in the mid 80's. Superconductive applications have already been in place in other sectors i.e. MRI for many years. Nevertheless, in the field of rotating machinery the application of superconductivity is still on a research level. Recent developments indicate that the first niche applications might not be that far away. HTS electrical machines have been reported to be more suitable for low speed high torque applications and therefore the application of this technology in wind turbines seems a prominent option and could represent a viable alternative for the +10 MW power range.

The force density of the conventional wind turbine generators is rather constant in the range of 30 - 60 kN/m² [10]. With the application of superconductors this figure could dramatically change due to simultaneously larger magnetic field and larger current densities. As a consequence, very high power density can be achieved resulting in machines that are much lighter and much more compact than conventional machines. According to [11], a 6 MW HTS direct drive wind turbine generator would only weigh about 20% of the mass of a conventional electrically excited direct drive synchronous generator and only 50% of an

Chapter 1 Introduction

optimized permanent magnet direct drive generator. Moreover, these machines have a very high efficiency almost at the complete range of operating speeds resulting in higher energy yield. This set of advantages provides a strong motivation to research groups and parties in the industry to investigate the application of HTS machines to wind turbines.

The objective of this thesis is to make an overview of the state of the art of superconducting generators focusing on their potential application to large offshore direct drive wind turbines, analyze the tradeoffs among the various options and give a rough design of a 10 MW generator with the intent to estimate its feasibility.

Throughout the initial literature survey it clearly emerged that the application of superconductivity on rotating machines is technically possible. A large number of designs and prototypes of synchronous machines having a superconducting rotor field winding have already been developed. Through these efforts many technical challenges have been faced and the technical feasibility of the concept proved. The majority (if not all) of the produced prototypes have a rotor HTS winding with 1G (BSSCO) tapes and copper armature winding. This is due to the large AC losses of the 1G and 2G (YBCO) HTS tapes, which result in an unacceptable required cooling power and in turn to a drastic cost increase and overall efficiency reduction.

Magnesium diboride (MgB_2) is a newer HTS superconductor than the cuprates. Discovered in 2001, MgB_2 is a much simpler compound to produce and thus the material cost is lower. Moreover, it has much lower anisotropy than the other 2 materials and can be produced in filamentary forms that reduce the AC losses. There are no limits on the production of a continuous length of wire. In contrast YBCO and BSSCO have complicated production techniques and the lengths that can be produced are limited. Performance in this prospect is improving but is still far inferior to MgB_2 . On the other hand MgB_2 has a lower critical temperature, which restricts the cooling options and lower performance compared to YBCO. Nevertheless, the performance of MgB_2 is still by far superior to the conventional technology.

A fully superconducting machine with MgB_2 seems technically possible. By adopting in both stator and rotor HTS windings the advantages of superconducting technology can be fully exploited resulting potentially in a very small and light generator with advantages in the transportation and installation processes of wind turbines. The AC losses of the material seem low and this provides sufficient motivation to investigate further and evaluate if such a design is economically viable.

1.3 Thesis outline

The outline of this thesis is as follows. In Chapter 2 the motivations for the shift to HTS drivetrains will be analyzed through economical and background aspects. In chapter 3 an overview of the application of superconductivity to rotating machinery is given. The available options regarding the wires, the cooling system and the generator layout will be illustrated alongside some key mechanical aspects. In chapter 4 a rough design of the generator is done. The electromagnetic analytical model adopted is presented and the major

Chapter 2 Why HTS wind turbines?

design issues described. In chapter 5 the conclusion and recommendations for future work are illustrated.

Chapter 2 Why HTS wind turbines?

2.1 Landscape of the wind industry

2.1.1. Market status

Wind energy is a vital component of the renewable generation portfolio in a prevailing sustainable global context. Only in Europe the wind power's share of the total installed capacity over the last decade has increased more than fourfold from 2.2% in 2000 to 10.5% in 2011 with an annual average growth of the installed capacity of 15.6% [12]. Over the last two years Latin America (Brazil and Mexico mainly) and Asia (China and India are the main drivers) are leading the market growth reaching a 6% global increase in 2011 representing about 50 billion € investments for new wind power [13]. 2011 was also the second consecutive year during which the majority of new installations were outside the OECD zone.

Onshore wind has been the main part of the industry for a long time, but over the last decade the offshore wind market has been steadily growing in northern Europe. European countries, in different extents, have invested in this industry promoting the expansion of the market harvesting the abundant wind resource in the North Sea. In the U.S., the onshore market has been greatly developed reaching a cumulative capacity of 60 GW at the end of 2012. In contrast the offshore market has not yet initiated with the first offshore project Cape Wind still in the permitting process. However, in the U.S. Department of Energy's report "20% Wind Energy by 2030" is envisioned that wind power may supply 20% of all U.S. electricity, which includes a contribution of 4% from offshore wind power. In the rest of the world the wind market is also in expansion following the trend set by the major players.

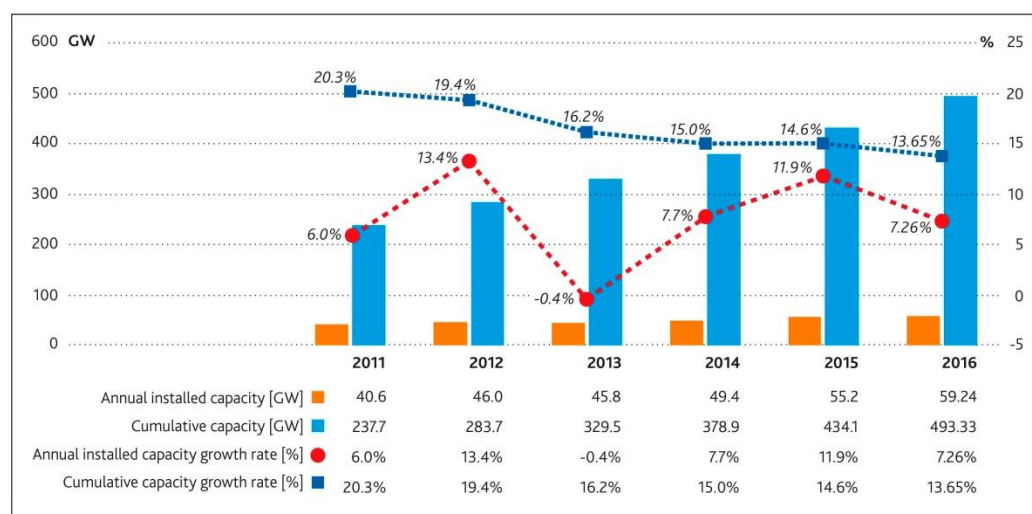


Figure 4 Wind market forecast for 2012-2016 source: GWEC 2011 annual report

Chapter 2 Why HTS wind turbines?

There are a few uncertainties that could affect the market expansion in the medium and short term (i.e. uncertainty over the European emissions trading system (ETS)), however overall the Global Wind Energy Council (GWEC) expects the annual market growth rate to be about 8% for the next 5 years [13]. The potential addition of new emerging markets could be a vital factor sustaining growth. For example Turkey has a rich and relatively unexploited wind resource. Turkey's minister of energy and natural resources in his speech in the opening session of EWEA 2013 announced a very aggressive strategy in renewable energy promotion aiming to attract investments for 10 billion \$ per year in order to meet the rise in their energy demand. With an estimated onshore capacity of more than 40000 GW Turkey aims to increment from current installed capacity of 2200 MW to 20000 MW in less than 15 years. Moreover, they also plan to make the market as domestic as possible with the creation on manufacturing units in points of the supply chain. The addition of such markets in the global context could only be beneficial.

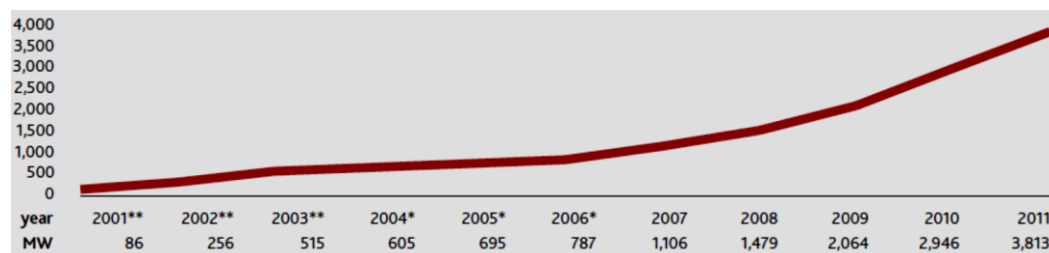


Figure 5 EU Offshore Total Cumulative Installed Capacity

Offshore wind development is a fast growing part of the market. Currently it only represents 2% of the total installed capacity, with 90% of the wind farm installations in northern Europe. However, there are strong indicators that offshore wind will be increasingly important in the global market context:

- Offshore wind is a major contributor in Europe's plan to consume 20% energy from renewables by 2020
- China aims to install 30 GW by 2020
- USA, Japan, Korea, Canada and India have shown grate interest and have great potential

Chapter 2 Why HTS wind turbines?

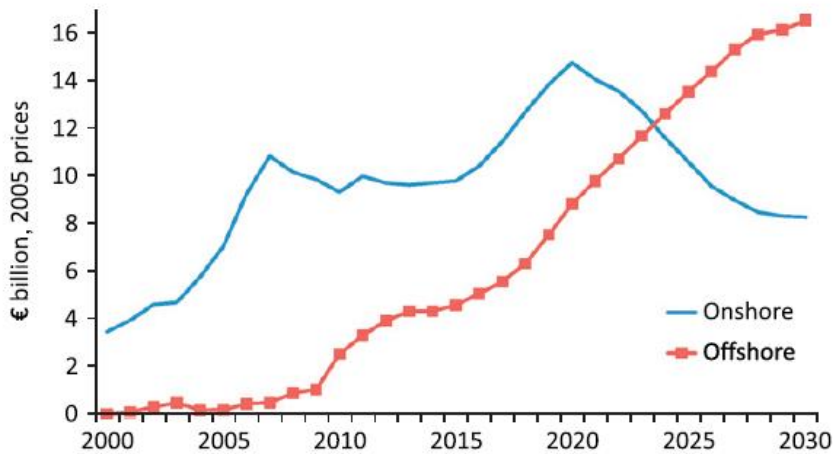


Figure 6 Predicted wind capacity investments in Europe [14]

Europe is leading massive offshore expansion with the UK holding an 87% share in new installations. Currently, almost 6 GW of offshore wind capacity is under construction with further 17 GW already consented and another 114 GW further planned [15]. The offshore wind business is in fact growing impressively, but this does not mean that is already a mature sector. Challenges need to be met and costs need to be lowered in order to reach the next step of development in deeper waters further offshore and make real massive offshore wind farms a reality (like the 1.5 GW farm off the Scottish coast).

In the very long term when the anticipated oil scarcity will occur, wind is regarded as one of the major energy sources, independently of the amount and percentage of other sources [16]. In this prospect the market can only expand. However, there are a few obstacles to overcome from a market perspective. Moving wind farms further offshore means the CAPEX of these projects increments. In concomitance with the adoption of new technologies and the assumptions of the related risk this implies an increment in the cost of capital. In addition to this the uncertainty over the regulations in many European countries (i.e. UK, Portugal) introduces more difficulties. From a policy perspective still a lot has to be done in order to encourage further the market development.

2.1.2. Drivetrain technological status

Extensive research and development over the last 30 years has resulted in increasingly efficient, complex and larger machines in power ratings as well as larger dimensions and weight. This has raised the impact of the cost of the installation process to the overall cost and has made imperative the processing of more efficient operation and maintenance schemes. In the prospect of lowering the impact of the associated costs each subsystem of a wind turbine has been carefully designed and optimized.

The generator and drivetrain subassemblies have known considerable evolution [17], [18]. In the early days of the industry, the wind turbines operated at constant speed and the drivetrain concept consisted of a gearbox connected to an asynchronous squirrel cage generator attached to the grid. Noise, load energy yield and power quality aspects have limited this topology to old turbines.

Chapter 2 Why HTS wind turbines?

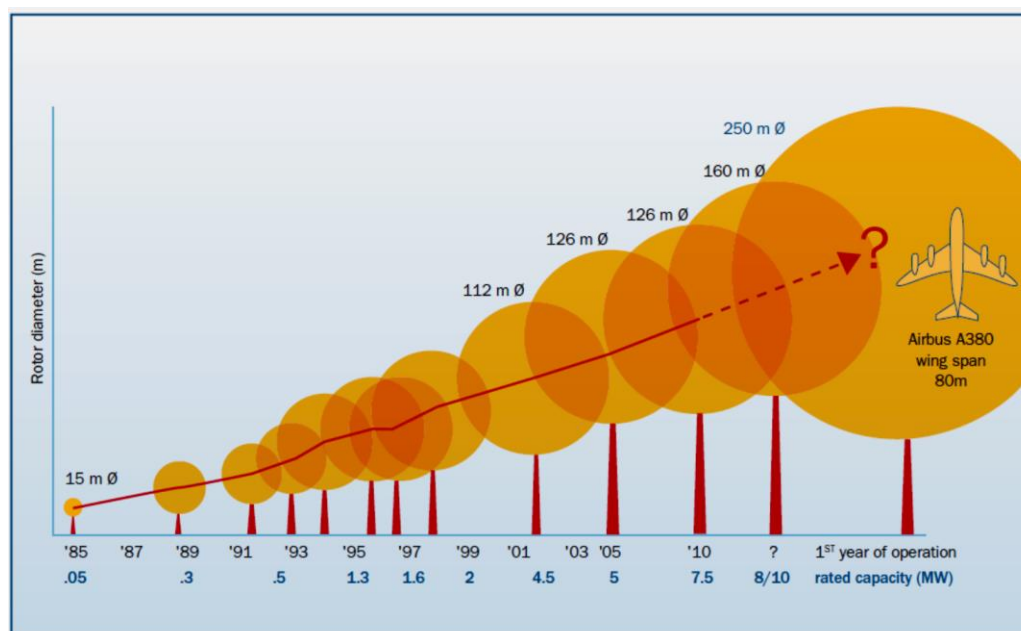


Figure 7 Development of power and rotor diameter of wind turbines [9]

Since the advent and establishment in the late 90's of variable speed machines the drivetrain has been further developed. Initially (and still dominating offshore) doubly fed induction generators with 3 stage gearbox were widely adopted. Their advantage was the use of a partial converter and a standard inexpensive generator but with limited speed range (approximately $\pm 30\%$ of the synchronous speed). Few manufacturers adopted models with a permanent magnet generator with a multi stage gearbox and a full converter (Vestas V112). The energy yield is higher but the converter was more expensive and had more losses compared to the DFIG.

As already mentioned after facing issues with the gearbox, direct drive solutions with synchronous generators have been investigated and have appeared on the market. The first topology to appear in the market was an electrically excited synchronous generator with a full converter (Enercon, Lagerwey). These generators are large and heavy increasing the structural requirements of wind turbines. Due to the large diameter of the machine and to non-fully standardized production these machines have suffered frequent failures. Therefore, in the prospect of moving to the 10 MW power range these generators would result in a difficult and costly installation process, whereas the tremendous dimensions would be a sensitive factor in the transportation and installation process especially in the offshore wind sector where the assembly on site is more difficult than onshore.

The application of $\text{Nd}_2\text{Fe}_{14}\text{B}$ Permanent Magnets (PM) at the rotor excitation field of direct drive generators was the next technological step. Enhanced efficiency at all loads and lighter designs than their electrically excited counterparts resulted in a widespread interest in this technology from the turbine manufacturers. Many configurations of this generator type (radial flux, axial flux, transverse flux) can be found in the literature each presenting advantages and disadvantages. A characteristic of this machine regardless configuration is that in average requires 600-700 kg of rare earth minerals per MW [19]. The sharp increase in rare earth materials price in 2010 has given rise to serious doubts regarding the economic

Chapter 2 Why HTS wind turbines?

viability of such generators. Many companies have maintained asynchronous generators or electrically excited synchronous generators in their commercial models while at the same time are investigating other options that will be more appropriate for the future. However, despite the price fluctuations for the time being some big market players like Alstom, Siemens and GE Energy have maintained their choice to keep direct drive permanent magnet generators for near future offshore multi MW turbines.

The intense R&D activity in this field is also reflected in the large variety of alternative proposed configurations. A certain interest has been shown in medium speed drives with one stage gearbox with the first commercial design form Multibrid (later Areva Multibrid). This concept combines some of the advantages of both geared and direct drive solutions:

- higher energy yield
- higher reliability
- lower generator cost
- smaller dimensions

For large offshore turbines the adoption of this drivetrain could result in an approximately 30% of cost saving per kW for a 5 MW machine and almost 14 % for a 10 MW machine with large reduction in diameter [20]. In terms of material consumption these generators are less sensible to rare earth material prices. In terms of reliability this drivetrain seems a prominent despite the presence of the gearbox. The reliability of the 1 stage gearbox is higher than the 3 stage gearbox, while the generator is more compact and could be more reliable than the direct drive. Some of the major manufacturers like Gamesa and Vestas decided to move towards that direction for their multi MW offshore models.

A variant of the medium speed drivetrain is a design reported in [21] with a brushless DFIG generator. This generator has the advantage to maintain the partial converter and omit the brushes and slip rings. The drivetrain is claimed to have both lower CAPEX and OPEX and be very reliable. However this machine type has rather complicated design and assembly. To date no commercial application exists.

Another drivetrain configuration found in the literature has a hydraulic gearbox in combination a mechanical gearbox and is commercialized by DeWind. The system consists of a mechanical gearbox attached to a hydraulic gearbox which in this way leaves the generator decoupled from the wind turbine. The converter is eliminated and there is a prospect in weight reductions of up to 20% for the drivetrain and of up to 10% for the nacelle [22]. In the same line of thought other proposals exist with gearboxes of variable transmission ratio connected to synchronous generators directly attached to the grid. The power electronics are eliminated while the generator rotates at fixed speed. It has been anticipated that the reduction in efficiency will be in the order of 1% whereas there will be a 10 % reduction in unplanned service and an associated increase of 0.4 % in availability. This could be an interesting proposal but there is a lot to prove in terms of performance and reliability. Bard is planning to make a commercial offshore turbine available with such topology.

In the field of hydraulic drivetrains a very innovative proposal comes from the TU Delft offshore wind research group [23]. The proposed system uses the wind to power a hydraulic

Chapter 2 Why HTS wind turbines?

pump which in turn reverses the working fluid in pipes. The pipelines from more turbines could be conducted to a central big generation unit of a similar type of the hydro-generators. The advantages that the system claims to have is that the power electronics are completely eliminated and fewer components are used with the potential for substantial cost saving. From an electrical view perspective, this system is definitely interesting since it adopts well proven and used generators that can also perform voltage and possibly frequency regulation with conventional methods. Such a thing would revolutionize the way of operating of wind farms and would at all effects constitute wind farms as conventional power plants.

Last but not least a considerable amount of interest exists on superconducting drivetrains with some big players like General Electric, AMSC, Advanced Magnet Lab and others that are researching and developing the technology. This technology is the subject of this thesis and will be described in detail in the next chapter.

Overall as stated in [24] currently there are 25 players actively developing new turbines for the offshore wind market: Of these, where the concept is known, almost half are direct-drive, one third is geared mid-speed and the rest are shared equally between geared high-speed and continuously variable transmission.

2.2 Bottlenecks in the development

2.2.1. Technological limits

The upscaling of wind turbines in the 10+ MW power range requires innovation in 2 linked aspects: the technological innovation of the machine and the optimisation in the supply chain. From a technological point of view the blades, the support structure and the drive train are the major areas where innovation is imperative. This statement does not underestimate the importance of other areas but implies that in these areas with the current state of the art it would be questionable if it is possible to make a viable +10 MW machine (for example blade materials and manufacture for this power rating could be extremely costly or even unviable). From the drivetrain perspective the current popular drivetrain options would face difficulties. Direct drive permanent magnet generators apart from being exposed to cost uncertainty, in that power range are huge and bulky. This affects the installation process. Geared turbines face similar issues with the difference that in that case the dimensions are not so huge, but that comes at an additional cost compared to the direct drive permanent magnet and with lower efficiency reducing the energy harvest.

As a matter of fact in the offshore wind sector weight and dimensions are influential factors in the cost and the required time to transport on site and successively install the components. Very bulky and heavy generators could require an on-site assembly. The transportation process is majorly influenced by the dimensions of the turbine in terms of the usage of the available vessel deck space from each turbine. The installation itself among other important site specific factors (i.e. the seabed) is majorly influenced by the weight of the components, which determines the required crane capability. Each crane has a capacity in terms of weight that can be lifted at a certain height [25]. Heavier components have the consequence that more offshore lifts and/or more powerful cranes are required which in turn creates more demanding vessel requirements.

Chapter 2 Why HTS wind turbines?

Vessel availability is a key aspect for offshore installation. The combination of turbine size, mass and water depth in some cases has effectively limited supply to a single vessel [26]. The effort in the industry is to minimize the number of required offshore lifts in order to reduce the installation time and thus the associated costs. Bulkier and heavier components would also require more performing vessels and more time to install thus raising costs and incrementing the inevitable risks related to weather conditions. In addition to this, onshore logistics requirements (ports and assembly sites) would be also affected especially during the installation of huge farms.

As a consequence, it is clear that with the current technological options moving in the 10 MW range apart the structural challenges presented in constructing the various parts of the turbine (i.e. blades) it would most probably present huge difficulties in the whole transportation and installation and this could have an impact on the cost of the energy produced and potentially making wind energy less competitive. In order to meet these challenges innovation is required. In the future designs of offshore turbines the installation and transportation should be seriously taken into account. The components should be designed aiming at an integration of the entire nacelle design. Ideally this will produce offshore turbines that can be assembled onshore, transported and installed as one piece with one offshore lift. If this concept is possible will be a major driver for faster and cheaper wind farm erection.

2.2.2. Material scarcity

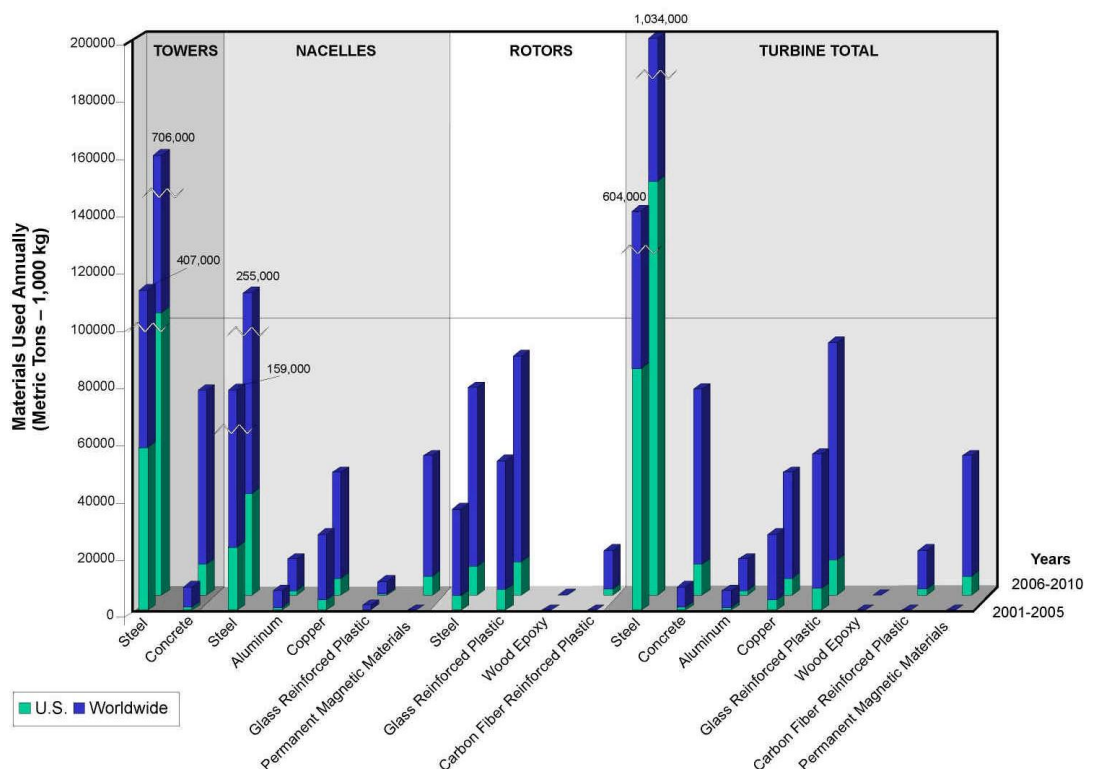


Figure 8 Wind turbine material usage [27]

The materials which majorly contribute to the construction of a wind turbine are steel, concrete, composite materials, permanent magnets (PM) and copper. The materials

Chapter 2 Why HTS wind turbines?

related to the drivetrain are steel (or equivalent) which provides the structural mass and copper and permanent magnets as active materials. The price of steel has presented fluctuations with an impact in turbine pricing [27]. However, steel will not be analyzed further as it is a major contributor to the turbine overall and not the drivetrain itself (in the tower there is only steel).

In the long term (after 2030) in a totally renewable generation scenario vast amounts of wind turbines should be installed to meet the energy demand. In [16] one such scenario is proposed with wind power alongside solar power (concentrated heat solar and photovoltaic cells) as primary sources, complete electrification of terrestrial transport and other major activities and the use of some carrier for storage, probably hydrogen as well as other means of energy storage like batteries, compressed air etc. Even if this is not the only scenario, it is indicative of the order of magnitude of the materials and resources that should be deployed to meet the objective of a fully sustainable future.

In this context, assuming that copper is used as a basic material for generators and cables (of whatever kind i.e. transmission distribution etc.) then this would mean that around 60-70% of the global copper reserves would have to be consumed in order to accomplish the complete electrification of society. This fact by itself would increment the price of copper to the precious metals levels. One could argue that even if the calculation is exact the known reserves of copper could increment and thus limit this negative effect. However, even in that case in order to meet the enormous demand the whole supply chain of copper would be stressed to the limit and this will also raise the market price. As a consequence, the use of copper should be rationalized to uses where it is indispensable and other options might be preferable for certain applications.

PM's are technically an appealing option for wind turbine generators. Unfortunately, this is not also reflected in their economic dimension. PM's are made from Rare Earth Elements (REE). In contrast to their name these materials are not scarce on earth. Their natural abundance could potentially be such that it would be possible to use them for wind turbine generators especially considering the fact that relatively small fractions of the total mass are REE. The problem lies in the anomaly of their global supply chain.

REE find application in many fields: magnets, catalysts, phosphors, metal alloys, military applications (smart bombs, missile guidance systems), telecommunications etc. As a consequence there is a continuous demand for REE. Combining this with the fact that half of the world's population is part of emerging economies it is straightforward to understand that there will always be a steadily increasing demand for these materials. China actually has approximately 50% of the world's reserves of REE. However, in 2010 China produced 97% of the world's rare earth elements, bringing itself in a near monopoly situation. The successive export quotas imposed from the government (60 % export reduction from 2009 to 2010) and the willingness of the government to suppress illegal mining has caused a very sharp increase in REE prices.

As already mentioned China possesses 50% of the REE world reserves. Due to lack of competitiveness and severe environmental impacts major mining of REE has ceased in other parts of the world in the 80's and this has led to the actual China's dominant position.

Chapter 2 Why HTS wind turbines?

Currently limited production and processing capability exists elsewhere. Since the prices have started heavily fluctuating efforts have been made to initiate mining operations elsewhere i.e. Canada, Australia etc. The drawback is that on the one hand a considerable amount of time is required before these new capital intensive mining operations start to cover a part of the demand (a project in the US initiated in 2010 will start mining in 2015) and on the other hand mining is only one small part of the supply chain. Generally speaking the supply chain apart from mining consists of separating the elements, refining, alloying and manufacturing of components. China has a dominant position in almost all phases. As a consequence it produces 95% of REE raw materials, 97% of REE oxides, is the only exporter of REE metals and produces 90% of metal alloys, 75% of NeFeB magnets and 60% of SmCo magnets [28].

Recycling of REE is also a quite difficult task [29]. REE's are chemically very similar. This yields a great difficulty in the separation from ore bodies. In addition to this, the processes used to recycle them (i.e. melting) may degrade the magnetic properties. Moreover, contaminants from machining processes, adhesives used to secure the magnets position and the nickel coating used for corrosion protection pose additional issues in the recycling itself and at the quality of the recovered material.

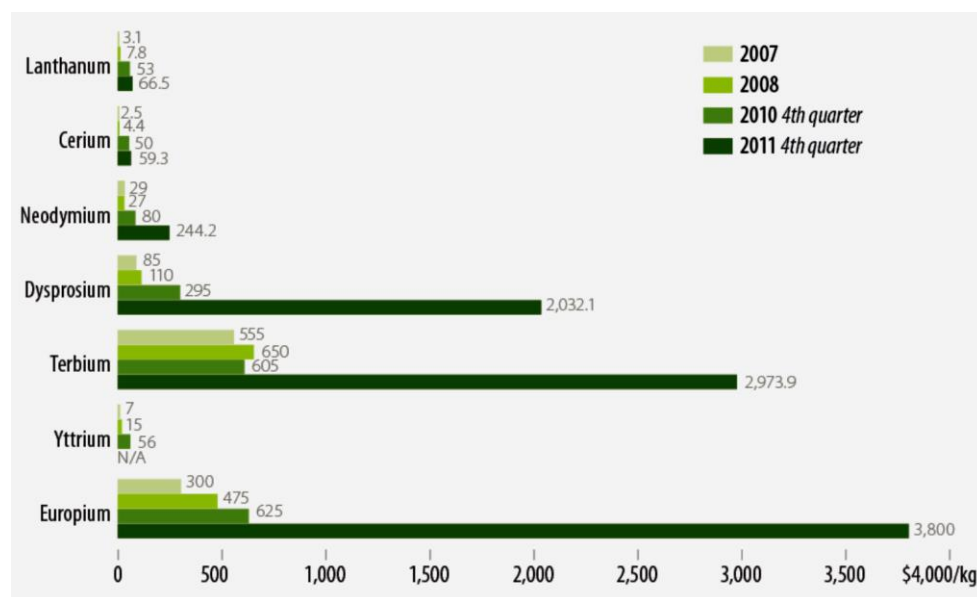


Figure 9 Some REE oxide prices 2007-2011 [28]

In final analysis this situation has not occurred occasionally. China has pursued its strategic objectives in this field with admiring methodology. They also have the necessary expertise and have built up a knowhow on the field that is not easy to imitate. As a consequence, it can be concluded that in the short and medium term price fluctuation are almost a certainty, whereas in the long term it will necessitate a tremendous amount of resources and skilled manpower to alter the situation in the global market of REE. Last but not least, it should also be considered that REE mining has a very severe environmental impact. Therefore, in a sustainable future scenario it might not be a very good option to produce energy with small ecologic footprint but on the other hand produce the necessary devices in a totally unsustainable and polluting way.

Chapter 2 Why HTS wind turbines?

2.3 Why HTS drive trains

The application of superconductivity in wind turbines could represent a valid and viable alternative for the 10 MW power range. At first glance there could be obvious advantages from the application of more power dense machines than the current ones. In addition to this there are more advantages also from perspective from the offshore sector as well as in the life cycle assessment. High power density results in machines that are much lighter and much more compact than conventional machines.

In reinforcement of the last statement comes a study from the NREL [30] comparing three concepts namely geared generator, a PMDD and an HTS generator concept from the AMSC. The comparison was conducted considering the rest of the parameters of the turbine the same for all three concepts. The study concentrates on three power levels namely 3, 6 and 10MW. The study concludes that the larger the power rating the bigger the potential of the HTS technology to make the difference. Moreover, the other options are fruit of a mature technology, whereas HTS technology with the introduction of new components could potentially achieve better results once it matures. However, the study also highlights that there is a significant amount of technological risk in adopting HTS drivetrains and this risk could only be mitigated if a smaller turbine than 10 MW is first produced and tested.

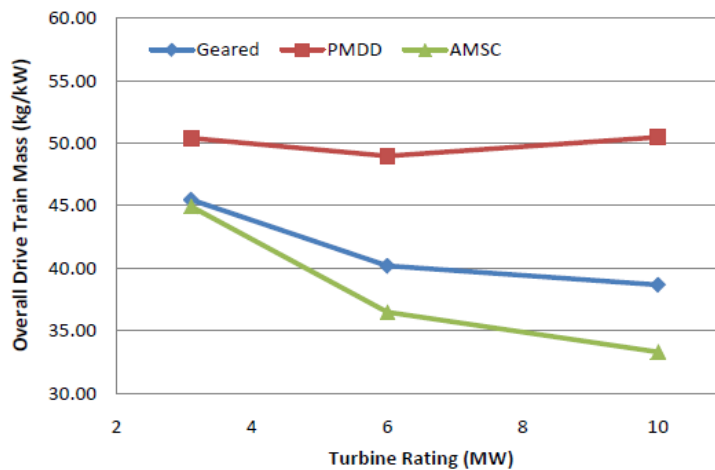


Figure 10 Comparison of overall drive train mass for geared, PMDD, and AMSC turbines [30]

Chapter 2 Why HTS wind turbines?

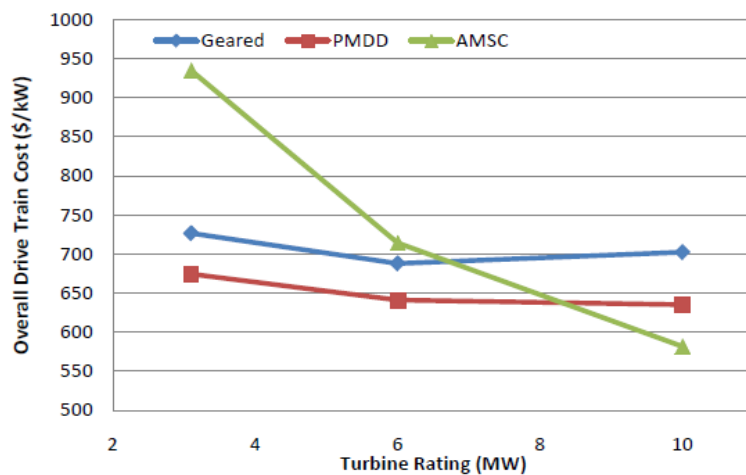


Figure 11 Comparison of overall drive train cost for geared, PMDD, and AMSC turbines [30]

The substantial weight and dimensions reduction may have a major impact in the offshore business. Even in case the percentages and numbers given above are not proved to be exact, they give a clear indication of the trend. In addition to this, the efficiency increase almost at the complete range of operating speeds results in a higher energy yield and a lower cost of electricity produced.

A more recent study [24] regarding innovation in wind turbines indicates the potential of OPEX reduction through innovation in the drivetrain. The study defines a 4 MW reference turbine and studied the potential advantages from the introduction of 8 MW turbines in 2020. The reference turbine is defined as a market-weighted average of four products at this scale available for final investment decision (FID) in 2011: AREVA M5000-116, Siemens SWT-3.6-120, REpower 5M (126m) and the Vestas V112-3.0MW. The analysis successively concentrates into upscaling the reference turbine into higher power ratings calculating the potential reduction of the cost of energy and the factors behind it. As it can be seen from figure 12 the increase in power rating has the biggest impact on the reduction of the cost of energy: more than 10% for an 8 MW turbine in 2020. The increase in turbine power rating increases the CAPEX per megawatt but reductions in balance of plant and installation costs and OPEX, coupled with increases in AEP, outweigh the additional cost.

Chapter 2 Why HTS wind turbines?

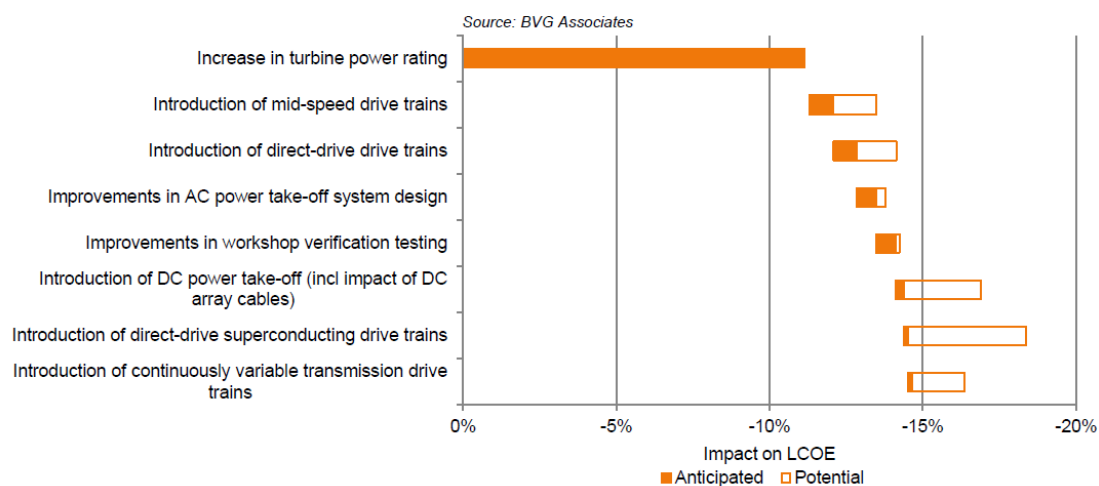


Figure 12 Anticipated and potential impact of turbine nacelle innovations for a wind farm with 8MW-Class Turbines FID in 2020, compared with a wind farm with 4MW-Class Turbines on the same Site Type with FID in 2011

The second largest potential contributor in driving down the cost of energy is the adoption of superconducting drive trains. The potential benefits are multiple. Apart the already mentioned mass and dimension reduction there is a striking 2% reduction in the overall turbine CAPEX. Naturally there is uncertainty over wire prices and this is highlighted in the study. Furthermore there is a 10% reduction in OPEX and an increased energy capture especially at partial loads. In the study it is however stated that the full potential of this technology will be realized in projects with FID beyond 2020. As a consequence the application of superconducting technology could represent a major technological breakthrough that in combination with the upscaling could bring grid parity at reach.

From a materials point of view HTS technology is by far superior. Minor quantities of copper are adopted in the superconducting wire as stabilizer material in fully superconducting machines. Copper can be also used at the stator winding making substantial reduction compared to electrically excited generators. Thus the use of copper in a far future scenario could be left to applications where technically it might be more convenient.

REE's are also not used in large quantities. 1G tapes adopt Bismuth while 2G tapes contain Yttrium, which are both REE's. This is exact, but the amount contained in these tapes is not comparable to the amount of REE's in PM's. For example as reported in [19] in 1 km of YBCO tape there are approximately 51g of Yttrium. Assuming that for a 5 MW offshore turbine 188 km of HTS tape is required this means that 9.5 kg of Yttrium are required. Compared to the 700 kg/MW consumption in PM direct drive generators this is negligible.

Moreover, these tapes are not the only candidate as an HTS wire. Magnesium diboride (MgB_2) is another commercial product which should be taken seriously into consideration. It is a simple compound with relatively abundant components. Magnesium is one of the most abundant elements on earth and can even be obtained from sea water [31]. Boron is not extremely abundant, but has on the other hand significant reserves that have not been exploited with an estimated almost 400 years of reserves with a steadily increasing demand [32]. From a reserves point of view it seems that MgB_2 has virtually no obstacle in

Chapter 2 Why HTS wind turbines?

widespread use and no danger of monopoly situations like REE's, while 1G and 2G tapes might not be in danger in the medium and short term, but have a certain degree of uncertainty for the future.

A question that should be addressed in order to have a clear picture of the materials involved regards the availability of cryogenic fluids. The major industrial source of cryogenic fluids except helium is from air liquefaction [33]. As a consequence, most cryogenic fluid are obtained through costly processes in terms of cost and energy but still have potentially a low chance to become scarce. Helium is produced through natural gas liquefaction and this is not always true for all natural gas reserves. There are some requirements regarding the concentration of helium in the natural gas reserve [34]. With the depletion of natural gas this could bring a serious shortage in the helium availability. Hydrogen has a large variety of production method that could also be sustainable i.e. from biomass, through electrolysis etc. Moreover in many future scenarios is indicated as possible a carrier energy carrier and therefore the associated technology with its production and use can only be expected to improve and become cheaper. As a consequence, by choosing carefully the more abundant cryogenic fluid and by setting up the necessary safety systems to monitor concentration where required (hydrogen and oxygen systems) there are no risks on running into situations like the actual market of REE's.

As it emerges from the illustrated arguments, the introduction of superconducting technology may provide substantial benefits and an added value in the offshore wind sector. However, it has also emerged that there is a technology risk. In the next chapter the technology will be described in detail and an assessment of the challenges will be made identifying the extent that have been met.

Chapter 3 Superconductivity and its application to rotating machinery

3.1 Introduction to superconductivity

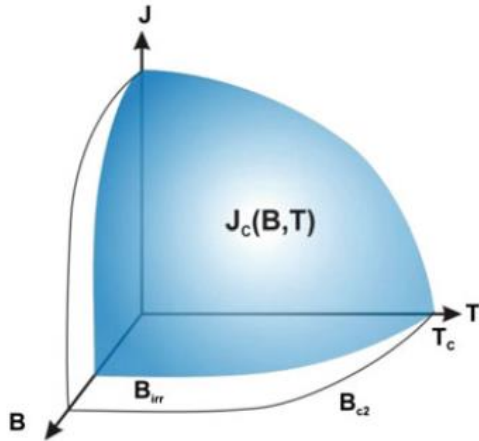


Figure 13 Surface of the critical current density of a superconductor spanned by the temperature, the magnetic field and the current density [19]

Superconductivity is the phenomenon of complete suppression of the electrical resistance manifested in some materials after cooling them down lower to a certain temperature and if the value of the magnetic field does not exceed a certain value. Superconductors differ fundamentally in quantum physics behavior from conventional materials in the manner by which electrons, or electric currents, move through the material [35]. This fundamental difference apart the absence of electrical resistance gives to superconductors a set of unique characteristics like the possibility to carry high current density, the exclusion of externally applied magnetic field (Meissner effect), the high sensitivity to magnetic field etc.

Due to these outstanding characteristics, since its discovery in 1911 by the Dutch scientist H.K Onnes superconductivity has been considered as the holy grail of electrical engineering with the possibility of constructing extremely high field magnets stimulating the engineering fantasy. Current commercial application of superconductivity is found in MRI, NMR, high energy physics accelerators and industrial separation of kaolin clay. Intense R&D activity is introducing superconductivity in power transmission (cables, fault current limiters, transformers), in energy storage and in rotating machinery (both motors and generators). There are strong indications especially in the power transmission sector that the first niche applications are already taking place.

Superconductors are classified in two groups: type I and type II. This classification is based on the phase transition of the material from superconducting to normal. For type I when increasing the external field beyond the upper critical value H_c the material passes from the superconducting state to normal. For the type II there are two critical fields H_{c1} and H_{c2} . When the field is below H_{c1} , the material is in the Meissner state and no flux penetrates [36]. When the field is between the H_{c1} and H_{c2} the material is in the mixed state and is partially penetrated. When the field passes the H_{c2} limit the material is in the normal state.

Chapter 3 Superconductivity and its application to rotating machinery

In practice H_{c2} for type II superconductors is very high and this makes them technologically useful. Type I superconductors are usually pure elements while type two superconductors are all the compounds.

All the useful superconductors are type II and are distinguished based upon their critical temperature in:

- low temperature superconductors (LTS)
- high temperature superconductors (HTS)

There is no sharp limit on the temperature in this distinction. With LTS are referred the materials that operate at liquid helium temperature whereas with HTS are indicated the materials that operate at higher temperatures.

3.2 HTS wires

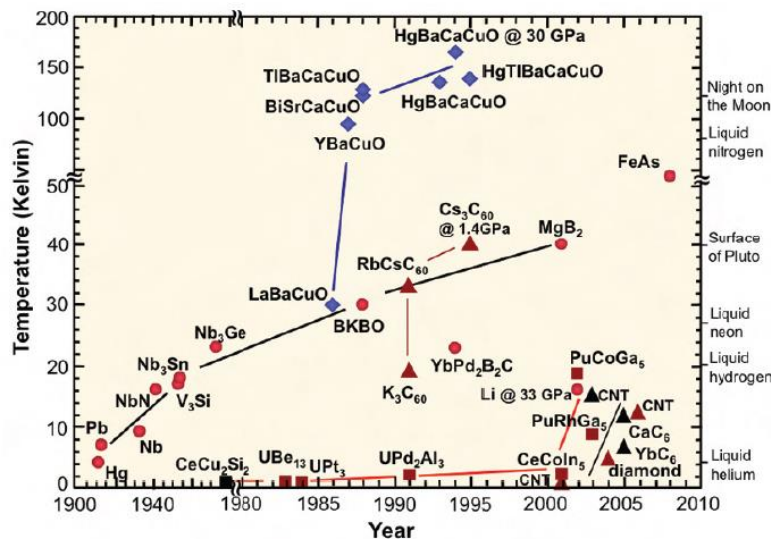


Figure 14 Discoveries of superconductors by year and critical temperature [35]

Material	T_C (K)	Anisotropy	Order of departing, current density at 4.2 K J_d ($A\ cm^{-2}$)	Critical current density at 4.2 K J_C ($A\ cm^{-2}$)	H_{c2} at 4.2 K (T)	H_{in} at 4.2 K (T)	Coherence length, $\xi(0)$ (nm)	Penetration depth $\lambda(0)$ (nm)	Normal state resistivity $\rho(T_C)$ ($\mu\Omega\ cm$)
NbTi	9	Negligible	10^7	$\sim 10^6$	11–12	10–11	4–5	240	60
Nb ₃ Sn	18	Negligible	10^8	$\sim 10^6$	25–29	21–24	3	65	5
MgB ₂	39	1.5–5	10^7	$\sim 10^6$	15–20	6–12	4–5	100–140	0.4
Bi2223	110	50–200	10^8	$\sim 10^7$	>100	0.2 (77 K)	1.5	150	40–60
YBCO	92	5–7	10^8	$\sim 10^6$	>100	5–7 (77 K)	1.5	150	150–800

Figure 15 Properties of LTS and HTS superconductors

The first commercially available superconducting wire was from NbTi (LTS) and was produced by the researchers in Westinghouse [37]. The development of Nb₃Sn followed and continuous improvements of the wire performance have been registered. The discovery of HTS materials occurred in 1986. From this category 3 products have become commercially available namely 1G BISCCO tapes, 2G YBCO tapes and MgB₂ wire.

BISCCO and YBCO are produced in the form of tapes whereas MgB₂ has a certain versatility in the form of the wires produced and can also be circular. In addition to wires, HTS superconductors can be manufactured as bulk material. This type of material could lead

Chapter 3 Superconductivity and its application to rotating machinery

to a cost reduction alongside other potential advantages. However, some issues like the magnetization process of the material itself introduces practical difficulties and for the time being it seems that still this technology is far from practical applications. As a consequence, this topic is not further treated in this thesis. In the following subsections firstly an insight on the important wire properties and the way to interpret them will be given. Successively a brief description of each superconductor will be presented in the sequence of their discovery. Finally, a discussion on the wire will be done analyzing the tradeoffs in the choice of the wire.

3.2.1. Wire properties

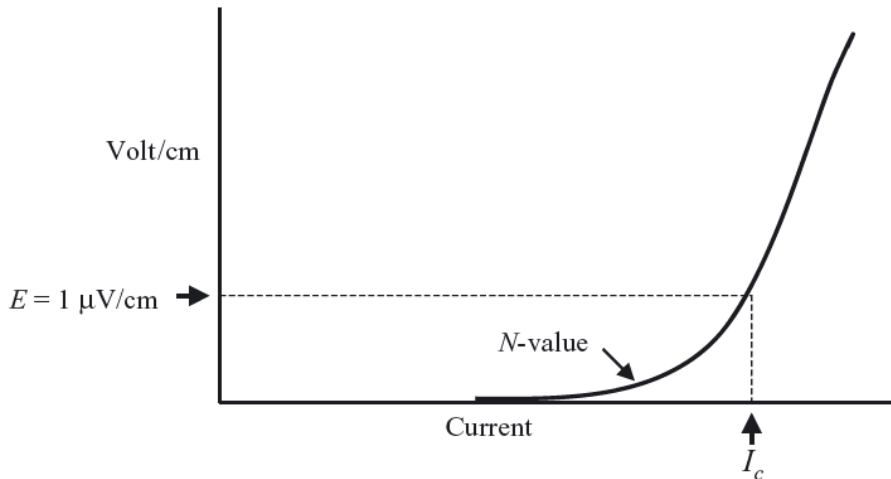


Figure 16 Typical V-I curve of a superconducting wire [38]

As already mentioned all HTS materials are type II superconductors. Due to their nature the transition from the superconducting to normal state is not abrupt but gradual. As a consequence the concept of critical current density needs some further definition. The industrial standard is to use a reference value for the voltage drop over the wire and define the value at which this occurs as the critical current. The accepted reference value is set to $1 \mu\text{ V/cm}$ even if there is trend to lower it to $0.1 \mu\text{ V/cm}$. Thus, a superconducting wire is characterized by a VI curve which represents the voltage drop along the length of the wire as a function of the current. This is modeled with the following power law [38]:

$$E(I) = E_c \left(\frac{I}{I_c}\right)^N \quad (1)$$

Where: $E(I)$ is the longitudinal voltage drop across the wire, E_c is the electric field criterion, I is the current in the conductor, I_c is the critical current, and N is the exponent. A higher N value produces a sharper transition in the VI curve and indicates a higher material quality.

In practice the values of the upper critical fields are extremely high. For example YBCO and BSSCO at 4 K have H_{c2} exceeding 100 T [39]. However, this field is strongly influenced by temperature and this is reflected in having to specify all 3 properties for every operating point namely temperature, current density and field.

Chapter 3 Superconductivity and its application to rotating machinery

An important parameter that should be mentioned is the engineering current density (J_e). The critical current density (J_c) refers to the superconducting fraction of the wire, while J_e refers to the entire cross section of the wire. HTS wires and tapes are made by many superconducting filaments embedded in a matrix of normal metal, such as Cu, Al, or Ag. Such embedding provides protection against magnetic flux jumps, thermal quenching and give mechanical strength [39]. Moreover, in the design of devices there are also other materials such insulation and extra mechanical support to cope with the forces on the windings. As a consequence J_e is a key figure in the design.

3.2.2. YBCO

Yttrium barium copper oxide, or YBCO, is the first high temperature superconductor discovered with a critical temperature above the melting point of nitrogen. Since its discovery in 1987 extensive research and development has taken place. YBCO is also called the second generation high temperature superconductor (2G HTS) being the second HTS product made commercially available. Currently, YBCO is the most performing HTS with the highest achievable fields and current densities.

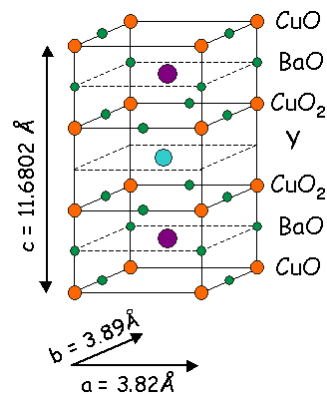


Figure 17 Layered atomic structure of YBCO [40]

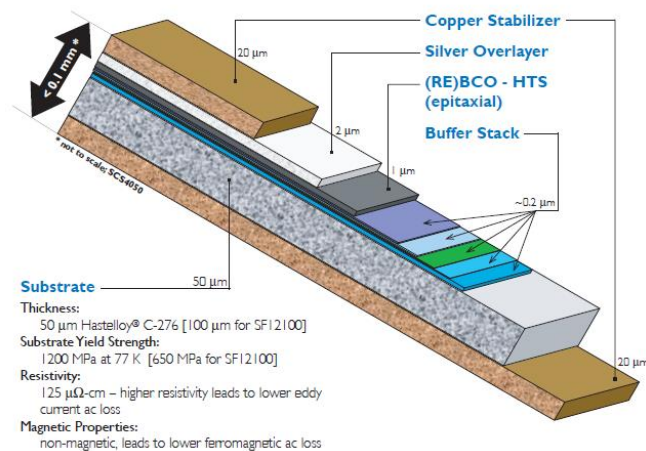


Figure 18 YBCO tape from Superpower

Chapter 3 Superconductivity and its application to rotating machinery

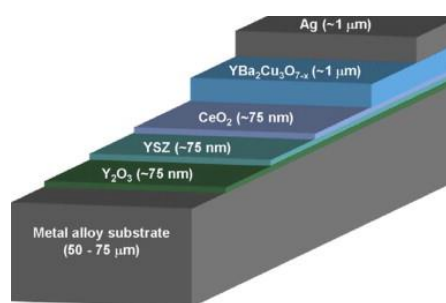


Figure 19 YBCO tape from AMSC

Being a cuprate, the material structure consists of a number of oxide layers with a rare earth atom in the middle. The number of layers and the rare earth atom can be changed in order to create different variants material with different properties. Other metals that can be used as the rare earth element besides Yttrium (Y) are Lanthanum (La) and Gadolinium (Gd).

Unlike the LTS materials, YBCO has a very small grain boundary. These grains should be aligned with each other with a maximum acceptable disorientation of 5 before compromising performance. YBCO is very brittle by nature. Mechanical stresses like bending or even the self-induced magnetic forces can damage the material especially in applications related to very high fields. Therefore to produce the material as a wire, coated conductors are made instead of conventional wires. These coated conductors consist of only about 1 volume percent of superconductor material and the rest provides mechanical strength and thermal conductance [41].

Most coated conductors are produced with either the rolling assisted biaxially textured substrates (RABITS) technology or the ion beam assisted deposition (IBAD) or variants of these technologies [42]. Due to the required high quality of the material, the production process is more related to the production of semiconductor material rather than LTS or conventional cables. The two processes (IBAD and RABITS) are different, but the end results are similar with (small) differences in properties like cost, maximum bending angle, critical current, ac losses etc. For both technologies it is challenging to produce long wires of more than 1 kilometer while ensuring high quality at reasonable prices. Especially the length is a major issue due to the small grain boundary of YBCO material.

3.2.3. BSSCO

Bismuth strontium calcium copper oxide, or BiSCCO, is also a cuprate high temperature superconductor and was discovered in 1988. Although discovered later than YBCO it was made commercially available earlier than YBCO, becoming the first generation HTS wire (1G).

The properties of BiSCCO and YBCO are quite similar. The crystal structure also consists of oxide layers, but there is no rare earth metal like for YBCO. BiSCCO is also very brittle and needs to be coated to improve the mechanical strength. Compared with YBCO, the mechanical properties are still worse for BiSCCO tapes.

Chapter 3 Superconductivity and its application to rotating machinery

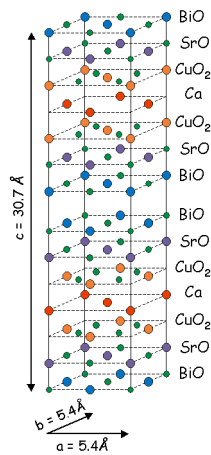


Figure 20 Layered atomic structure of BiSCCO [40]

However, there are differences like the higher anisotropy (an order of magnitude higher), the need of silver coating for BiSCCO wires and above all the inferior performance of BiSCCO: the irreversibility field and the current density are higher for YBCO. The critical temperature however, is somewhat higher for BiSCCO. Despite the disadvantages since it was the first available most prototypes deploy this type of material and as a consequence is more tested and reliable and thus is kept in production and can claim a market share.

Many companies like American Superconductor have ceased their efforts on BiSCCO wire and are nowadays more focused on YBCO wire. However, some companies like Sumitomo Electric and Bruker EST are still investing in BiSCCO wire. In 2004 Sumitomo introduced the controlled-overpressure (CT-OP) sintering method to produce their dynamically innovated BiSCCO wire called DI-BiSCCO [43]. This method is an improved version of the conventional Powder in Tube (PIT) method. With this production process Sumitomo produces wires with competitive critical values and single piece lengths of more than 1500 meters. Laminated wire is also available to reduce AC losses [43]. The downside of any production process of BiSCCO wire is that you need to sheath the wire with silver due to the properties of the material and this sets a rather high lower cost limit set by the high silver price.

3.2.4. MgB₂

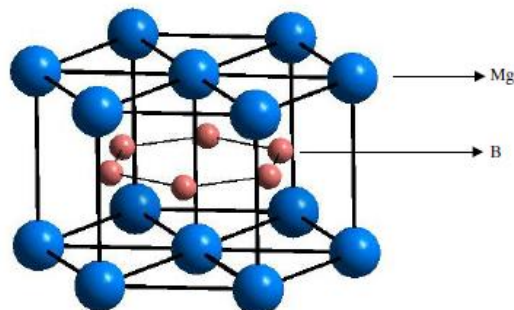


Figure 21 Crystal structure of MgB₂

Magnesium diboride is a relatively new superconductor discovered in January 2001. It is a material known since the 50's, but only at that time it was discovered that it was

Chapter 3 Superconductivity and its application to rotating machinery

superconductive at a temperature around 40K. In figure 4.9 the crystal structure is depicted. The B layer is considered to be responsible for the superconductivity state [44]. The material's properties are closer to the low temperature superconductors rather than the high temperature superconducting materials.

Unlike the cuprates, MgB₂ has lower anisotropy, larger coherence length, and transparency of the grain boundaries to current flow, which makes it a good candidate for applications. Moreover, higher critical current densities (J_c) can be achieved by oxygen alloying [45]. In addition to this MgB₂ has a density of 2.6 g cm⁻³, which is much lower than the other superconductors making it the most suitable candidate for lightweight applications.

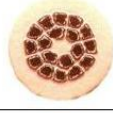
Higher Filament Counts (54)		Lower AC Loss for Stator
Al ₂ O ₃ Dispersion Strengthened Copper		Lower AC Losses for Transformers
Resistive Matrix		Wire for Fault Current Limiter
Rectangular Wire		Better Packing for electromagnetic coils
Nb Barrier All Copper Matrix		Improved Wire Stability
Wire-in-Channel		Stability and Strength

Figure 22 Possible wire configurations from Hypertech

MgB₂ is a brittle material like the HTS materials. Typical polycrystalline MgB₂ has a grain size of 10 nm–10 μm. The exact degree of anisotropy of MgB₂ to a certain extent is still under discussion, also depending on the geometry of the material. In [44] is reported 1.5–5 (parallel to perpendicular component of the magnetic field) and is low compared to the anisotropy of the HTS cuprates. This low anisotropy means there is no need of texturing as in the case of HTS and wire geometry can be used with higher J_c. Due to the large coherence length, higher than the interatomic spacing, the weak link problem is not severe in MgB₂ [45].

The normal state of MgB₂ is metallic and the normal state resistivity is much lower than that of other superconductors and is 0.4 μΩcm [44]. MgB₂ has a very sharp T_c of 39–40 K and has a very narrow transition width of less than 1 K. The grain boundaries are a current limiting factor in other superconductors. In MgB₂ not only they are transparent to the current, but also enhance flux pinning resulting that the overall J_c increments as the grain size decreases [45].

Chapter 3 Superconductivity and its application to rotating machinery

MgB₂ has the potential to become a good low AC loss superconductor. The MgB₂ strand is such that the barrier and sheath material can be interchanged and so a conductor with a more resistive matrix than the standard multifilament wire can be produced, thus reducing the external field-induced eddy current losses. The dominant factor in external field losses is the filament size. The filamentation and reduction of filament size is much easier in MgB₂ compared to YBCO-coated conductors [46]. With respect to transport current losses, MgB₂ has the traditional advantage of a wire as compared with a tape (losses proportional to the width or radius) and therefore can be quite low for MgB₂.

The fabrication techniques of other low and high temperature superconductors can be applied to MgB₂. One of the big advantages of the fabrication of MgB₂ conductors compared to the other superconductors is that the MgB₂ phase forms at lower temperatures and high grain connectivity and better superconducting properties can be achieved with heat treatment in short durations [44]. In fact there is no fundamental barrier to the production of km long MgB₂ conductors.

There are mainly 3 techniques for the production of MgB₂: the diffusion method, the coating techniques and the powder in tube method (PIT). The diffusion method consists of Mg diffusion in B fibers and is a straightforward and well known method. The first wire samples were produced in this way. The low phase homogeneity makes it suitable for the production of short samples. The coated conductor techniques are well established methods and are used to produce YBCO. The properties of the wire produced are very good, but scaling up this method in order to achieve satisfactory wire lengths is difficult.

The PIT method is also the one adopted to produce Bi-2212 and Bi-22223 tapes. It consists of filling metal tubes or sheaths with precursor powder in air or inert environment (usually argon). The tubes are successively rolled into wires and this is followed by heat treatment in vacuum or oxygen protective atmosphere. The sheath material must provide mechanical support to the superconductor and at the same time should allow mechanical working of the wire and should not react with the superconductor. The sheath is usually made of Cu, Ag, Ni, Nb, but also other materials and alloys have been tested i.e. Ti, Cu-Ni. The Cu sheath yields an enhanced thermal stability of the wire. There are basically two variants in the PIT method: the ex situ and the in situ method. The difference lies in the powder. In the ex situ method the powder is already MgB₂, while in the in situ technique the tubes are filled with stoichiometric Mg and B, are then rolled and successively are subject to high temperature heat treatment (650-800°C). The ex situ method is more reliable in obtaining homogeneous and dense cores, however limits the sinterability and the effectiveness of doping. The in situ conductors are more prone to porosity than the ex situ ones [44].

During the literature survey three companies emerged as the major producers of MgB₂ wire: Hyper Tech (USA), Columbus (ITA) and Hitachi. Hyper Tech and Hitachi adopt an in situ technique while Columbus an ex situ method.

Hyper Tech developed and patented the continuous tube forming and filling (CTFF) process to make a powder metallurgy based wire of the MgB₂ superconductor, which adopts an in situ method. To manufacture a multifilament wire, numerous monofilaments

Chapter 3 Superconductivity and its application to rotating machinery

containing the superconducting powder must be stacked within a tube and then drawn down to the required wire diameter and length. Hyper Tech has manufactured monofilamentary and multifilamentary wires of up to 6 kilometers in length. Columbus superconductors manufacture MgB_2 wires based on the ex situ technique. The company produces wires for both DC and AC applications. They claim that they have a production capability of wire length of 1-5 km.

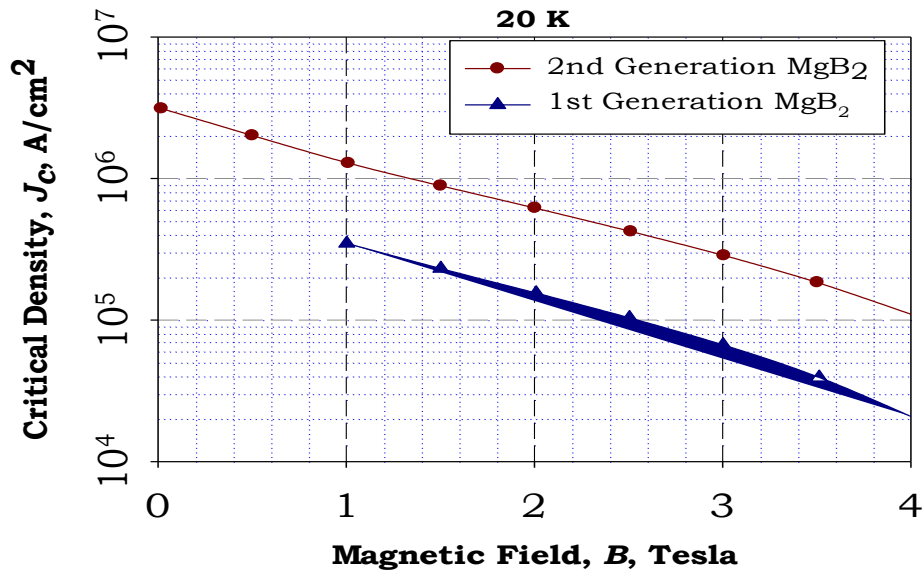


Figure 23 MgB_2 evolution of performance [47]

In figure 23 the recent announcement of development of second generation MgB_2 wires can be seen. The result is significant and bridges the gap in performance with the cuprates. This result was achieved by obtaining higher purity in the wire composition. It should be also stated that it was obtained for a short sample. However, Hypertech expect to achieve the same standards of the first generation wire within 3 years and therefore for a potential demonstrator intended to be operated in the mid-term this is the wire to consider. The salient characteristic of MgB_2 wire is its very low cost compared to the other superconductors. Hyper tech has declared that typical MgB_2 0.8 mm round wire costs \$5-7/m (a factor of 8 approximately less costly than YBCO) currently. Moreover, they expect in the next 2 years or less to get to \$1-2/m for MRI applications. In this price range the use of more superconducting material in order to achieve the same performance as with other HTS superconductors could be justified.

3.2.5. Stability of HTS wires

Stability is a very important issue in superconducting technology. It could certainly be subject of a dedicated study. The intention of the author is not make an extensive analysis but to expose some concepts that need to be taken into account when designing a superconducting machine. It is evident that compared to LTS, HTS materials are inherently more stable [36]. This is due to the operating temperature which heavily influences the heat capacity and therefore the higher the temperature the higher is the energy that is required to produce a temperature rise. Moreover, due to the less sharp transition from the superconducting to the normal state HTS wires have a higher capability to handle

Chapter 3 Superconductivity and its application to rotating machinery

overcritical current with subsequent lower Joule heating. Thus, HTS wires have in principle a larger stability margin and quenches are not as intense as for LTS wires.

The quench can be simply defined as the transition from the superconducting state to normal state. During a quench the stored magnetic energy will dissipate to heat. Some of the reasons why this occurs are: wire movement, flux jump, resin cracking and loss of cooling power [48]. The consequences of a quench can be insulation breakdown, mechanical strain and even irreparable damage of the coil.

The quench once it takes place successively propagates in both longitudinal and transverse directions [49]. The velocity is not the same in both directions since due to the presence of insulation the heat capacity and heat conductivity are different. The minimum propagation zone (MPZ) is defined as: a normal zone in a superconductor which is larger than the MPZ will grow; a smaller one collapses and full superconductivity will recover [50]. The stability of superconducting magnets is generally evaluated in terms of the minimum quench energy (MQE) and the normal zone propagation velocity (NZPV). MQE is the energy required to create the MPZ. The propagation velocity depends on the conductor geometry, material properties and operating conditions [51].

Thorough analysis is required to determine these parameters for a particular design with choices that need to be made regarding the configuration of the cooling system, the amount of stabilizer in the wire etc. The objective of this thesis is not to make extensive calculations on this matter, but to make reasonable assumptions. As a consequence a few concepts are exposed.

MQE of MgB_2 is 2 to 3 orders of magnitude higher than LTS superconductors, while NZPV is 1 order of magnitude lower [52]. More specific experimental data from Hypertech wire tested by the TU Twente reveals that MQE is in the range 2-100 mJ and NZPV 1-100 cm/s [47]. The NZPV for YBCO is 0.1 cm/s [53] and for NbTi at 4.2 K is around 20–40 m/s [52]. Ideally from a device designer perspective on the one hand it is desirable to have a wire that is improbable that quenches as the other hand if the undesirable phenomenon occurs to have the possibility to protect the device. If active protection schemes are adopted it is desirable to easily detect the quench. MQE plays an important role how easy it is to quench. Therefore a higher MQE is desirable. The NZPV indicates how the quench diffuses in the winding. In LTS with such velocities the propagation is easy. In HTS the propagation velocity is lower. As a consequence the stored energy is dissipated in a smaller volume causing local hot spots. Moreover, detection with a lower NZPV is problematic. MgB_2 suffers less this problem than YBCO.

In a “real” machine the operating temperature of a coil is determined upon the balance of cooling power and generated losses. If the balance is altered a transient is caused. Superconducting machines are designed to settle these transients into acceptable temperature levels. As a consequence, instead of considering the coil’s critical current it is important to consider the coil’s “quench current” which is defined as the current above which the winding temperature and voltage become unstable and raise with time [54]. The quench current is a system property since it also accounts for coil properties, cooling system and magnetic field to which the wire is exposed.

Chapter 3 Superconductivity and its application to rotating machinery

In conclusion, it can be said that HTS wires are more stable, but this does not mean that stability is not still an issue. In depth analysis is needed for the correct assessment of the operating point of the coils. In the next chapter where a design will be proposed some assumptions will be made regarding stability and calculations in this field will not be performed.

3.2.6. Discussion on wires

Both BISCCO and YBCO are produced in the form of tapes. BISCCO was the first material to be commercial available and therefore is by far the more used in prototypes. YBCO is characterized by very high magnetic fields and high critical current at relatively high temperatures. These materials suffer the pronounced effect of anisotropy (YBCO less than BISCCO). As a consequence the orientation of the field majorly influences the performance of the tape. An important parameter that needs to be taken into account is the perpendicular component to the wide face of the tape of the flux density. J_e is heavily dependent on this component: the higher the perpendicular component the lower is J_e . In both tapes their complex structure makes them difficult to handle. They have both low mechanical strength and should be laminated to a stronger metal to withstand the applied forces. Moreover, their production methods make it difficult to produce continuous pieces of long lengths of high quality wire. The maximum available length of YBCO is around 500 m [38]. Both these materials suffer significant losses if exposed to AC fields. For this reason they are exclusively used in the excitation field winding of synchronous machines and never in the armature.

In addition to this, both materials suffer a homogeneity problem which means that J_e is not uniform in a given conductor with the part of the least J_e determining the performance of the tape [38]. This fact combined with the already mentioned dependence of J_e to the orientation of the field gives an idea regarding the restrictions in the design of coils. Although BISCCO tapes have a higher critical temperature, they give good performance characteristics at temperatures around 20 K, while YBCO has a good performance even at 77 K. In this prospect, the choice of YBCO could lead into a simpler and less costly cooling system compared to BiSSCO and MgB₂. In figure 24 is depicted a comparison between typical 1G and 2G tapes at 77 K [38].

Magnesium diboride has a simple bimetal structure. The natural abundance and the low price of Mg and B combined with the simpler production process make it a cheaper alternative to the cuprates. It has lower anisotropy and this make it possible to produce in a variety of wire geometries which in turn yields versatility to the design of coils [38]. This compound is lighter than the cuprates and its production process does not set any practical limit in the wire's length produced. Currently wires with lengths up to 6 km have been reported [55]. On the other hand the wire performance is by far inferior to YBCO and the expected operating temperature would be much lower. However, the possibility of producing MgB₂ wire in various wire geometries makes it possible to reduce the AC losses and could consequently be the only suitable candidate for the armature of a fully superconducting synchronous machine. Its low cost renders this material attractive even if more superconductors would be required to produce a given magnetomotive force compared to YBCO.

Chapter 3 Superconductivity and its application to rotating machinery

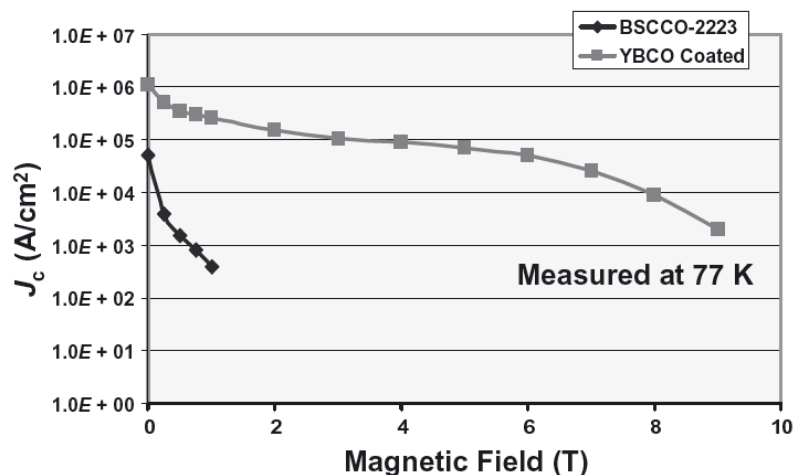


Figure 24 Performance comparison between typical 1G and 2G wires [38]

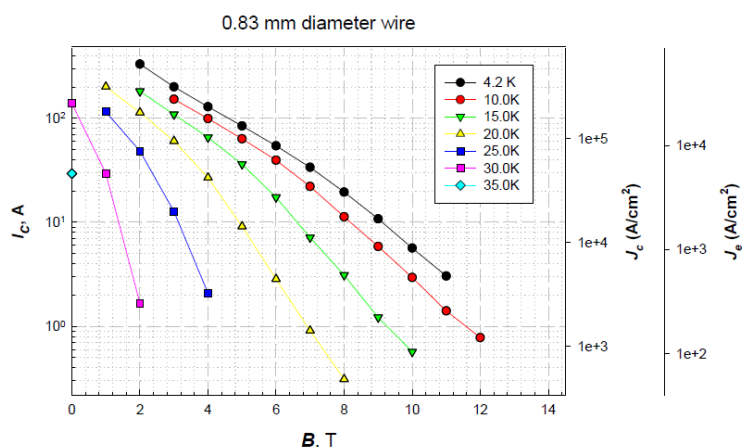


Figure 25 Typical MgB₂ Hypertech wire performance over Temperature [48]

Comparing the characteristics of the three HTS products it turns out that currently there is no preferable option on the choice of a material for electrical machinery. The very high magnetic field achievable with YBCO combined with its reduced cooling requirements stimulate imagination for constructing electrical machines well beyond the conventional flux density levels. However, the question that arises is whether the fragile tapes of the material can withstand the significant forces developed. BiSSCO on the other hand is more reliable on this prospect having being more tested. In both cases the cost is a major issue with the industry aiming to significant cost reductions compared to today for further diffusion. In addition to this the wire length should be incremented for application in large machines. MgB₂ represents a low cost option, with no real barrier in producing long wires. Moreover at present is the only suitable superconductor for AC use with acceptable losses potentially leading to a fully superconducting machine and thus fully exploiting the potential of the technology. The downside is that the cooling power is more demanding to reach the 20 K region where MgB₂ is expected to operate. However, as it will be put into evidence in a later section, prototypes incorporating cuprates do not usually operate at the liquid nitrogen range but at a range from 20 K at 50-60 K. In stability terms the three wires seem to have similar properties apart the NZPV which is more favourable in MgB₂.

Chapter 3 Superconductivity and its application to rotating machinery

3.3 HTS generator topologies

In this section the principal HTS generator topologies will be presented. In principle a superconducting electrical machine has a set of characteristics that lead to significant advantages. These include the already demonstrated advantages of [42]:

- Enhanced efficiency at all loads
- Higher power density
- Reduced weight and dimension

As well as the potential advantages of:

- Reduced acoustic noise
- Lower life cycle cost
- Reduced capital cost
- Superior negative sequence capability
- Enhanced grid stability
- Lower maintenance requirements

These advantages were evident since the beginning of the development of such machines with the commercial availability of low temperature superconductor (LTS) wire in the 60's. The first demonstration of a rotating synchronous superconducting field winding was built at the Massachusetts Institute of Technology (MIT). Successively, research programs on large synchronous superconducting machines have been carried out by General electric, Siemens, Westinghouse and others, which resulted in a number of prototypes]. However the positive aspects of these machines were largely offset by the extreme cost, the complexity and the technical challenges mainly related to the cooling system which in turn arrested the diffusion of this technology and mostly restricted the research to very large turbogenerators. The commercial availability of HTS wires has given new momentum in the research for this technology resulting in a variety of prototypes and designs. From the literature survey some basic design trends have emerged.

The electrical machines can be classified according to the direction of the flux lines to:

- Radial flux machines
- Axial flux machines

The literature survey indicated that the vast majority of the constructed HTS machines until now are of the radial type. The axial flux topology has not been as extensively developed yet and this has resulted until now in prototypes with fairly moderate power ratings. Nevertheless, this machine topology is interesting, because it could lead to further miniaturization of the design since the machine's linear dimension could be used more effectively by increasing the number of rotor plates and stator units [56].

Due to the already discussed performance of the available HTS tapes in a large number of designs the machines had an HTS rotor field winding and a conventional stator copper winding. Therefore another type of classification is:

- Machines with HTS field windings

Chapter 3 Superconductivity and its application to rotating machinery

- Fully superconducting machines

HTS generators have fundamental differences compared to the conventional electrical machines. Above all is that the presence of iron is not required. As a consequence another way to distinguish HTS generators is:

- Magnetic core rotor and airgap stator winding
- Iron on both stator and rotor
- Air core machines

The magnetic core rotors are constructed in a similar way as in conventional machines. The rotor core material (iron) minimizes the requirement of the HTS wire and this reduction is effective even if the machine operates at the saturation flux density levels (i.e. 2T) [57]. The machine has a high moment of inertia, comparable to conventional machines. Even if the flux density levels are lower than the air core generators, the torque densities are many times not inferior to air core machines and this is due to the fact that smaller coils and simple mechanical construction increase the speed and power density [42].

The rotor can be at cryogenic (cold rotor) or “room” temperature (warm rotor). The warm rotor design has reduced cold mass. As a result the cool down period is short and therefore the machine is insensitive to the induced eddy currents. However, the support structure is more complicated because on the one hand it should limit the heat transfer from the iron core to the winding and on the other hand it should transmit the torque from the winding to the rotor body [57]. Connecting structures of different temperature could give rise to considerable thermal stresses [58] and therefore the design and the material of the construction should be carefully evaluated.

The cold rotor design has the disadvantage to increase the cold mass of the machine and as a consequence the cooling system requires more power. In the design process the eddy current losses should be evaluated as they affect the winding and should be removed from the cooling system. The advantage of this design is that the windings do not necessitate connecting structures at different temperatures and therefore the whole structure is mechanically simpler [57].

Air core machines require a significantly higher amount of HTS wire in order to get magnetized [57]. The winding support structure should be designed to carry all the torque of the machine. This limits the application of such a design to lower speed applications, due to the large centrifugal forces applied at the windings at high speeds [42]. One material that can be used is Glass Fiber Reinforced Plastics (GFRP). This material is very strong and shows no ferromagnetic effects, meaning it behaves magnetically similar to air. The major downside of this material is the high cost. The windings are vacuum sealed to provide insulation. The electromagnetic shield protects the windings from the asynchronous stator fields, carries the high transient torque during faults and provides damping for low frequency torsional oscillations [59]. The moment of inertia is much lower compared to the other topologies. With the elimination of the iron, there are no eddy current losses and the flux density can be increased well beyond the conventional machines operational levels. This machine topology has a large magnetic air gap and thus has a low synchronous reactance. As

Chapter 3 Superconductivity and its application to rotating machinery

a consequence there is reduced magnetic coupling between the rotor and stator fields and thus the machine has superior steady state stability [60].

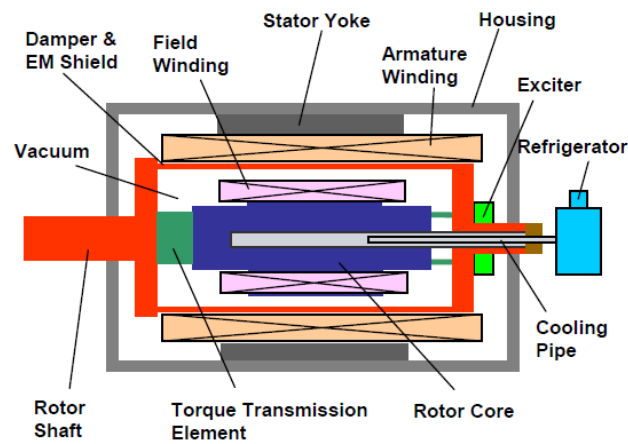


Figure 26 HTS machine with radial flux topology and cold rotor core [57]

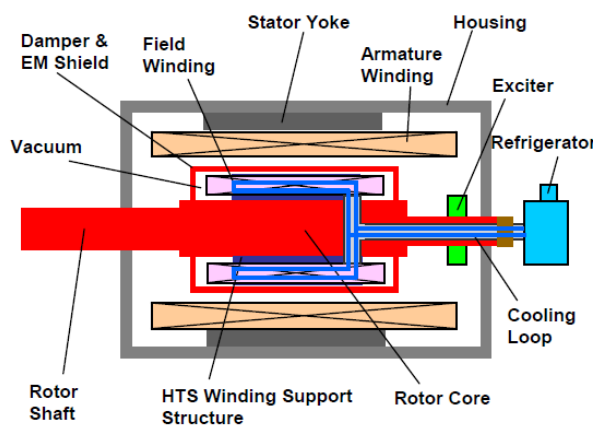


Figure 27 HTS machine with radial flux topology and warm rotor core [57]

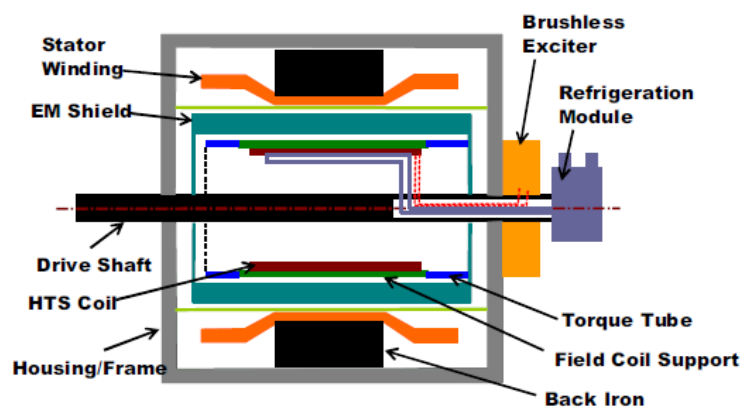


Figure 28 Air-Core Electric Machine Topology [59]

Chapter 3 Superconductivity and its application to rotating machinery

For the stator of the superconducting generators there are two fundamental choices: A conventional (or semi-conventional) copper stator winding or a superconductive armature winding. With the products currently commercially available, as already mentioned, the only possible candidate would be MgB_2 . During the literature survey no evidence has emerged on a prototype of a fully superconducting machine. Therefore, not considering for the time being the option of superconducting coils, two solutions are described in the literature. Firstly, it is possible to adopt the current state of the art in the stator windings construction: stranded copper winding supported by magnetic teeth. This is a robust, reliable and proven solution, which also affords currently dominant maintenance approaches in the industry [60]. However, it is subject to saturation and produces harmonic distortion.

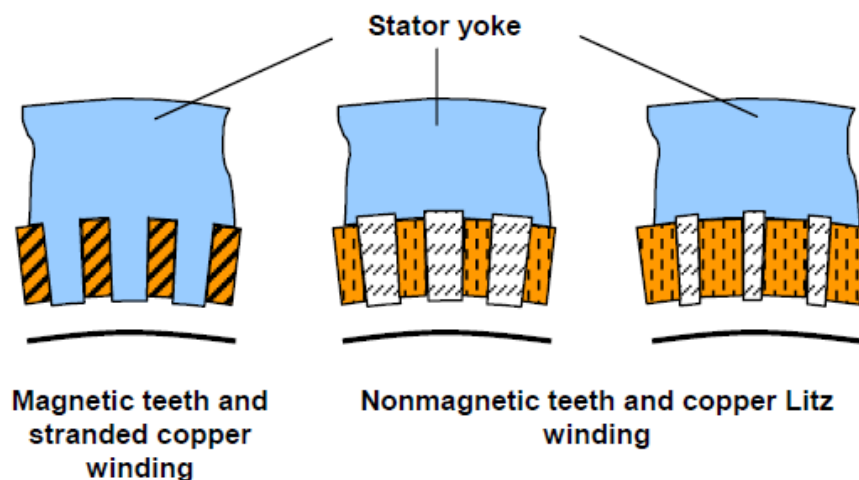


Figure 29 Different stator topologies of HTS machines [57]

In order to achieve higher levels of flux density, enhance efficiency and fully take advantage of the superconducting technology, the magnetic teeth could be replaced by a non-magnetic material (Fiber Reinforced Plastic). In this way higher flux densities could be realized and hence higher power output. As a consequence, the isolation of the winding would increment in order to withstand the higher voltage. Nevertheless, this is not necessarily a disadvantage, because it could be beneficial to generate power at a higher voltage level. An interesting solution would be to adopt liquid cooling for the stator winding using some fluid that performs both cooling and isolation of the windings. Another consequence of the replacement of the stator teeth is the change of the magnetic field distribution. There are no more slot harmonics and the transversal flux components are increased [57]. The magnetic air gap is also increased (higher reluctance). For this reason the windings are made of Litz conductors (small diameter insulated and transposed copper strands) in order to minimize losses. The armature reaction is decreased and therefore the generator shows a reduced dependency on load changes [5]. Air core designs mount this kind of ironless stator configuration [60].

In order to increment the utilization of the stator teeth, the non-magnetic teeth could be constructed with a reduced width (designed only to fulfil the mechanical requirements) and replace the space with more copper to increment the ampere turn loading [57]. As a result this design modification enhances the power density, but introduces

Chapter 3 Superconductivity and its application to rotating machinery

an additional mechanical requirement for the support structure of the windings that should be able to provide mechanical stability under all operating conditions.

Another interesting topology is the superconducting homopolar machines. This topology was one of the first to be developed with the advent of LTS wires. Homopolar machines have the advantage that superconducting coils are stationary and do not experience torque thus, simplifying the support structure, the cooling mechanism and overall driving down costs. On the other hand, the use of iron in many designs does not allow raising the flux density beyond the conventional levels and does not yield the compactness of other types of superconducting machines [38]. Moreover, a large number of designs adopt brushes to collect the current from the rotor. This is a source of wear and losses reducing the efficiency. However, this topology could be prominent for some applications.

3.4 Cooling systems

The cooling system is one of the most challenging parts of a superconducting machine. Instability or underestimation of the heat power that should be removed leads to the immediate damage of the coils. Moreover, constructional features as it is for example the rotary joint that should connect the cryocooler to the rotor, add cost, complexity and a possible source of failures to the system. In this section the cooling systems for HTS generators will be discussed. Firstly the cryostat will be described. Successively, the available options regarding cryogenic fluids and cryocooler types will be briefly presented. Finally a short illustration of the heat transfer mechanism between the coil and the fluid will be given highlighting sensitive parameters.

3.4.1. The cryostat

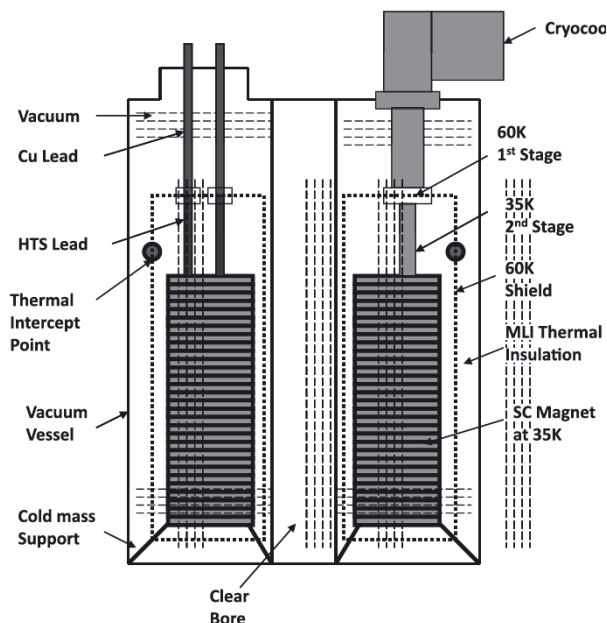


Figure 30 Cryostat for an HTS magnet [38]

Chapter 3 Superconductivity and its application to rotating machinery

The cryostat is the container that houses all the necessary components for the operation of the coils. It comprises the vacuum vessel, the HTS coils, the current leads, the cold mass support, an intermediate temperature radiation shield, a multi-layer insulation and the cryocooler. The cryostat thickness can be estimated around 50 mm in the 50-80 K region and around 100 mm in the 20-50 K range [61]. The current leads supply current to the coil and can be made from conventional conductors or HTS. Due to the additional thermal loads they introduce and due to the fact they can represent a source of heat leakage proper design is imperative and the HTS option is the preferable one. The radiation shield intercepts radiative heat loads from room temperature surfaces to the operating temperature surfaces. The cryocoolers can be single or double stage. Usually a single stage is sufficient to achieve a working temperature of 30 K. An example of a cryostat for an HTS magnet is depicted in figure 30. In many cases a step of precooling with LN is adopted in order to reduce the power required from the cryocooler at low temperature.

3.4.2. Cryogenic fluids

In figure 31 the properties of cryogenic fluids are listed. A common characteristic of all the coolants is that either they should be replenished or they should be designed in a closed cycle system. Among the coolants H_2 and O_2 are not the preferred options due to the hazards associated with their use. In case they are adopted careful monitoring is required. Liquid nitrogen is by far the less costly and more abundant fluid. However, its temperature range restricts its use. Liquid neon is an attractive coolant for its properties, but is costly and not readily available in large quantities.

Property	He	H_2	Ne	N_2	O_2
Boiling temperature (T_s), K	4.22	20.39	27.09	77.39	90.18
Triple point, K	—	13.96	24.56	63.16	54.36
Heat of vaporization (liquid), kJ/kg	20.9	443	85.9	199.3	213
Heat of vaporization (liquid volume), J/cm ³	2.6	31.1	104	161	243
Density (T_s , liquid), kg/m ³	125	70.8	1206	807	1141
Density (T_s , vapor), kg/m ³	16.9	1.33	9.37	4.60	4.47
Density (293 K), kg/m ³	0.167	0.084	0.840	1.169	1.333
Density (T_s , liquid)/ Density (293 K)	749	843	1436	690	856

Figure 31 Properties of cryogenic fluids [62]

LTS magnets require operation at extremely low temperatures and thus the choice is restricted to LHe with a major impact in the system complexity and cost. HTS leaves a wider choice open for discussion and considerations. For applications adopting BISCCO or YBCO tapes there is more freedom in deciding the operating temperature and as a consequence there can be a variety of suitable coolants. In contrast the operating temperature of MgB_2 restricts the available options.

Chapter 3 Superconductivity and its application to rotating machinery

3.4.3. Cryocoolers

Cryocoolers are the heart of the cooling systems. Reliability and redundancy are important in evaluating a cryocooler and a cooling system. Proper design of the system means proper choice of the cryocooler. An important aspect of cryocoolers is that their efficiency is not high. In addition, cryocooler efficiency decreases as the temperature decreases and due to the Carnot penalty the amount of power required to subtract a given heat power increases as the temperature decreases. As a consequence when deciding the operating temperature of superconductors a careful balance is needed between the enhanced performance at lower temperature and the increased cooling power required.

Cryocooler research in the past 20 years has led to significant advancements. Lifetimes of 10 years are possible for space cryocoolers, whereas 5 years for commercial applications. Efficiencies can be as high as 20% of the Carnot efficiency, with typical efficiencies for commercial products around 10-15% of the Carnot efficiency [63]. Two main types of cryocoolers exist based on the adopted thermodynamic cycle: recuperative and regenerative cycles. In recuperative cycles the gas flows in one direction with steady low and high pressures in the appropriate locations, whereas regenerative cycles operate with oscillating flows and pressures. Currently the most popular option for HTS coils is the use of regenerative cycles [38].

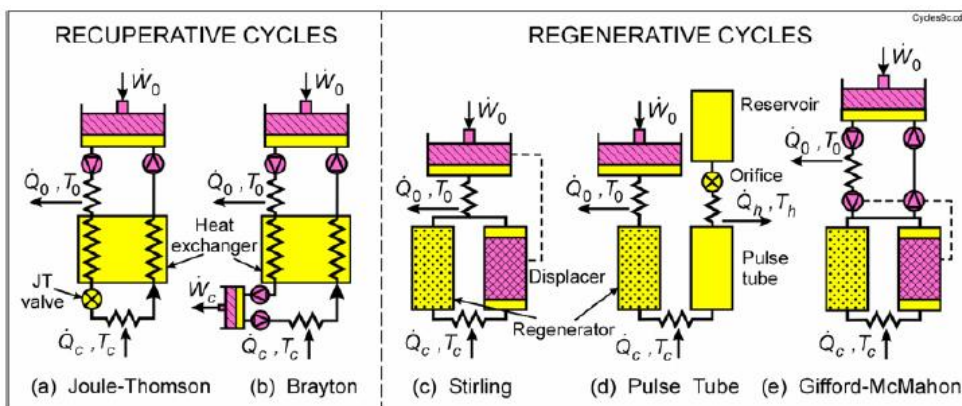


Figure 32 Schematics of the five common types of cryocoolers [63]

I. Recuperative cycles

Both types of recuperative cycles are characterized by steady flow and steady pressure and therefore temperature oscillation and vibration are inherently low. These cycles are analogous to DC electrical systems. High effectiveness heat exchangers are required in both cycles. The cold end can be separated from the compressor by a large distance reducing the electromagnetic interference (EMI) and the vibration associated with the compressor's operation.

The Joule Thomson (JT) cryocoolers consist of a compressor, a counter flow heat exchanger, a JT valve and a reservoir. The expansion occurs with no heat input or production of work and therefore occurs at constant enthalpy [64]. As a consequence a disadvantage of this type of cryocooler operating with pure nitrogen or argon is that very high pressures are required, due to the fact that the JT expansion provides cooling in real gases where enthalpy is a function of pressure. At room temperature both fluids have small pressure dependence

Chapter 3 Superconductivity and its application to rotating machinery

on the enthalpy and as a consequence the JT effect decreases. The use of mixed refrigerants can improve performance [63]. These mixtures usually consist of adding high boiling point components (i.e. ethane, methane). Another disadvantage of the JT cryocooler is the susceptibility to plugging by moisture of the very small orifice. In addition to this, this device has low efficiency when used in a closed cycle mode. Compressor efficiencies are very low when compressing to such high pressures. For temperatures below about 70K the use of a second compressor and a neon or hydrogen working fluid are required. The main advantage of this cryocooler is that there are no moving parts at the cold end and therefore it can be miniaturized resulting in short cooling-down times. The mixed refrigerant cryocoolers have achieved lifetimes of over 10 years [63].

In Brayton cryocoolers cooling occurs as the expanding gas does work. The Brayton cycle is commonly used in large liquefaction plants with the addition of a JT final expansion stage, which is called the Claude cycle. The working fluid used in the turbo-Brayton cryocoolers is usually neon when operating above 35 K, but helium is required for lower temperatures. An advantage of the Brayton cryocooler is the very low vibration associated with rotating parts in a system with turbo expanders and centrifugal compressors [63]. This low vibration is often required with sensitive telescopes in satellite applications, such as with the Hubble telescope. The expansion engine provides for good efficiency over a wide temperature range, although not as high as some Stirling and pulse tube cryocoolers at temperatures above about 50 K. The low-pressure operation of the miniature Brayton systems requires relatively large and expensive heat exchangers. The expansion turbines are also expensive to fabricate, especially in very small sizes [65].

II. Regenerative cycles

As already mentioned these cycles operate with oscillating flows and pressures, analogous to AC electrical systems. The oscillating pressure can be generated with a valve less compressor (Stirling, Pulse tube), or with valves that switch the cold head between high and low pressure source (Gifford McMahon (GM)). In these devices heating occurs as the pressure is increasing and cooling as the pressure is decreasing. The regenerative heat exchanger (regenerator) consists of a matrix of solid porous material through which the gas flows. The matrix must have a high heat capacity, a good contact with the gas and a low flow resistance. These devices are simpler and cheaper than the ones used for the recuperative cycles, even though high performance is always required.

Stirling cryocoolers consist of a piston, a compression space, a displacer, a regenerator and an expansion space. The displacer replaced the cold piston of the early designs. In the PV diagram the ideal cycle is represented by two isotherms and two isochors. The motion of the displacer is synchronized with the motion of the piston (nearly sinusoidal) and typically is 90 degrees out of phase. With this condition the mass flow in the regenerator is approximately in phase with the pressure change [65]. The cycle is reversible and heat is exchanged at two fixed temperatures. The cold piston is rather impractical and so frequently it is substituted by a displacer. The displacer is a solid body that drives the gas from the cold to the hot end and vice versa, in a synchronized motion with the piston and thus requiring ideally no work [64]. Stirling cryocoolers were majorly developed for space applications after the introduction of flexure bearings to support the piston and a displacer to avoid rubbing

Chapter 3 Superconductivity and its application to rotating machinery

contacts. Lifetimes of at least 10 years can be expected. Usually the lifetime of the device exceeds the lifetime of the accompanying electronics [63]. A major disadvantage of this type of cryocooler is that it is inherently subject to vibrations and electromagnetic interference (EMI). Shielding of the cryocoolers and the use of dual opposed pistons has been adopted when coupling this cryocooler to SQUIDs [65]. Although Stirling cryocoolers are more efficient than GM and can provide considerable cooling powers they are bulky and heavy.

The GM cryocooler finds widespread application i.e. in MRI and cryopumping where the working fluid is helium and the pressure in the 10 to 30 bar range [64]. Moreover, they are the most popular option for HTS magnets. The cold head contains a regenerator and a displacer, which are usually combined in one body and is separated from the compressor. This in turn allows the adoption of lower cost commercial compressors also mitigating the vibration problem caused by the operation of the compressor. The varying pressure is obtained by connecting the cold head periodically to the high and low pressure sides of a compressor through a rotating valve which is synchronized with the motion of the displacer. A disadvantage of this type is the inherent irreversibility due to the operation of the valves. However, the cycle frequencies of the compressor and the displacer are uncoupled and as a consequence the swept volume of the compressor can be 50 to 60 times smaller than that of the cooler resulting in a cost reduction by the use of cheap commercial compressors [64]. The use of these cryocoolers in the semiconductor fabrication equipment resulted in intense development which led to improvements in reliability and cost reduction. Maintenance intervals of one to two years are typical for these devices. The adoption of regenerators made with rare earth materials with high heat capacities allowed GM cryocoolers to achieve temperatures up to 4K. These compressors are available in multistage devices allowing the achievement of temperatures as low as 2 K. Usually, a two stage device is sufficient to reach 4K whereas single stage devices could be capable of reaching 20 K. There is large commercial availability of GM cryocoolers [63].

The Pulse tube cryocoolers (PTR) have the constructional advantage that the displacer is a column of gas and not a solid metal. As a consequence PTR's have higher reliability, lower cost, lower vibration and less EMI compared to Stirling cryocoolers. Early PTR's did not reach the efficiency of the Stirling cryocoolers. However, with the insertion of the double inlet and the inertance tube the achievable efficiencies are comparable to the Stirling type, reaching 20% of Carnot at 80 K [63]. Most devices of this type constructed until now have had small cooling capacities i.e. 60 W at 80 K. However, recent advances have raised expectancies that larger capacities i.e. 1 kW might be available in the future. In that case the adoption of PTR's could simplify the cryogenic design and avoid many of the disadvantages of the other options.

3.4.4. Heat transfer mechanism

A description of the cooling system without mentioning the heat transfer mechanism between coils and cryogenic fluid would only give a limited point of view. The real challenges are identified into effectively designing a cooling scheme that would

Chapter 3 Superconductivity and its application to rotating machinery

guarantee an efficient heat transfer and thus that the coil is stably in equilibrium at the desired operating point.

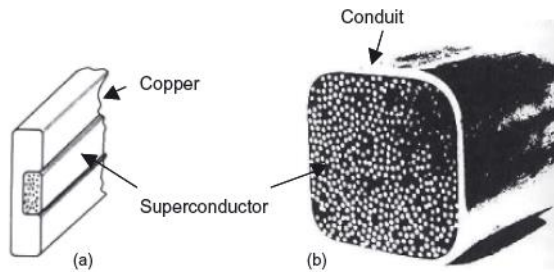


Figure 33 (a) bath cooling conductor (b) cable in conduit [38]

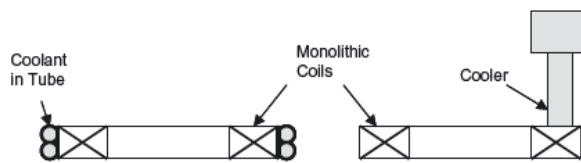


Figure 34 Conduction cooling scheme [38]

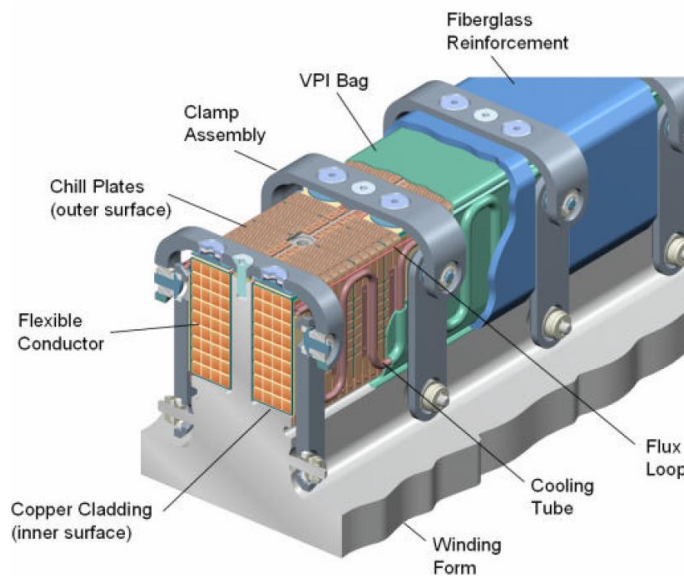


Figure 3-1 - TRC Winding Pack

Figure 35 cable in conduit

The superconducting magnets (LTS and HTS) are cooled using the following techniques [38, 66]:

1. Bath cooling
2. Forced flow cooling
3. Conduction cooling

LTS magnets (NbTi and Nb₃Sn) are generally cooled by submerging them in liquid He (option1). The heat generated in the coils is absorbed by the phase transition of the coolant from liquid to gas and thus employing the latent heat of evaporation. The operating

Chapter 3 Superconductivity and its application to rotating machinery

temperature is guaranteed until the heat flux is less than the He can remove (critical heat flux). The majority of MRI and particle accelerator magnets are cooled in this way. This system is inherently stable since the heat capacity of the cold mass (superconducting strand and volume of liquid cryogen) is very large [36].

Forced flow cooling can be achieved in 2 ways: either both superconductor strands and cooling tubes are contained in a conduit or the cooling tubes are attached in the side of the conduit containing the superconductor strands. This method is more effective and more controlled than option1. Careful design is needed to ensure that no hot spots are generated within the conduit. Mechanical issues are also important due to more materials coming into contact. The thermal contraction properties should be matched in materials that contact each other to avoid stresses.

In option3 the coils are epoxy impregnated to create monolithic structures which are robust and easy to handle. These coils are then cooled from their outside surface by conduction ensuring a good contact. This can be achieved in 2 ways: either coils come to contact with tubes carrying coolant or directly to a cryocooler.

The choice of the heat transfer mechanism greatly influences the mechanical design of the machine. In the design phase apart the correct assessment of the cooling budget a proper mechanical design that ensures the good contact in conduction cooling or enough flow rate and surface contact with the cooling channel in forced cooling is imperative.

3.5 Demonstrators

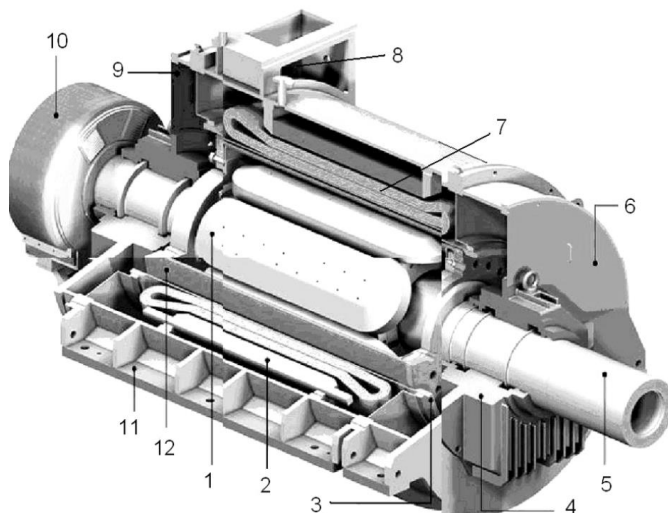


Figure 36 Construction of a 5 MW synchronous motor with 1G BSCCO HTS rotor for ship propulsion. 1 — HTS rotor coil, 2 — stator yoke, 3 — electromechanical shield, 4 — bearing, 5 — drive shaft, 6 — motor enclosure, 7 — stator copper coil, 8 — power terminal box, 9

There are several companies and research groups that have produced some demonstrators to prove the concept in various applications. In the following paragraphs some of the most important achievements will be briefly presented. It is certain that the analysis is not exhaustive as new prototypes from different parts of the world are continuously developed and thus it is impossible to know them all.

Chapter 3 Superconductivity and its application to rotating machinery

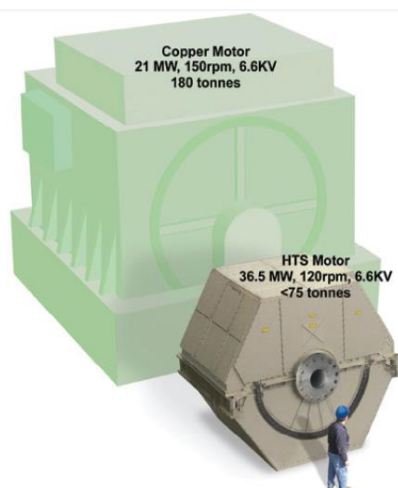


Figure 37 Dimension comparison of the 36.5 MW motor with a conventional 21 MW motor

AMSC has developed the 1G and 2G tapes. The first prototype build by AMSC was a 3 phase 5 MW 230 rpm 6 poles synchronous motor. This motor adopted BSCCO 1G windings, had salient poles, a voltage of 2.4 kV at the terminal and an armature current of 722 A. The copper stator is liquid cooled. This was a critical milestone in the subsequent development of the 36.5 MW motor. The AMSC has designed in collaboration with the U.S. Navy a 9 phase 36.5 MW 120 rpm HTS motor operating at 30 K with a weight of 75 tons. The armature voltage is 6 kV with a rated current of 1270 A and a rated torque of 2.9 MNm. The rotor is an air core rotor design with an oil cooled stator winding which achieves high stator utilization [42].

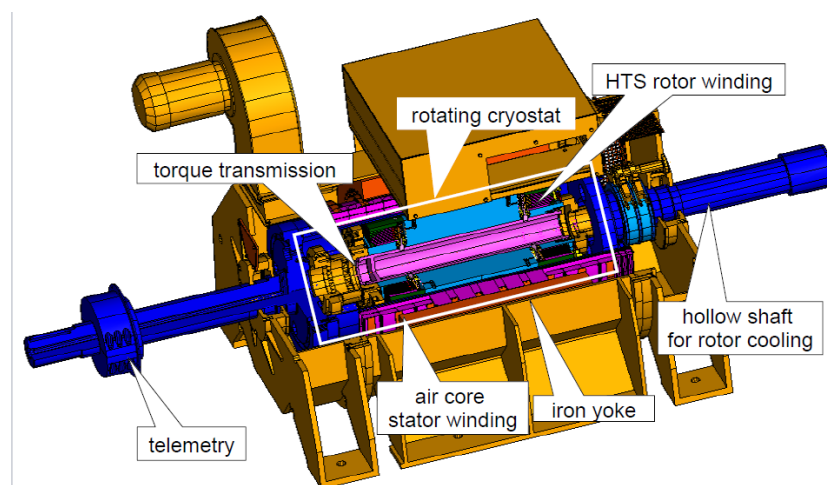


Figure 38 Schematic of the Siemens 400 kW HTS machine

Siemens has been researching superconductor technology in all its possible applications (transformers, cables, machines) since the early 70's with LTS materials and later on with HTS materials. This intense R&D resulted in the first design and testing for 2 years of a 4 pole 400 kVA machine and successively to the design and testing of 4 MVA model. Both models have an operating temperature around 25-30 K.

Chapter 3 Superconductivity and its application to rotating machinery

The 400 kVA model has a nominal torque of 2600 Nm at 1500 rpm with a rated voltage of 400 V. The field windings employ flat pancake coils of BSCCO-223 conductors with Mg reinforced Ag sheath resulting in a peak flux density of 1.1 T at the outside surface of the rotor and 2.5 T within the HTS winding. The cryocooler deployed is a commercial GM cryocooler with Neon and proved itself to be highly reliable after 2.5 years of continuous operation even at high speeds [67]. The efficiency of this model is 96.8% (including cooling) compared to 95.7% for a conventional machine [68].



Figure 39 The Siemens 4 MVA HTS machine

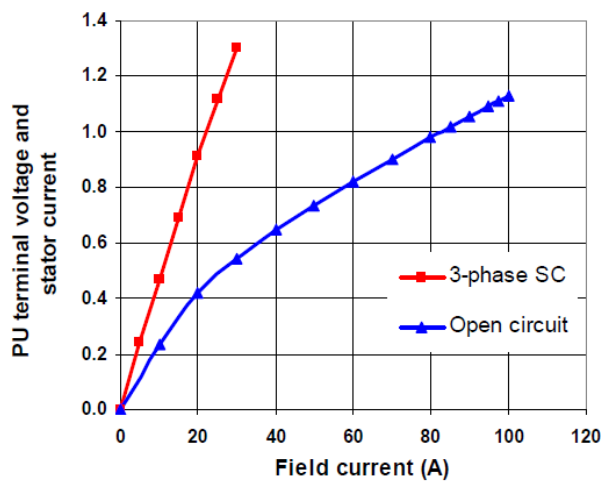


Figure 40 Open circuit and short circuit characteristic of the 4 MVA HTS machine

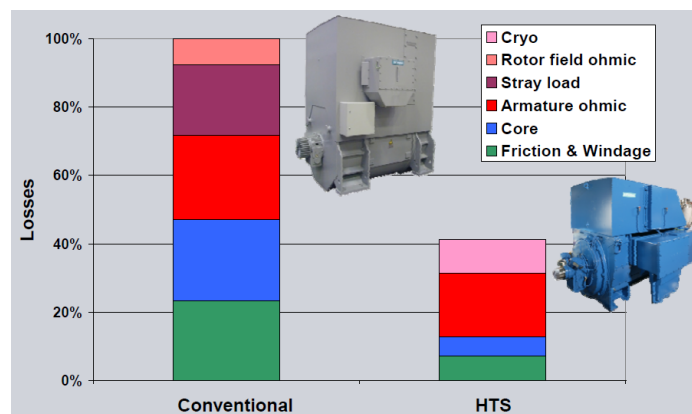


Figure 41 Fractions of losses of the 4 MVA HTS machine and comparison with a corresponding conventional machine

Chapter 3 Superconductivity and its application to rotating machinery

The 2 pole 4 MVA 3600 rpm model has an armature voltage of 6.6 kV with an air core Litz wire winding surrounded by an iron yoke and supported by non-magnetic FRP elements. The rated current is 350 A and the nominal torque is 10.6 kNm. The d axis synchronous reactance is 0.41 pu. The machine has a cold rotor design and demonstrated an efficiency of 98.4% (96.1% conventional machine) at $\cos\phi= 0.8$ and 98.7% (97% conventional machine) at $\cos\phi= 1$ [69]. In figure 42 a comparison between the 4 MVA generator and a Siemens conventional machine of the same power rating can be visualized.

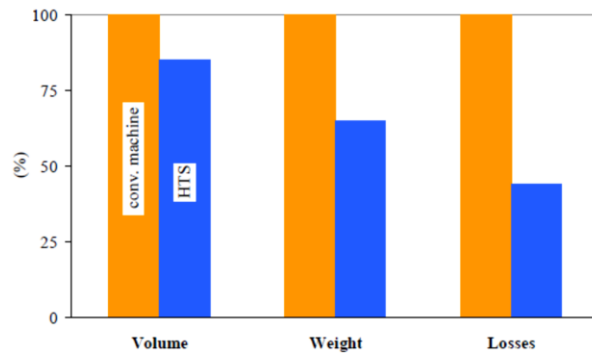


Figure 42 Comparison of volume, weight and losses

Converteam supported from the UK department of trade is leading a consortium that designed and manufactured the Hydrogenie superconductor turbine for the hydro power station in Hirschaid (DE), retrofitting an existing generator and thus keeping the conventional copper armature. The station is scheduled to start operation in the near future. The machine is a 1.789 MVA 214 rpm HTS Hydro generator. The armature voltage is 5.25 kV and the rated torque 80.3 kNm. The design has a warm iron rotor, thus the use of cryogenic steel was not necessary and the amount of cold mass is minimized. The field windings are made of Bi-2223 tapes with an operating temperature of 30 K. The coolant adopted is helium gas in a Stirling type cryocooler [70].



Figure 43 Full rotor assembly of the Hydrogenie generator

General Atomics has constructed a prototype of a 3.7 MW DC homopolar motor for marine propulsion and is planning to develop a 25 MW motor [71]. The 3.7 MW motor has 1m of diameter and 1.8m of axial length. The salient characteristic of this prototype is that it deploys a stationary HTS winding.

Chapter 3 Superconductivity and its application to rotating machinery

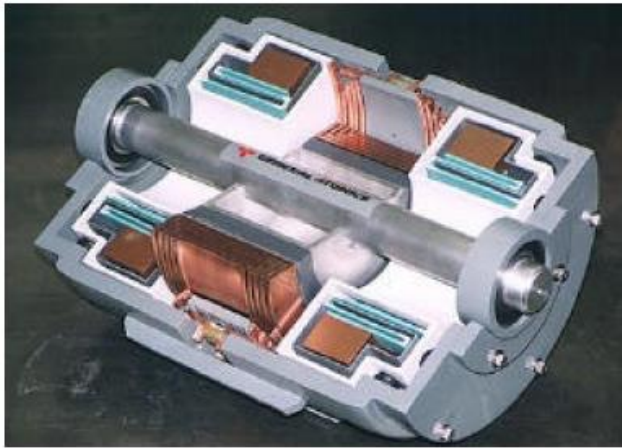


Figure 44 Longitudinal section of HTS DC homopolar motor from General atomics

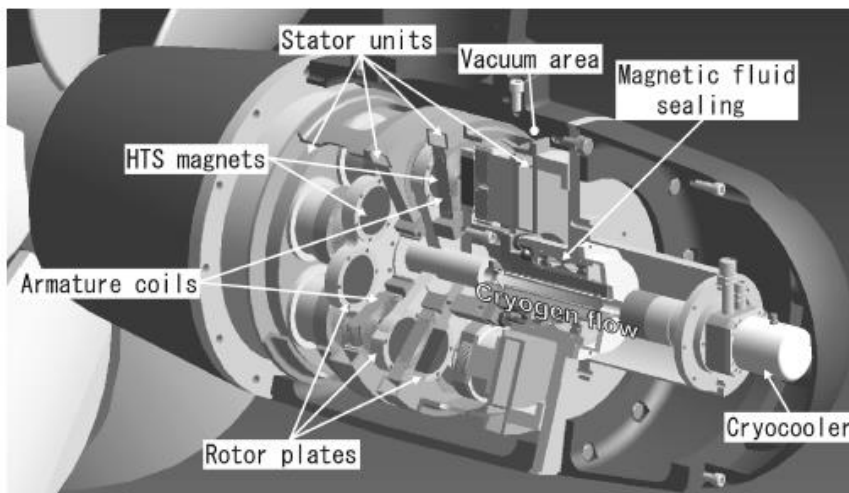


Figure 45 Conceptual diagram of an axial-gap type HTS motor with podded-propulsion system

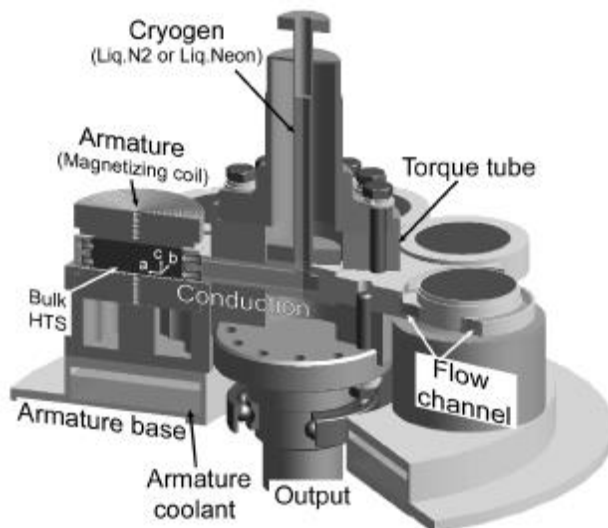


Figure 46 Schematics of the axial flux bulk motor

Chapter 3 Superconductivity and its application to rotating machinery

Axial flux motors for marine propulsion have been developed by a Japanese research group that consists of Tokyo University, Kitano Seiki (Japanese company) and the University of Fukui. In particular two motor types have been developed: one employing bulk material on the rotor and one employing Bi-2223 wire. The first one was designed for the propulsion of small ships (<500 t), while the second one was designed for the MW class of ship propulsion systems.

In Figure 46 the structure of the bulk motor is depicted. The pole field magnets consist of melt – textured $GdBa_2Cu_3O$ bulks that could provide a field over 3T at 77K. This design has 8 pole field bulk magnets on the rotor. The armature coils are vortex type copper windings that perform both the armature coil function and the magnetizing coil function. The armature consists of 6 poles and has no iron. Cooling and magnetization occurs inside the motor. The bulks are cooled by a lateral flow of cryogen and are positioned in such a way to exploit the larger thermal conductivity in the a-b crystallographic plane resulting in a more effective cooling compared to an immersed rotor design and a shorter cooling time [72]. The rotor and stator units are kept in vacuum. The bulk material is magnetized with the pulsed field magnetization method (PFM), which yielded a flux density over 0.6 T on the surface of the armature coil. In order to achieve the PFM the armature windings are vortex type. This coil applies a conical field distribution profile having the maximum flux density along the center of the bulk. During the magnetization process considerable electromagnetic forces develop on the coil (up to 1 kN). In order to protect the coil the mechanical support is carefully designed and is made of glass reinforced plastics [72]. This motor design has no collector rings or current leads to excite the field pole magnets and so provides a high redundancy. Overall the structure is simple, small, light and easy to maintain. The motor was designed for the output of 15 kW at 720 rpm, however in the evaluation test it has been operated with a 3.1 kW output at 720 rpm. A problem encountered in this design is the fact that the pulsed magnetization does not yield a homogeneous and isotropic flux density distribution inside the bulk material, which influences the operating efficiency of the motor [73].

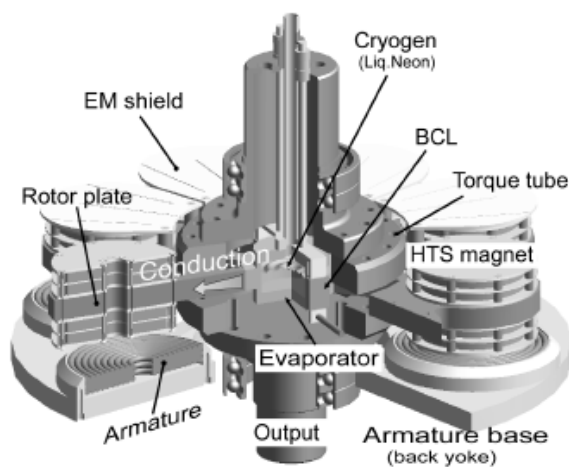


Figure 47 Schematics of the axial flux BiSSCO motor

Chapter 3 Superconductivity and its application to rotating machinery

The motor with BISSCO wire has a similar design apart the fact that it is vertically arranged. This machine has a larger power output due to the higher total magnetic flux. The evaluation test yielded a power output of 100 kW at 230 rpm. The rotor adopts a coreless design. The field pole coils are double pancake coils (DPC). There are 16 DPC's on the rotor forming 8 split type field poles. The windings generated a flux density over 1.4 T with a 200 A DC current. LNe was used as cryogenic fluid operating in a GM cryocooler. In order to enhance performance the concept utilizing bulk materials has been further developed by adding more rotor (twinned rotor) and stator plates, which results in a motor torque increase. The rotor and stator geometry are identical to the previous design. The motor has a rated output of 16 kW at 760 rpm with a maximum trapped field of 0.7 T [72]. Apart the power increase and the power density increase, the main advantage of this motor is that both line and phase voltages have a considerably better waveform [73].

The University of Southampton has constructed a 100 kVA 3000 rpm synchronous generator [74]. In the development process more designs have been made on the same line of thought. All the designs are 3 phase 2 pole 100 kVA 3000 rpm HTS generator with hybrid salient pole rotor and BSCCO tapes operating at liquid nitrogen region. There are cored and air core designs, but both are in cryogenic temperature (the cored design operates in slightly higher temperature whereas the coreless design operates at 64 K) and both deploy flux diverters in order to keep low the flux density perpendicular to the broad face of the tape [75]. In the cored designs the rotor core is constructed with a 9% Ni steel which demonstrates good mechanical and magnetic properties. The rotor winding are made with a 40 turn BiPb2223 flat pancake coils. The stator is conventional [74].

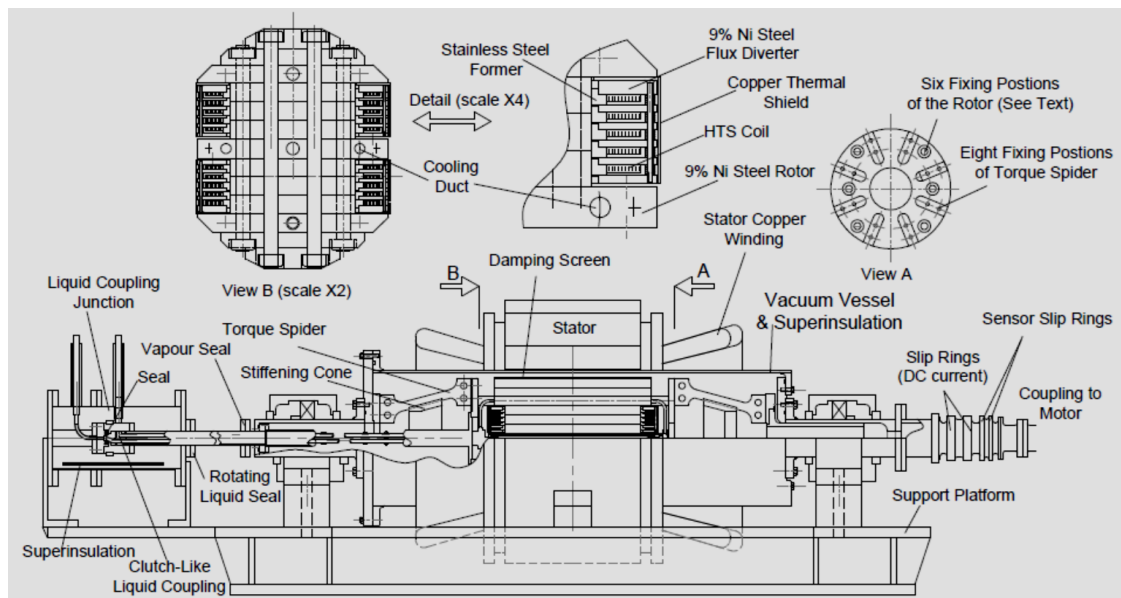


Figure 48 Overview of the Southampton HTS generator

In the coreless design there was first an attempt to completely eliminate the flux diverters, by creating an elimination of the perpendicular component of the flux density by adjacent coils. However, this introduced problems in the end coils and therefore in the latest design flux diverters have been put at the top and bottom of the winding [75]. In figure 50 the two coreless designs are depicted. The difference between them lies in the location and

Chapter 3 Superconductivity and its application to rotating machinery

subsequently at the temperature of the pole pieces. In figure 9 the final rotor design is shown after performing optimization [76]. In Figure 51 is depicted the torque transmitting device (torque tube), which is constructed from fiberglass (G10). The use of flux diverters introduces a fundamental difference in the machine's design: without flux diverters the perpendicular value of the flux density at the tape determines the critical. In contrast when flux diverters are deployed it is the parallel component that determines the required operating temperature [77].

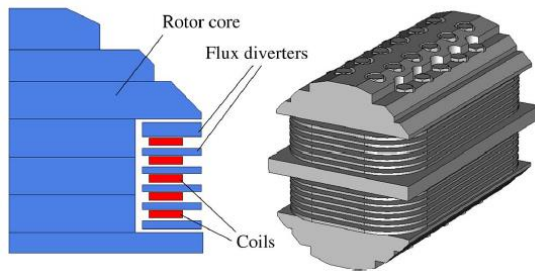


Figure 49 Cross section of the cored rotor

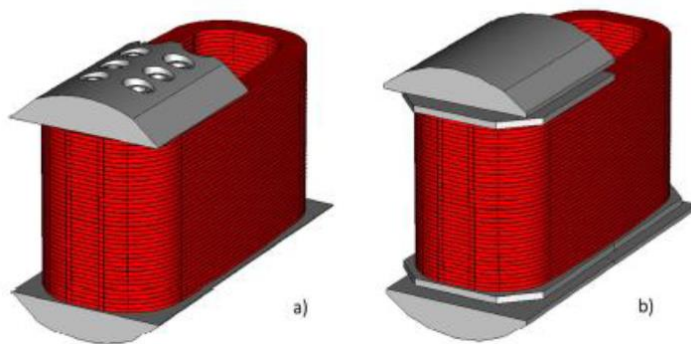


Figure 50 Coreless designs with (a) pole pieces inside (b) outside the cryostat



Figure 51 various parts of the torque tube during assembly

Chapter 3 Superconductivity and its application to rotating machinery

A Russian research group (NII Electromach) has built a prototype of a high voltage 5 MVA 40 kV HTS synchronous generator [42]. The machine has an HTS field excitation winding, stator ferromagnetic core and an airgap stator winding. The rotor support structure is made of non-magnetic steel. The rotor is a rotating cryostat and carries the racetrack coils. The stator (armature) winding consists of multilayer saddle-type concentric coils with advantages in terms of manufacturing assembly and cooling.



Figure 52 5 MVA 40 kV HTS synchronous generator

Other motor prototypes found in the literature survey are:

- A German company has reported the construction of various prototypes of HTS reluctance motors [78].
- A Korean research group has constructed a prototype of an HTS induction motor [79]
- A Japanese research group has also manufactured an HTS induction motor [80]

3.6 Designs of HTS wind turbine generators

Integrating the presented generator topologies in the harsh environment of a wind turbine is not an easy task. Moreover, since the design of HTS superconducting machines is at its relatively early stages, there is no consolidated practice and therefore there is a lot of space for “out of the box” thinking. In this section some of the designs of superconducting wind turbine generators found in the literature will be presented aiming to present them as examples. There are a lot of research groups investigating this field with little published information. For example Advanced Magnet Lab is developing an HTS wind turbine with double helix technology but with barely any in depth description so far. The designs presented here are only the ones that have a rather detailed description.

A 10 MW class wind turbine generator has been proposed in [81] with a diameter of 5m. The design adopts circular field HTS coils and concentrated copper stator windings with both axial and radial airgaps. The machine is designed to operate with a flux density of 10 T

Chapter 3 Superconductivity and its application to rotating machinery

and a field coil current density of 1.68×10^8 A/m² at 20 K. The advantage of using circular coils is that they are easy to wind and manufacture and the magnetic force around the coil is more uniform. The disadvantage is that the design requires long lengths of wires produced and that the support structure is costly and complicated.

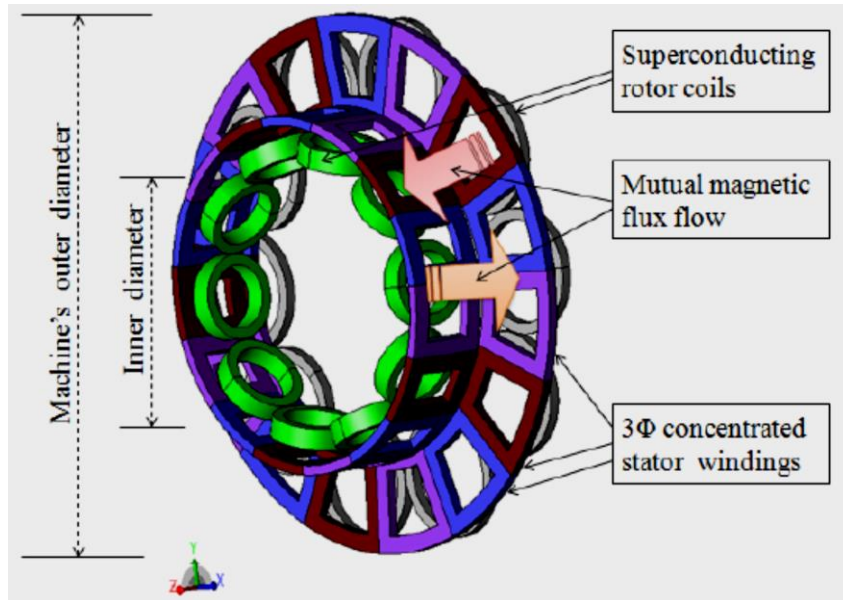


Figure 53 Model structure of a 10-pole wind turbine generator [38]

This design investigates the tradeoffs regarding the adoption or not of back iron. In the air core model the active mass of the generator is 20 tons for a required length of superconducting wire of 1000 km, whereas the back iron model weighs 50 tons for a required length of 750 km of wire. The adoption of back iron has been calculated through FEM that yields a 30% increase in the flux linkage thus reducing the wire requirements.

In [82] the design of a 10 MW fully superconducting generator was proposed. This design adopts BISCCO or YBCO tapes for the DC field winding and MgB₂ wires for the armature. The generator has a diameter of 3.67 m and a length of 1.5 m with a rated rotational speed of 10 rpm. The operating temperature is 20 K and the AC losses have been estimated to be less than 1 kW.

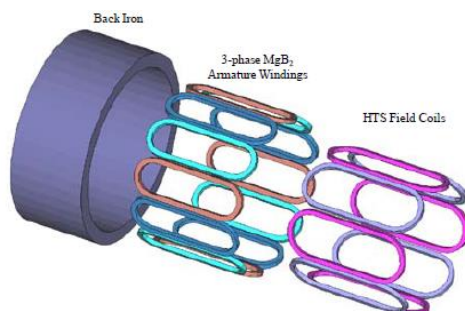


Figure 54 Fully superconducting wind turbine generator

The armature windings have a concentrated winding structure whereas the field coils have a typical for HTS racetrack structure. The armature voltage is 3.3 kV and the line current is 1.7 kA. In that paper three possibilities are investigated for the flux density level at the armature

Chapter 3 Superconductivity and its application to rotating machinery

winding namely 2 T (A), 2.5 T (B) and 3 T (C), which in turn revealed that a 10 MW fully superconducting generator could be possible with a total wire requirement around 500 km.

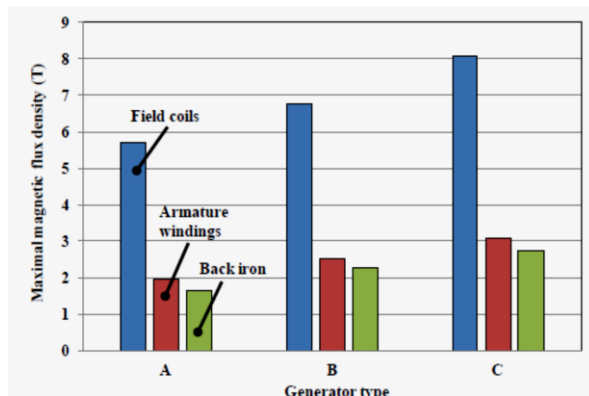


Figure 55 Flux density levels

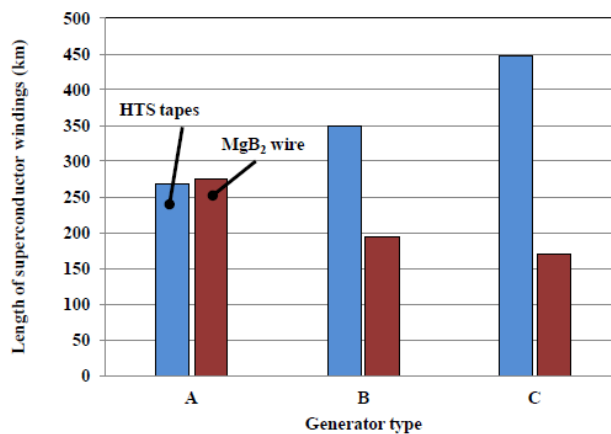


Figure 56 Wire length

In [83] a homopolar generator has been proposed. The superconducting coil is a large circular winding and is fixed to the armature winding. As a consequence, this machine has the advantage that the HTS coils are stationary and experience no torque. This results in a simpler design of the support structure and of the cooling mechanism. The rotor has a varying reluctance structure with many modular C-shaped magnetic core structures which divert the flux and create a varying flux on the armature coils. The gaps in the magnetic core structures could be filled with non-magnetic material to increase the stiffness of the structure.

This topology could potentially have a very high reliability: stationary coil and rather simple construction. On the other hand, the design adopts iron. This results that the weight of the machine is slightly higher than a permanent magnet direct drive of the same power and 40% heavier than the expected weight of an HTS machine. The flux density is in the conventional range around 1.4 T. In order to enhance performance the winding arrangement could be modified to create two opposing magnetic fields and thus have a bipolar generator. Two separate superconducting field windings can be used one attached to the armature coil like the homopolar design (inner) and one fixed to a back iron that diverts flux. Both windings carry DC current at the same direction.

Chapter 3 Superconductivity and its application to rotating machinery

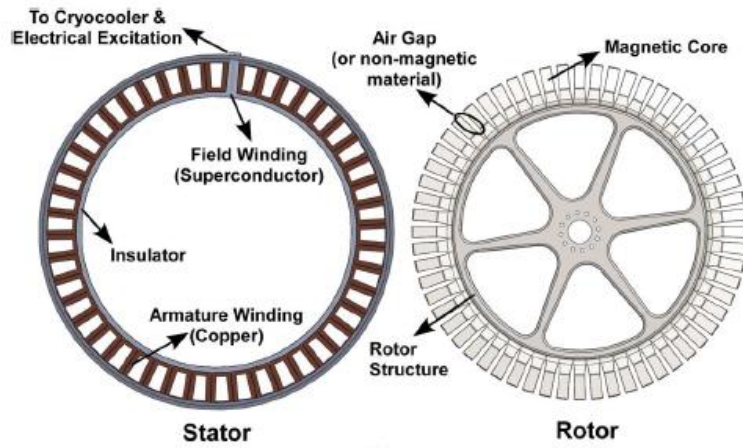


Figure 57 Stator and rotor components

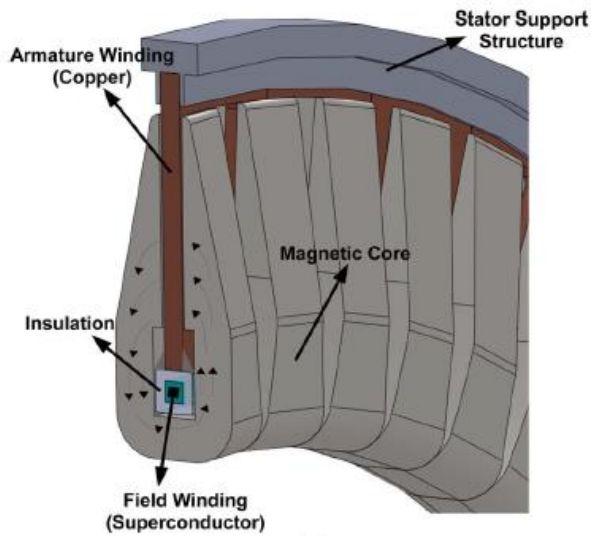


Figure 58 cut through view

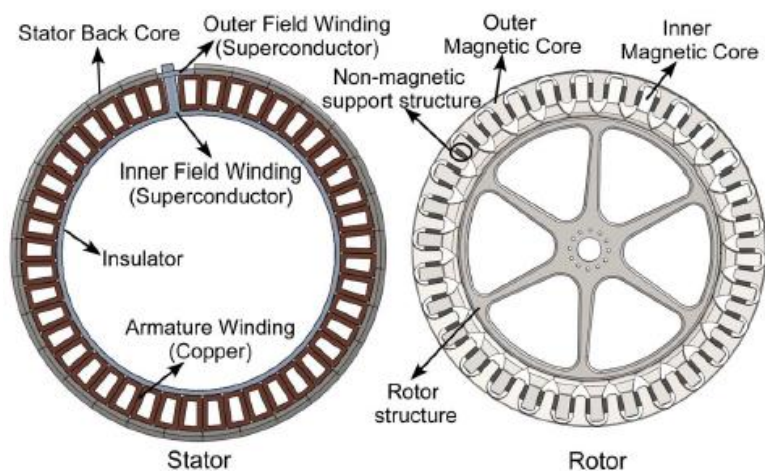


Figure 59 Stator and rotor components

Chapter 3 Superconductivity and its application to rotating machinery

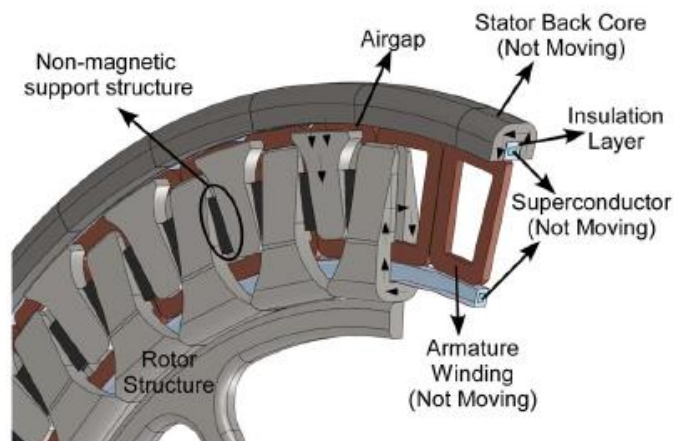


Figure 60 cut through view

The magnetic flux created by the two coils is carried through rotating inner and outer magnetic cores linking it with the armature windings. The proposed design of the bipolar generator is a 6 MW 12 rpm generator with a rated torque 4.7 MNm. The machine has a diameter of 12 m with a mass of 134 tons. The biggest advantage of this generator is that it only requires 43 km of superconducting wire and therefore is potentially a very low cost generator.

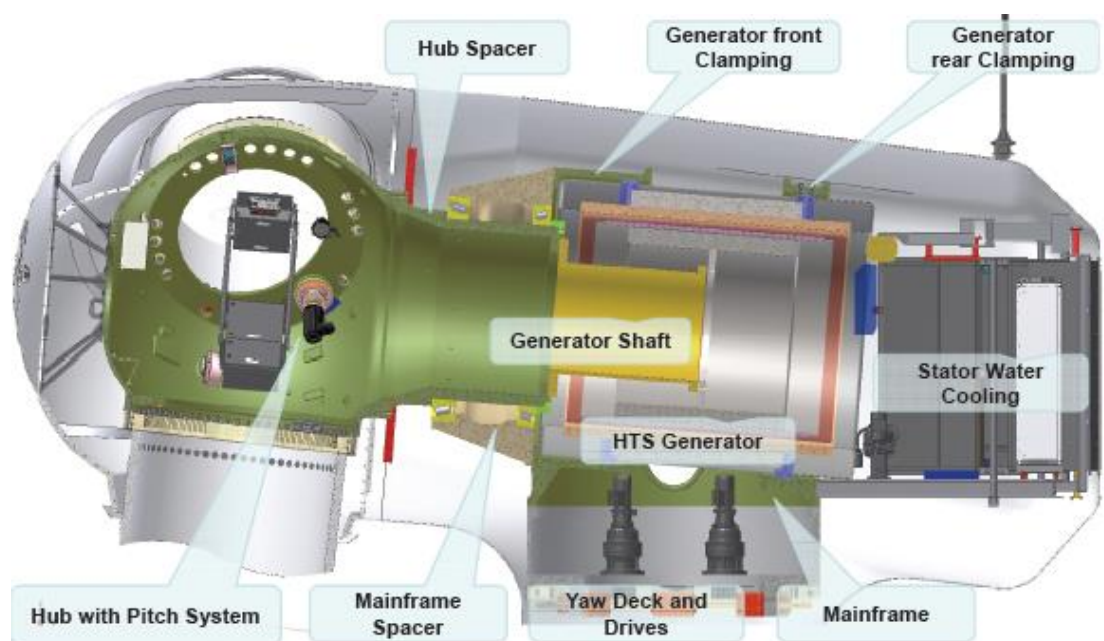


Figure 61 AMSC Sea Titan concept

AMSC under its subsidiary Windtec GmbH is developing wind turbine concepts with HTS generators like the sea Titan which is a 10 MW 10 RPM with 94% efficiency (including the converter) and a rotor diameter 190 m. The generator diameter is 4.5 m with 4 m axial length. This is an aircore generator with a large mechanical airgap (2 cm). The electromagnetic airgap due to the absence of iron is higher. The estimated size and weight of this device are sensibly lower than conventional concepts. The top mass is estimated less than 500 tons instead of around 850 tons for a direct drive and 750 tons for a geared turbine of the same power rating [84].

Chapter 3 Superconductivity and its application to rotating machinery

Converteam has also developed an HTS wind turbine direct drive generator conceptual design. It consists of a superconducting generator with an air gap stator winding and an HTS rotor with non-magnetic pole bodies [85]. The machine is an 8 MW 12 rpm generator intended for use with a turbine having a diameter of 160 m and a shaft torque of 6.5 MNm. The HTS generator itself has a diameter of 5 m and a length of 2 m with a weight of approximately 100 t [86]. This generator is intended to operate with YBCO 2G coils which are expected to become competitive in terms of cost within 5 to 10 years [87].

A 10 MW direct drive wind turbine HTS generator study utilizing both coils and bulk materials has been reported by the University of Tokyo [88]. The arc shaped bulk superconductors are used to create magnetic shielding for the HTS coils. The stator is made of copper and the rotor has a coreless structure. In figure is depicted the rotor structure, which consists of 7 superconducting coils of 7 m diameter. The axial length is 1.82 m. The current density is 290 MA/m².

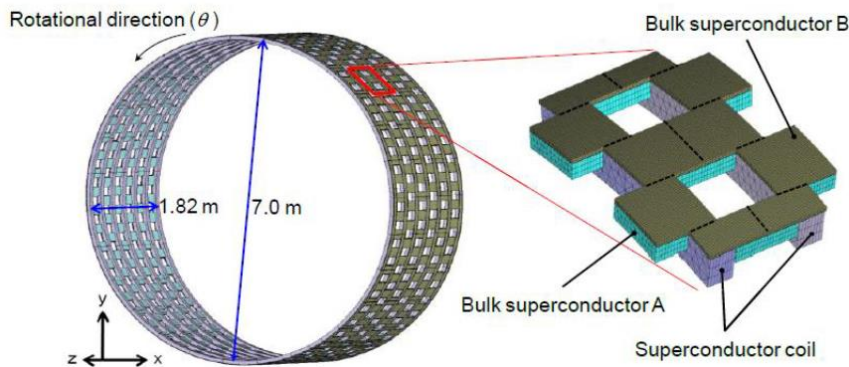


Figure 62 Rotor structure

The principle is that adjacent coils carry opposite current and so a cusp-shaped magnetic field is generated. The bulk superconductors shield the magnetic field generated by the HTS coils and generate a stronger and a weaker part alternately in the rotating direction around a set of bulk superconductors. In figure this principle is illustrated for a configuration of 8 poles. There are 2 types of bulk material in the structure: one that produces field modulation in the rotational direction (A) and those who reduce the leakage flux (B). The generated magnetic field has 110 poles. The maximum flux density on the coil is reported to be 12 T. The operating temperature is around 20 K. Because the bulk material is well capable of steering the field the resulting perpendicular field on the HTS windings of the coils can be decreased. As a result the coils can produce the high fields of more than 10 Tesla. The downside of this method is that a rather large amount of bulk material is needed and has to be cooled in conjunction with the HTS coils. Also taking into account the increased weight of the bulk material and the increased thermal mass (resulting in a longer cooldown time), this topology might be too expensive.

With the same principle of operation other designs have been reported. In particular, there is a design which has 12 superconducting field coils generating a 12-pole magnetic field and is intended for application to direct drive wind turbines [89]. The rotational speed is 10 rpm and the operating temperature is 20 K. The maximum flux density at the face of the coil is lower than 10 T. In figure 64 the structure of this design is depicted.

Chapter 3 Superconductivity and its application to rotating machinery

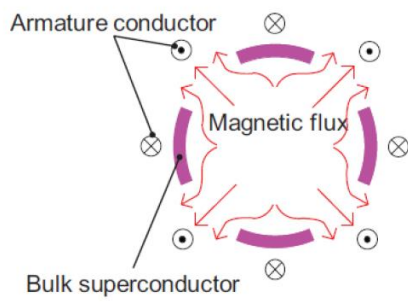


Figure 63 Magnetic flux lines in the cross section perpendicular to the rotation axis

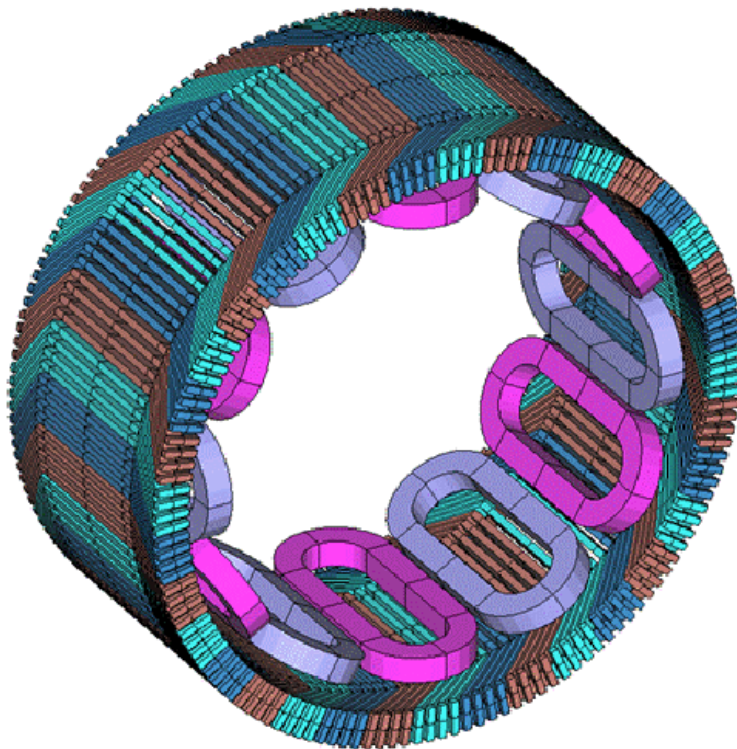


Figure 64 Armature and field coils of the 12 pole generator

Chapter 4 Rough Design of a 10 MW HTS wind turbine generator

4.1 Introduction

The design of a fully superconducting machine differs in many aspects from the design of a conventional machine. Firstly, the omission of iron and the large effective airgap means that the traditional computational methods are inadequate: the flux density cannot be assumed to cross the airgap perpendicularly and thus does not only consist of a radial component. The division between mutual and leakage flux is not easily identifiable like in conventional machines. In conventional machines the main flux is the one that crosses the airgap, whereas the leakage flux consists of the one linking the iron teeth and of the end leakage. In air-core machines there are no teeth and the field is two dimensional with the simplifying assumptions.

The adoption of the air-core topology has some consequences. The windings are experiencing torque and significant Lorentz forces due to the high field and high current densities. The machine has inherently low synchronous reactance. This on the one hand gives a stiff operational behavior and on the other hand means that fault situations will give rise to forces and currents of larger magnitude which increments the support structure requirements. Iron also acted as a heat sink for the windings.

The fact that the machine operates at cryogenic temperatures sets limitations on the suitable materials. The construction materials should guarantee strength and endurance in thermal stresses and should provide support for the windings. At the same time the heat leakage through the materials should be minimized. The insulation should withstand the low operating temperature and the stress that arise from thermal contraction of different materials in the insulating wire. HTS wires are not typically sold as insulated products and depending on the technique used to produce the wire there are restrictions on the suitable materials.

As it emerges there are a large number of often conflicting parameters to be taken into consideration and the detailed design of such a machine goes well beyond the scope of this thesis. The objective of this chapter is to provide an insight in the basic design options and present a rough design of a 10 MW HTS wind turbine generator. The structure of the chapter is as follows. In section 4.2 some basic parameters for a 10 MW wind turbine are discussed and the speed range of the generator is defined. In section 4.3 the HTS generator concept is illustrated. In section 4.4 the winding design is presented. In section 4.5 the electromagnetic design of the generator is given and successively in 4.6 the losses are evaluated. In section 4.7 the estimations about the cooling system and the torque tube exposed. Finally in section 4.8 the summary of the calculated generator parameters is given.

Chapter 4 Rough Design of a 10 MW HTS wind turbine generator

4.2 A 10 MW wind turbine

In this section some basic calculations are presented in order to make an assessment of the rotational speed range of the generator. It is known that many of the parameters that are mentioned here in order to be properly set a larger study of aerodynamic and structural aspects is needed. This is out of the scope of this thesis and therefore basic rough calculations are done.

The electrical power output of a direct drive wind turbine is given by:

$$P = \frac{1}{2} \rho V_{wind}^3 \pi R^2 C_p \eta_g \eta_c \quad (1)$$

Where: ρ is the density of air, V_{wind} is the wind velocity at hub height, R is the rotor radius, C_p is the power coefficient of the turbine, η_g is the generator efficiency and η_c is the converter efficiency.

For large modern wind turbines the value of $C_p = 0.52$ is achievable [90]. The generator efficiency for the sake of this calculation can be assumed to be 94%. The efficiency of multilevel converter for a 10 MW wind turbine can be assumed to be 99% [91]. Assuming that the rated wind speed of the turbine is 12 m/s then in order to produce 10 MW of rated electrical power a rotor of approximately 80 m radius is required.

The tip speed ratio is defined as:

$$\lambda = \frac{\omega * R}{V_{wind}} \quad (2)$$

Where ω is the angular velocity of the turbine. The trend in offshore turbines is to increment the tip speed with respect to onshore turbines but not too much due to excessive loading. It is assumed that the tip speed is kept at a maximum of 90 m/s. Assuming that the tip speed ratio is 7.5 and that the cut in wind speed is 4 m/s this yields a rotational speed range from 3.6 to 10.7 RPM. It is very likely that these values could change after making tradeoffs with mechanical aspects. However, as already mentioned this is not subject of this thesis and therefore these are the values that will be further assumed.

In many designs for future direct drive wind turbines like for example Alstom Heliade, it is claimed that the coupling of the direct drive generator to the rotor occurs through a structure that transmits pure torque at the generator and transmits the wind loads to the support structure. Since this concept has been claimed also in other drive train configurations it is assumed that it is technically possible and that the proposed turbine concept adopts this system. Thus, the generator's support structure has to be designed only to withstand the transmitted torque. Naturally this is not the only source of loading since the coils experience significant Lorentz forces.

4.3 HTS generator concept

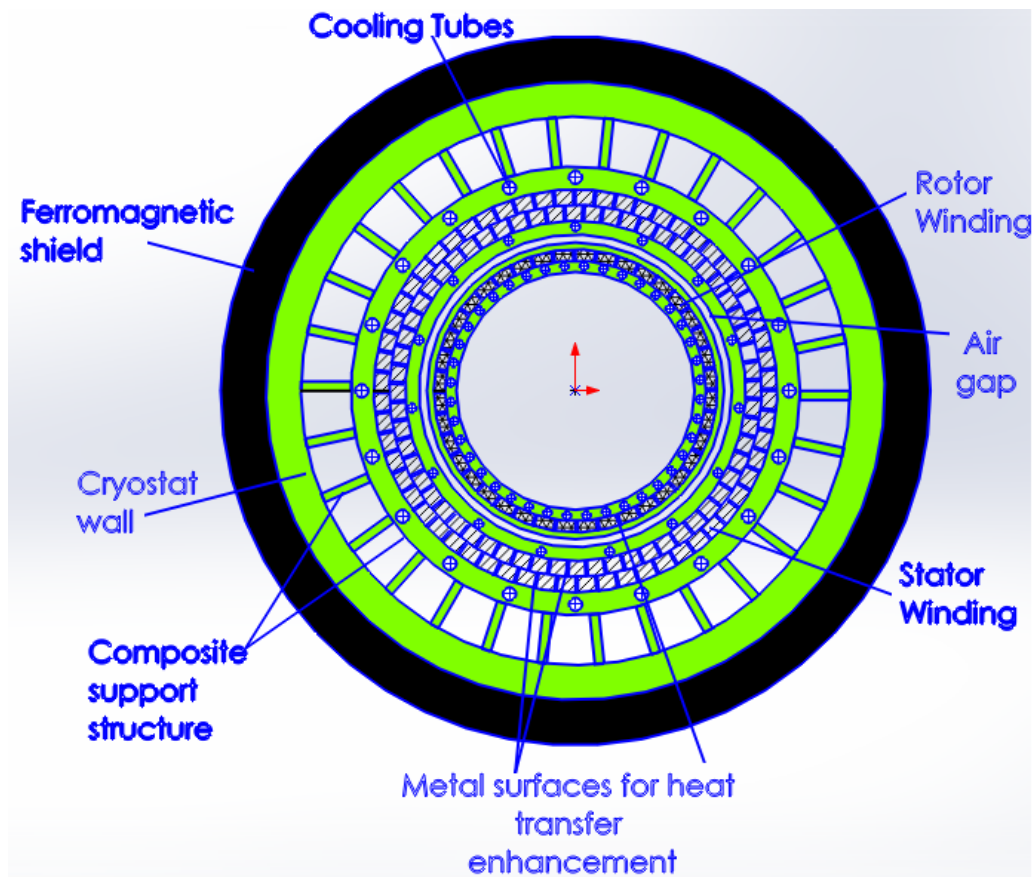


Figure 65 MgB_2 fully superconducting generator concept cross sectional view

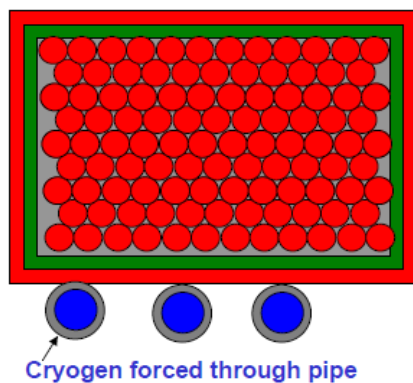


Figure 66 Adiabatic winding concept [92]

The general outline of the generator is a fully superconducting machine with a non-magnetic rotor body housed in a single cryostat with an environmental shield that encloses the generator and eventually an electromagnetic shield (EM) for protection of the rotor coils. Stator and rotor coils are both supported by a composite support structure. The major driver for the choice of composite material is weight. As heat transfer mechanism the proposed design adopts the adiabatic forced flow winding concept [36],[92]. The winding operates under high quality vacuum and is globally conduction cooled by the circulation of cryogen in

Chapter 4 Rough Design of a 10 MW HTS wind turbine generator

pipes. The pipes are in contact with a metal surface that acts as a heat sink. In order to enhance the thermal conductivity within the winding a substance is added in the winding making it almost a monolithic structure.

The choice regarding the adoption of the EM shield has a significant impact on the design. The EM has primarily the functionality to protect the rotor coils from AC fields and to damp the transient oscillations. The EM is made from a conductive material (copper or aluminum) and should be able to withstand the significant forces developed during faults. The two mentioned materials might not be able to bear such loads and oversizing could introduce problems to the damping torque [38]. For this reason the solution usually adopted is to either reinforce the conductive material layer with a stainless steel support or with a composite support.

MgB₂ is a low AC loss HTS and thus the question that arises is whether the use of the shield is necessary. For the damping function, since the generator is operated coupled to a full converter (required for variable speed operation) it can be provided by this device. As a consequence the shield would only have the role of protecting the windings. Without the shield the effective airgap is reduced, the coupling is enhanced and the amount of ampere turns required for the same flux density at the stator winding mean radius minimized. With a single cryostat there would be no thermal function for the shield. Thus aiming at a low weight generator the EM shield is not adopted in the design.

The environmental shield is included in the design. The function of this shield is to enclose the generator's field and generally to provide mechanical support to the stator, whereas in the proposed design it would provide support to the cryostat. It can be ferromagnetic or conductive. In the first case it will be from laminated iron. The disadvantage is that it is heavy, although it attenuates well both AC and DC fields outside the machine, enhances the field in the machine and provides a stiff support structure. A conductive shield is a lighter option although it is not the preferable one. This is due to the incomplete attenuation provided (only AC fields) and to the fact that cannot be located in close proximity to the armature to avoid excessive losses and its demagnetizing effect [38]. As a consequence the volume of the machine is increased. The ferromagnetic environmental shield is assumed to operate at room temperature in order to reduce the cold mass and avoid the use of more expensive material

The power rating is 10 MW. The phase RMS voltage is set to 10kV. As a consequence the steady state RMS rated phase current is approximately 340 A. It will be assumed that this current is applied from a full converter to the armature, as it is the usual scheme of connection of variable speed direct drive wind turbines. The flux density level of the generator at the stator winding radius could be set at a much higher value respect to conventional machines. Fields of 3-4 T at 20 K are technically possible for recent 2nd generation MgB₂ wire. However, this is at the expense of a lower current density with subsequently more wire needed to produce a given magnetomotive force (mmf). With a more conservative approach the aimed peak flux density is set to 2 T at the stator winding radius. The corresponding field in the rotor winding area is not calculated due to the

Chapter 4 Rough Design of a 10 MW HTS wind turbine generator

analytical electromagnetic model adopted. For the calculations are used the values of J_c corresponding to 3 T.

The operating temperature is fixed to 20 K in order to obtain satisfactory performance of the wires. The performance could be enhanced by lowering the temperature, but at the expense of higher costs for the cooling system and the use of less efficient devices that make the cooling system heavier and bulkier. This temperature has the consequence that the thickness of the cryostat will be approximately $t_{cr}=100$ mm [93].

The number of pole pairs is set to be $p=10$. The motivation for this choice is that as reported in [93], this number of pole pairs decreases the harmonic content in the winding. Moreover, as reported in [94] a 20 pole machine is desirable because it yields a better efficiency and weight compared to machines with lower pole pairs and less wire consumption compared to machines with a higher number of pole pairs.

The HTS armature winding experiences AC fields and thus produces losses. MgB_2 is a low AC loss superconductor. Nevertheless, this is true for low frequencies i.e. 1-2 Hz. As calculated in section 4.1 the turbine's speed range is expected to be from 3.6 to 10.7 RPM. Since this is a direct drive machine with $p=10$ the electrical frequency range of the generator is set to be from 0.59 to 1.8 Hz. At this point it should be stated that such a low frequency could provoke problems to the converter's operation through additional thermal cycling (thermal constant of the converter lower than the frequency). However, this issue is a subject that has to be taken into account further in the design process of the electrical system of the wind turbine and thus for the purpose of this thesis is not considered.

The stability of the generator is not studied. Quench protection is a complex task that requires an in depth analysis. As a general comment it can be said that the superconducting armature will act as a fault current limiter in case of faults. Naturally this ensures the mechanical integrity of the generator, but not the stator HTS coils. In LTS machines voltage detection schemes are used to detect the quench voltage and once discovered heating of the coils is used to propagate the quench energy in a larger volume. In HTS the situation is not critical as in LTS and therefore a fault current limiter in series with the armature or a connection with a SMES could guarantee the integrity of the armature.

The current reaches the HTS coils through current leads that are made with normal conductor or with HTS. The design of the leads is not done in this thesis. It is assumed that HTS leads are used. For the rotor excitation there are a couple of schemes reported in [118].

4.4 Winding design

4.4.1. Wire adopted

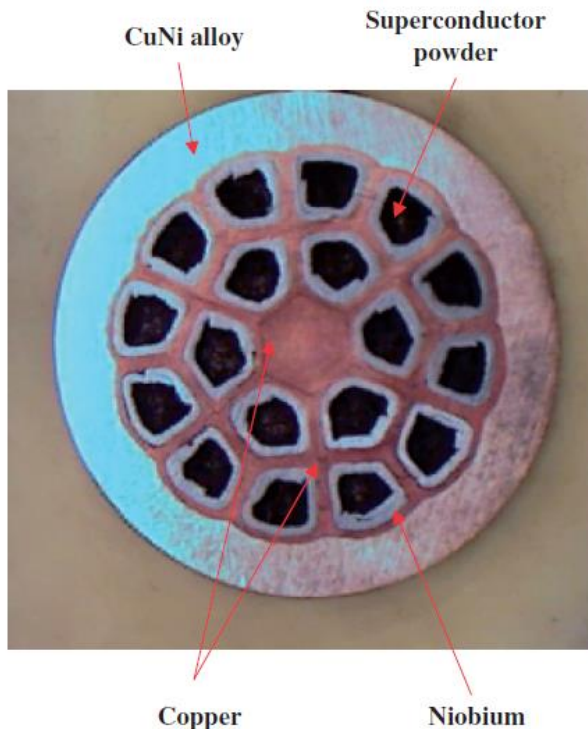


Figure 67 18 filament Hypertech wire cross section [95]

The material that has been chosen is MgB_2 due to the fact that currently seems the only viable HTS for AC use. In particular the reference products for this thesis are the Hypertech wires. As already mentioned in chapter 3 superconducting wires do not only contain superconductor material. The addition of a matrix material is necessary for the stabilization of the superconductor and its protection from undesired phenomena like the flux jump. In LTS wires copper is used as stabilizer. For MgB_2 wires initially a ferromagnetic matrix was used due to reaction of copper and MgB_2 during the heat treatment of the wire at $650\text{ }^\circ\text{C}$ for the formation of the compound [50]. In order to avoid this problem and use copper as stabilizer due to its better properties a barrier sheath is used around the superconducting filament which is usually made of niobium, but could also be from nickel, iron or titanium [95]. In a similar way copper is used as matrix material contained in another high resistivity sheath in order to reduce the eddy currents in the matrix. This sheath is usually made from monel or a copper nickel alloy or glicop (copper based with the addition of aluminum oxide particles).

The addition of copper enhances the thermal conductivity and electrical resistivity in normal state, provides another current path when the wire experiences the transition from the superconducting state and enhances mechanical strength. The amount of copper added in the wire is directly linked with the minimum propagation zone. In [96] Wilson has calculated the extension of this zone in terms of the heat generated in the superconductor after a quench event and the heat removal. From these formulas emerges the dependence

Chapter 4 Rough Design of a 10 MW HTS wind turbine generator

of the extension of the zone to the amount of copper added in the wire. However, there are also other conflicting tradeoffs that should be studied because an effect from the massive addition of copper is to have a lower engineering current density and an increase in eddy current losses. As a consequence it is clear that the exact amount of copper added to the wire is subject of a more in depth study regarding stability linking electromagnetic and heat transfer properties that goes beyond the scope of this thesis.

Hypertech MgB₂ wires usually contain a superconducting material fraction from 13% to >25% depending on the mentioned stability considerations and the application for which the coil is intended to be used [97]. For the calculations in this chapter it is assumed that the superconducting fraction is 25% in order to have a reasonable engineering current density (when also considering insulation) but also some stability margin from the amount of copper added. The reference product for the performance is the 2nd generation MgB₂ wire with a performance curve as given in chapter 3. These results as mentioned in chapter 3 are recent and refer to a short sample. However, the company expects to produce it at the same standards as 1st generation wire within 2 years and therefore it will be assumed that this wire has reached these standards.

Hypertech is able to deliver a variety of shapes (circular, rectangular) and filament counts (up to 61 in a round Nb/Cu/Monel composite wire). The number of filaments and the filament diameter influence the AC losses, the mechanical performance of the coil and the stability. For the stator calculations, the maximum currently available cross section from the Hypertech brochure is assumed (2 mm diameter) with the maximum filament count (61) in order to minimize AC losses. For the rotor a larger cross section is assumed to increase the available transport current. Even if this is not clearly indicated in the brochure the company mentioned that it could be possible to have larger cross sections. 61 filaments are always assumed because due to the absence of an electromagnetic shield the rotor coils experience the armature reaction flux. It is very likely that more in depth studies will change the mentioned assumptions, because for example it could be that a lower filament wire is more economical for the rotor. However, in this thesis issues like current sharing between filaments, exact magnetic field in the winding zone and variation of the critical current density in the wire cross section are not studied and therefore the mentioned assumptions seem rational.

The superconducting wire requires insulation. The amount of insulation needed is determined by fault conditions and transients (thermal and electromagnetic) in the superconductor. A factor that lies in the basis for the choice of the insulating material is the way the winding is produced that is in a “wind and react” or a “react and wind” approach (alternatively called in situ and ex situ). When the first way is adopted insulation is added before the heat treatment at 650°C. This immediately restricts the choice. Hypertech in this type of coils applies S-glass braid or sol gel insulation [97] with the former showing better performance. In case react and wind is used then the insulating material may be different, but extra care is required in handling the wire. The in situ way is preferred due to its simplicity in fabrication, lower reaction temperatures and ease of addition of dopants in the wire. However, the ex situ way may offer a product that could be insulated more properly for a particular application and offers a wider range of high quality insulators.

Chapter 4 Rough Design of a 10 MW HTS wind turbine generator

Insulation at cryogenic temperatures is not a straight forward issue. LTS materials are typically sold as an insulated product, whereas for HTS there is no consolidated practice. Generally superconducting coils require turn to turn and layer to layer insulation. This means that the mechanical and the thermal properties of the composite structure of the insulated wire are highly anisotropic in all 3 directions [98]. Insulation is subjected to a number of different forces (shear, compression, tension and combinations of these) arising from both the magnetic and thermal loading. Thermal stresses arise as a result of the differences in expansion/contraction coefficients and local stresses arise at orthogonal interfaces even between materials with similar properties [98]. As a consequence it is clear that for the choice of insulation these parameters should be studied thoroughly.

As already mentioned the level of the insulation in superconducting machines is decided by transient events. During normal operation no significant voltage drop is present at the wire (in reality due to the non-sharp transition from superconducting to normal a small value is always present). In superconducting coils with a large amount of turns and thus high inductance, considerable voltage may arise during charging and discharging. Therefore in the determination of the insulation level a detailed study is needed regarding the expected events and the subsequent probability of appearance of a certain voltage level. In [99] it is proposed a systematic approach on the determination of the insulation level in LTS magnets. Such a study goes beyond this thesis and requires detailed calculation of the quench voltage taking into account all the operating conditions.

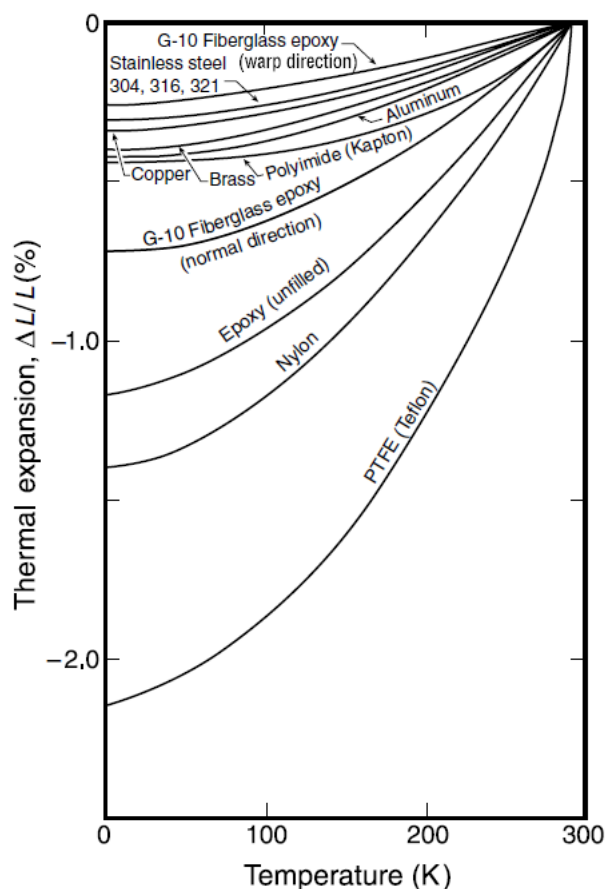


Figure 68 Thermal expansion coefficients of some materials

Chapter 4 Rough Design of a 10 MW HTS wind turbine generator

There have been investigations in the literature about HTS coils without turn to turn insulation [100], [101]. In these coils alternative current paths from layer to layer ensure the safe passage of fault current. The results are claimed to be satisfactory, but always refer to coils with small radii and rather low current i.e. I_c in the order of 100 A. In case this technique proves itself in a wider context it will bring significant advantages and cost reduction. However, in order to make such an assumption a more in depth study is required. Therefore with a conservative approach it is assumed that the coils necessitate insulation.

As already mentioned an important parameter is the thermal contraction of the materials. This can be a source of failures and quenches. Figure 68 depicts the thermal contraction coefficients for various materials. As it can be seen Kapton is one of the few polymers to have a similar thermal contraction/expansion as metals [102]. Therefore this choice ensures that there will be no major issues in this topic. In addition to this Kapton has excellent dielectric properties and an extraordinary high thermal conductivity for a polymer [103]. Kapton comes with an adhesive tape which ensures good contact with the conductor. Most probably the stator wire insulation is more stressed than the rotor and therefore a different choice might be better in terms of costs and performance. However, it is assumed that both stator and rotor wire is insulated with a layer of 0.5 mm thick of Kapton tape for ease of calculation and for lack of data that could prove another option is better. There are Kapton tapes that have AC dielectric strength of 236 kV/mm at room temperature. At cryogenic temperatures this value might change significantly but should remain at a safe level.

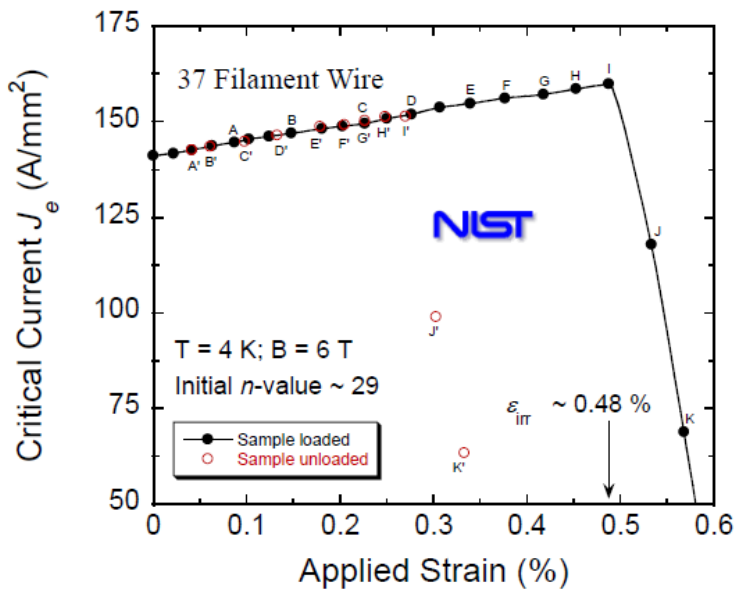


Figure 69 Hyperech 0.8 diameter 37 filament wire strain limit [47]

On the downside for the choice of Kapton comes that it can “only” survive till 400°C thus making it inappropriate for “wind and react” wire. As a consequence the “react and wind” technique is adopted. The handling of this reacted wire requires extra care (i.e. in the process of winding the coil). MgB₂ wires are brittle and suffer severe I_c degradation beyond a strain limit. Figure 69 depicts the dependence of the performance to the strain applied and

Chapter 4 Rough Design of a 10 MW HTS wind turbine generator

the strain limit for a reacted 0.8 mm diameter 37 filament MgB₂ Hypertech wire. The strain is defined as [104]:

$$\varepsilon\% = \frac{R_s}{R_c}(100) \quad (3)$$

With R_s strand radius and R_c coil radius respectively. This formula hides an underlying truth regarding the factors that affect this property. It is correct to use it in order to determine the minimum bending radius. However, in the formula it is used the strand diameter whereas the filament diameter plays a major role. More precisely the increment of the number of filaments and the subsequent decrease in the filament diameter increments the strain limit and thus the minimum bending diameter. For the same cross section the 7 filament wire has 0.37% of strain limit whereas for 19 filaments it is 0.4 % and for 37 filaments 0.48% [47]. The information for the 61 filaments is not available. What is certain is that MgB₂ will never achieve the performance of NbTi which is a pretty ductile conductor able to sustain almost 0.7-1% strain. Therefore the ultimate achievable strain limit for MgB₂ can be expected to be much lower. Although only 3 points are available and therefore this is not a very safe estimation method a linear polynomial fit in Matlab has indicated that for 61 filaments this value could be around 0.55%. As a consequence the minimum bending radius for a 2 mm diameter wire is around 18 cm and for a 3 mm wire is 27 cm.

As already mentioned the adopted heat transfer mechanism concept refers to adiabatic forced flow windings. In order to ensure that the winding operates under a uniform temperature profile and in order to enhance mechanical strength the coil should be impregnated with an agent who is:

- a good thermal conductor
- adheres well to both the polyimide and the metal
- is mechanically strong
- is electrically insulating
- has similar thermal contraction and expansion to the other materials

Tests have shown that the best results were obtained by using a wet-winding process with an epoxy filled with a high content of alumina (Stycast 2850) [105]. As a consequence this material is assumed for the coil impregnation in both stator and rotor.

For both rotor and stator the usual (for superconducting magnets) racetrack geometry is used. The racetrack coil width defines the number of layers in the coil. The height defines the number of turns per layer. The end radius of the inner layer should respect the minimum bending radius criterion. In both rotor and stator it is assumed that the wires are wound on stainless steel formers like in [97], [104] or an equivalently strong other metal surface that enhances the heat transfer. Table 1 reassumes the assumed wire properties.

Chapter 4 Rough Design of a 10 MW HTS wind turbine generator

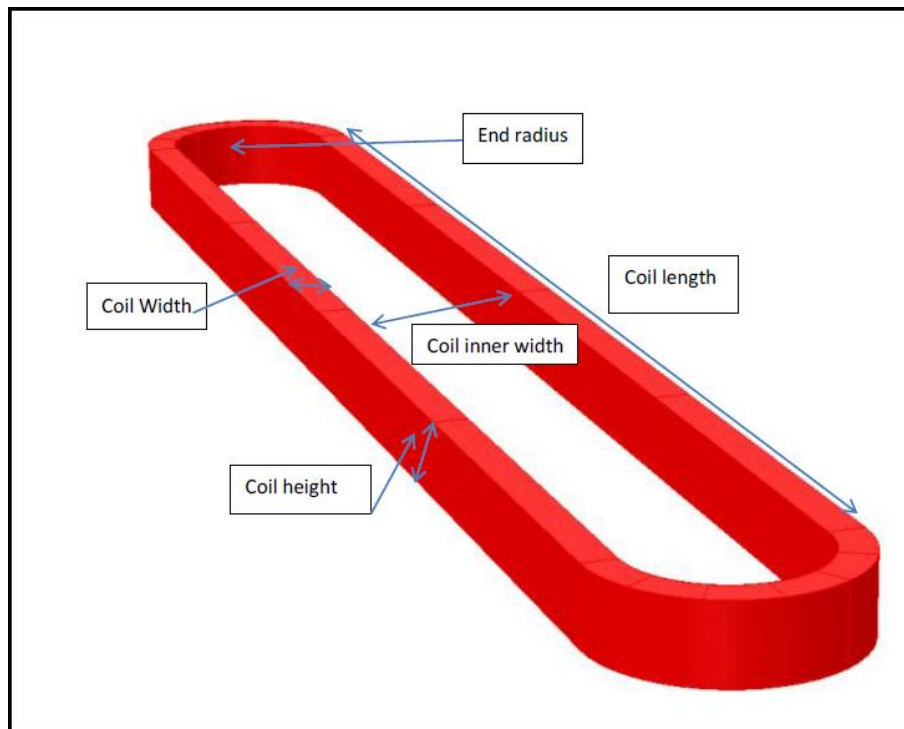


Figure 70 Racetrack coil geometry [115]

Table 1 Summary of the adopted wire properties

Wire type	round Nb/Cu/Monel
Impregnation	Stycast 2850
Filaments	61
Superconductor fraction	25%
Diameter	2-3 mm
Insulation thickness and material	0.5 mm Kapton
Total cross section diameter	3-4 mm
Strain	0.55%
Minimum bending radius	18-27 cm

4.4.2. Rotor

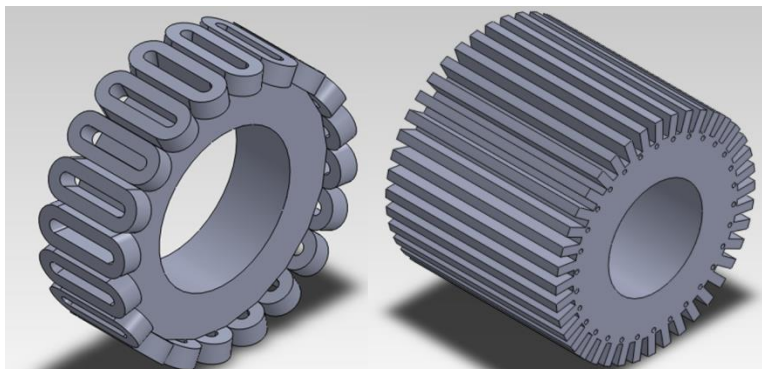


Figure 71 Rotor concept

Each rotor coil represents one pole. The field coils are mounted on a hollow composite structure with metal interfaces for heat transfer enhancement. More details on the torque tube layout and on the thermal design are in section 4.7.

Chapter 4 Rough Design of a 10 MW HTS wind turbine generator

4.4.3. Stator

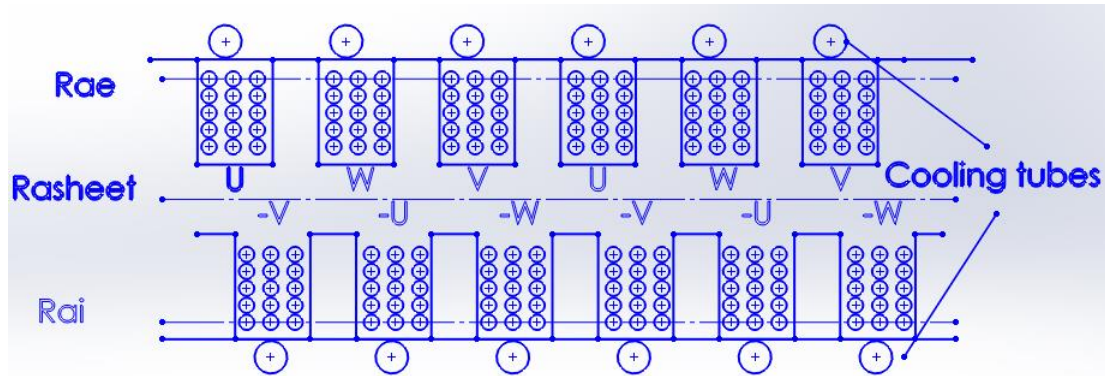


Figure 72 Double layer stator winding concept illustrating with and the external (R_{ae}), internal (R_{ai}) and sheet radii (R_{asheet}) of the winding representation

The substitution of iron with composite as host material for the winding has undoubtedly advantages but also introduces some difficulties in the design because the windings are no longer connected to a continuous stiff support neither are anchored to an effective heat sink. When designing non-conventional windings a balance between the phases in mechanical and electrical terms is required. There are few winding types like the spiral pancake winding arranged in 4 to 5 layers [113] and the helical windings [106] that fulfill the requirements.

In particular, the helical winding as discussed in [106] due to its smooth and regular shape may have less demanding structural requirements but also increase the power rating and lower the synchronous reactance. AML is already developing an MgB_2 fully superconducting wind turbine generator with double helix armature winding. The double helix produces a very smooth waveform and mitigates some of the disadvantages of the single helix winding. Moreover, its smoothness guarantees that there should be no particular problems to produce it with MgB_2 “react and wind” wire.

As a consequence it clearly emerges that in a more detailed and comprehensive design study this option should be certainly investigated. This investigation certainly requires FEM modeling with a full electromagnetic, thermal and mechanical model of the wire for an exact force/stress calculation which will verify the structural gains from this winding. Naturally this goes beyond this thesis and a more standard approach is adopted with racetrack coils.

For the stator winding the distributed winding approach is taking into account that the end connections should comply with the minimum bending diameter restriction. For 10 pole pairs and a 3 phase machine this means that there are 60 phase zones distributed in the periphery of the stator. For better spacing of the coils and in order to avoid the need for other types of end connections than circular the 60 zones are arranged in 2 layers as illustrated in figure 72. Each straight section of the racetrack coil represents a phase zone and is “contained” in a composite slot. The winding experiences forces that are transmitted through the composite structure to the cryostat walls and the environmental shield to the turbine structure.

4.5 Electromagnetic design

4.5.1. Equivalent current sheets

The presented analytical approach for the calculation of the electromagnetic field of the generator is based on the concepts illustrated in [107], [108], [109], [110], [111], [112], [113] for the treatment of air-core machines. The main concept in studying air-core machines consists in representing the effective winding distribution as a linear current distribution sine distributed over the periphery of the machine. This results by considering the ampere loading distribution over the periphery of the generator and successively evaluating its Fourier transformation.

$$K_r(\theta) = \sum K_{sheet}^v \sin(vp\theta) \text{ [A/m]} \quad (4)$$

Harmonic analysis can be carried out by considering separately each component of the current sheet. In this study only the fundamental is considered. As a consequence:

$$K_r(\theta) = K_r \sin p\theta \text{ [A/m]} \quad (5)$$

The amplitude of the equivalent current sheet is defined as:

$$K_r = \frac{2N_r k_w}{\pi R_{sheet}} * I_{sheet} \text{ [A/m]} \quad (6)$$

Where I_{sheet} is the current of the HTS coils, N_r is the total number of turns of the rotor and k_w the winding factor.

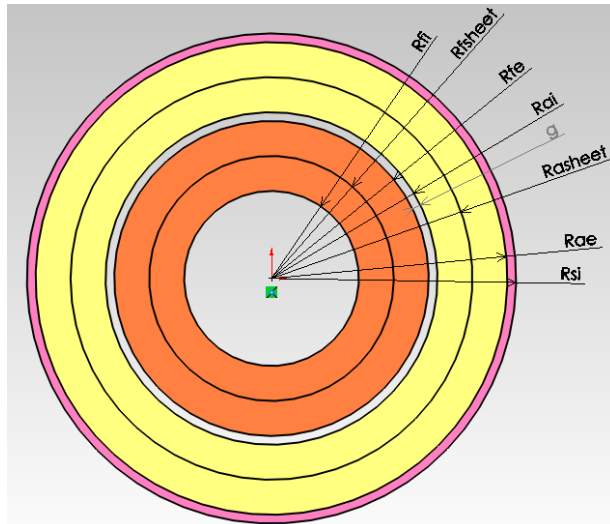


Figure 73 Cross section of the proposed generator

Figure 72 illustrates the proposed generator layout. The HTS windings (both field and armature) are represented as rings contained between an outer and an inner radius. The equivalent current sheet is assumed to be distributed along an intermediate radius, which is taken to be the average of the outer and inner radii. In order to correctly define the equivalent rotor current sheet amplitude the positioning of the HTS coils should be considered. In figure 73 the position of the racetracks is indicated in the generator's cross

Chapter 4 Rough Design of a 10 MW HTS wind turbine generator

section for a pole pair. The color depicts the direction of the current in the coils. In Figure 74 the effective rotor ampere loading of the machine is given for a pole pair. The sinusoidal signal depicted represents the fundamental of the considered current sheet distribution.

In a similar way the equivalent armature current sheet can be calculated. The only difference lies in the fact that there are three phases carrying currents displaced with respect to each other by 120° . The stator is divided into $2pm$ zones with p the number of pole pairs and m the number of phases. Each zone is carrying instantaneously current in the opposite direction (3 phases 10 pole pairs). Each current zone represents a side of a racetrack.

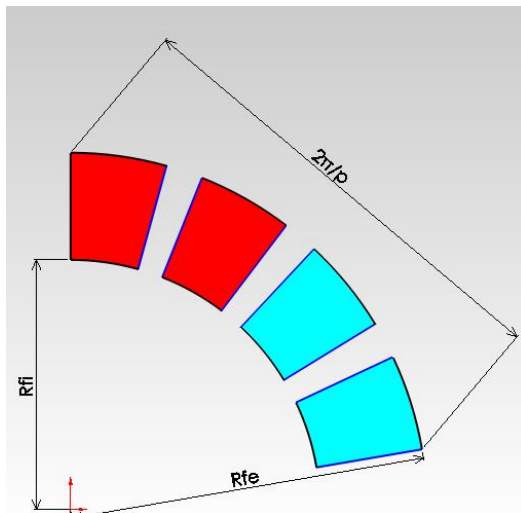


Figure 74 Positioning of the racetrack coils for a rotor pole pair

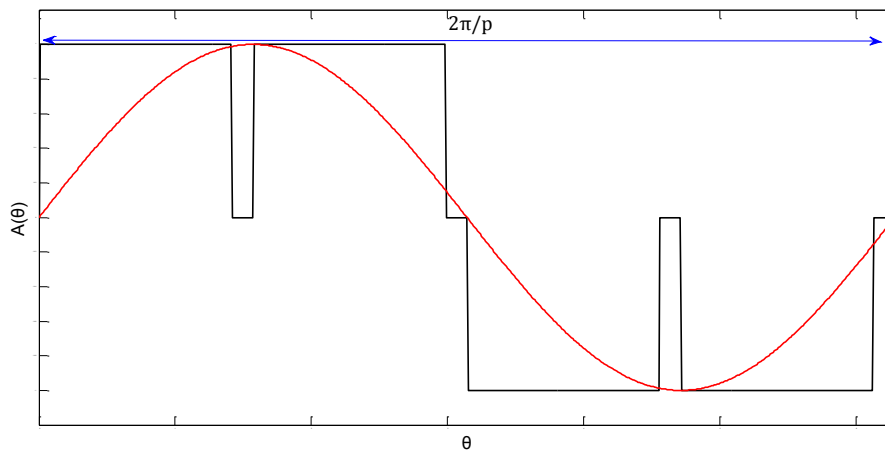


Figure 75 Ampere loading of a rotor pole pair and the fundamental of the sinusoidal current sheet

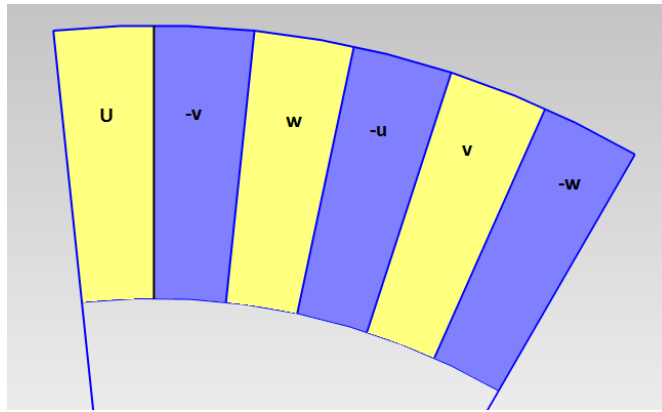


Figure 76 Stator pole pitch

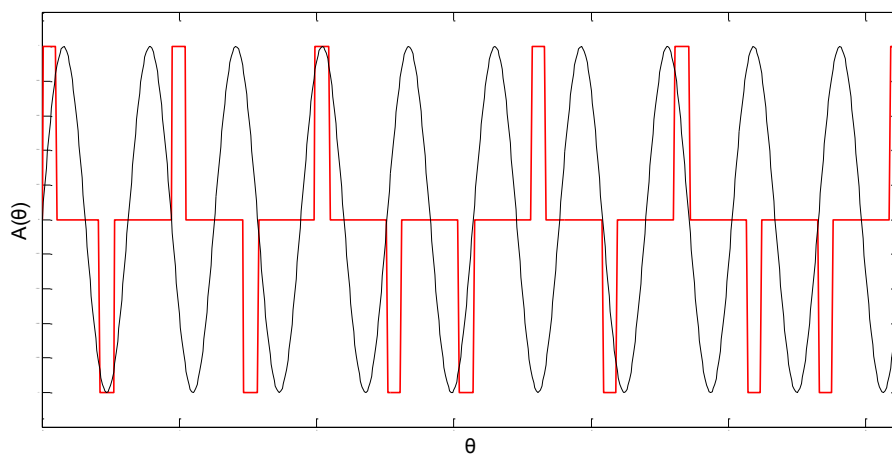


Figure 77 Stator ampere loading for phase a

In figure 75 a distance of two pole pitches of the stator is depicted. In figure 76 the ampere loading for phase a is given for a fixed moment in time together with the amplitude of the equivalent stator sine sheet sum of all three phases.

The stator electric loading is defined by:

$$K_s = \frac{3N_{phase} I_{phase} k_w}{\pi R_{sheet}} [A/m] \quad (7)$$

Where I_{phase} is the RMS current of phase a and N_s is the total number of series turns per phase.

4.5.2. Electromagnetic field of the generator

The main assumptions of the electromagnetic model are:

- End effects neglected
- Eddy currents neglected
- Only the fundamental is considered
- Windings carry currents only in the z direction
- Windings approximated by sine distributed current sheets

Chapter 4 Rough Design of a 10 MW HTS wind turbine generator

The starting point is Maxwell equations in a quasi-static state (displacement current neglected) and in particular Ampère's law and Gauss law for the magnetic field:

$$\nabla \times \vec{H} = \vec{j} \quad (8)$$

$$\nabla \cdot \vec{B} = 0 \quad (9)$$

These equations together with the constitutive equation (13) are the basic relations that describe the magnetic field in all the regions of the generator (windings, airgap, eventual iron parts and non-magnetic parts).

$$\vec{B} = \mu \vec{H} \quad (10)$$

The magnetic vector potential is given by:

$$\vec{B} = \nabla \times \vec{A} \quad (11)$$

The Coulomb condition required to define it unambiguously is:

$$\nabla \cdot \vec{A} = 0 \quad (12)$$

Using equation (10) and substituting equation (11) to equation (8) the following expression is obtained:

$$-\nabla^2 \vec{A} = \mu \vec{j} \quad (13)$$

Assuming that the current density has only a z component also the vector potential has only a z component. This means that the magnetic field solution has only x and y components or equivalently in cylindrical coordinates only r and θ components. The rotor field coils are represented by an equivalent sinusoidal current sheet distribution $K_r \sin p\theta$ with K_r the rotor electric loading defined by equation (6). With the assumptions made the magnetic vector potential will be proportional to $\sin p\theta$, for example

$$A = A_0(r) \sin p\theta \quad (14)$$

$A_0(r)$ is then the solution of the following equation:

$$\frac{d^2 A_0}{dr^2} + \frac{1}{r} \frac{dA_0}{dr} - \frac{p^2}{r^2} A_0 = 0 \quad (15)$$

This equation can be solved with the following boundary conditions:

- $K=0$ at $r=0$ and $r=\infty$
- B_r continuity at the various region boundaries
- H_θ continuity at the various region boundaries

The flux density can then be calculated by:

$$B_r = \frac{1}{r} \frac{\partial A}{\partial \theta} \quad \partial B_\theta = -\frac{\partial A}{\partial r} \quad (16)$$

Chapter 4 Rough Design of a 10 MW HTS wind turbine generator

The expressions of the flux density are given firstly for an air-core machine and secondly for a machine with stator back iron (r generic radius). The expressions are only given for the winding regions of interest:

$r < R_{\text{sheet}}$

$$B_r = \frac{\mu_0 K_r}{2} \left(\frac{r}{R_r}\right)^{p-1} \cos p\theta \quad (17)$$

$$B_\theta = \frac{\mu_0 K_r}{2} \left(\frac{r}{R_r}\right)^{p-1} (-\sin p\theta) \quad (18)$$

$r > R_{\text{sheet}}$

$$B_r = \frac{\mu_0 K_r}{2} \left(\frac{r}{R_r}\right)^{p+1} \cos p\theta \quad (19)$$

$$B_\theta = \frac{\mu_0 K_r}{2} \left(\frac{r}{R_r}\right)^{p+1} \sin p\theta \quad (20)$$

$r < R_{\text{sheet}}$

$$B_r = \frac{\mu_0 K_r}{2} \left(\frac{r}{R_r}\right)^{p-1} \left[1 + \eta \lambda_s \left(\frac{R_r}{R_{s1}}\right)^{2p}\right] \cos p\theta \quad (21)$$

$$B_\theta = \frac{\mu_0 K_r}{2} \left(\frac{r}{R_r}\right)^{p-1} \left[1 + \eta \lambda_s \left(\frac{r}{R_{s1}}\right)^{2p}\right] (-\sin p\theta) \quad (22)$$

$R_{\text{sheet}} < r < R_{\text{si}}$

$$B_r = \frac{\mu_0 K_r}{2} \left(\frac{R_r}{r}\right)^{p+1} \left[1 + \eta \lambda_s \left(\frac{r}{R_{\text{si}}}\right)^{2p}\right] \cos p\theta \quad (23)$$

$$B_\theta = \frac{\mu_0 K_r}{2} \left(\frac{R_r}{r}\right)^{p+1} \left[1 - \eta \lambda_s \left(\frac{r}{R_{\text{si}}}\right)^{2p}\right] \sin p\theta \quad (24)$$

With λ_s and η defined as:

$$\lambda_s = (\mu_s - 1)/(\mu_s + 1) \quad (25)$$

$$\eta = [1 - \left(\frac{R_{\text{si}}}{R_{\text{se}}}\right)^{2p}] / [1 - \lambda_s^2 \left(\frac{R_{\text{si}}}{R_{\text{se}}}\right)^{2p}] \quad (26)$$

Where μ_s is the relative permeability of iron. For the calculation of the armature reaction flux the same relations can be used, by specifying the appropriate radii, the appropriate current sheet amplitude and the appropriate region where the calculation is conducted.

After calculating the flux density due to the rotor field winding, the flux linkage of the stator winding can be calculated by applying stokes theorem:

$$\lambda = \iint \vec{B} \cdot d\vec{s} = \iint \nabla \times \vec{A} \cdot d\vec{s} = \oint \vec{A} \cdot d\vec{s} \quad (27)$$

The inductances can be calculated by dividing the appropriate flux linkage with the corresponding current. The following expressions for self-inductance and mutual inductances (coils at generic radius r) are given for air-core machines as well as for machines with stator back iron.

Chapter 4 Rough Design of a 10 MW HTS wind turbine generator

$$L = \frac{2\mu_0 (N_s k_w)^2}{\pi p} \text{ air-core machine} \quad (28)$$

$$\frac{L_{Iron}}{L} = [1 + \eta \lambda_s (\frac{r}{R_{Si}})^{2p}] \text{ stator back iron} \quad (29)$$

$$M = \frac{2\mu_0 (N_{s1} k_{w1}) (N_{s2} k_{w2})}{\pi p} (\frac{r_1}{r_2})^p \cos p\alpha \quad (30) \text{ air-core machine}$$

$$M = \frac{\mu_0 (N_s k_w)^2}{\pi p} \quad (31) \text{ balanced 3 phase winding air core machine}$$

$$\frac{M_{Iron}}{M} = [1 + \eta \lambda_s (\frac{r_2}{R_{Si}})^{2p}] \quad (32) \text{ stator back iron}$$

As in conventional machines with small airgap the mutual inductance is half of the self-inductance due to the assumed symmetry (cylindrical machine-symmetric air gap).

The current flowing in the stator winding is assumed that is coming from a converter. The current flowing in phase a is assumed to be of this form:

$$I_a = \sqrt{2} I_s \cos \omega_e t \quad (33)$$

The other phase currents are assumed to be displaced of $2\pi/3$ and $4\pi/3$ respectively. The star connection point is not used therefore

$$I_a + I_b + I_c = 0 \quad (34)$$

As a consequence

$$I_b + I_c = -I_a \quad (35)$$

The total flux linkage per phase is:

$$\lambda_a = L_{sa} i_a + M_{sab} i_b + M_{sac} i_c + \lambda_f \quad (36)$$

Due to symmetry the mutual inductance of phase a and b is equal to the one of phase b and c and the one of phase a and c.

$$\lambda_a = (L_{sa} - M) i_a + \lambda_f \quad (37)$$

The voltage equation for each phase with the generator's convection is given by:

$$v = -\frac{d\lambda}{dt} = -(L_{sa} \frac{di_a}{dt} + M_{sa} \frac{di_b}{dt} + M_{sac} \frac{di_c}{dt} + \frac{d\lambda_f}{dt}) \quad (38)$$

Working out this expression results in:

$$v = -L_s \frac{di_a}{dt} + e_a \quad (39)$$

L_s is the synchronous inductance in the classical circuit representation of synchronous machines without saliency. For the calculation of L_s , the inductance of each phase is calculated by formulas (28) and (29) and the result is multiplied by 3/2 to account for the other phases [109].

Chapter 4 Rough Design of a 10 MW HTS wind turbine generator

The RMS value of the induced voltage is given by [113] :

$$E_a = \sqrt{2} N_s k_w B_{so} R_{asheet} L \frac{\omega}{p} \quad (40)$$

The coupling coefficients show how tight is the coupling between field and armature. It is a measure of magnetic efficiency, in the sense of the utilization of the flux produced. The coupling coefficient influences the transient reactance. For the three topologies for which the solutions of the field have been given above, the coefficients are given by:

$$c_{aircore} = (r_f/r_a)^p \quad (41)$$

$$c_{conv} = \frac{2(r_f/r_a)^p}{1+(r_f/r_a)^{2p}} \text{ Infinitely permeable iron} \quad (42)$$

$$c_{back-iron} = (r_f/r_a)^p \sqrt{\frac{2(r_f/r_{si})^p}{1+(r_f/r_{si})^{2p}}} \quad (43)$$

4.5.3. Design parameters

The output power of a 3 phase generator is given by:

$$P = \left(\frac{\pi^2}{\sqrt{2}}\right) k_w K_s B_{so} D^2 l n_s \quad (44)$$

Where D is the stator winding mean diameter and l is the active length of the machine. The peak radial flux density at stator winding radius is set to $B_{so} = 2$ T. The electrical frequency is ≈ 1.8 Hz. Consequently $n_s = 0.17$ rev s^{-1} . The stator electric loading K_s is defined in (7). k_w is the winding factor and is assumed to be 0.9.

For a machine with a superconducting armature K_s could be assumed to be 600-700 kA/m [113]. Compared to 100-350 kA/m of conventional machines (the higher value is for water cooled airgap armature windings) it is evident that this represents a significant increase. Assuming $K_s = 600$ kA/m from equation (44) it is deduced that the product $D^2 l = 7.4$ m³. This means that assuming a cylindrical geometry the necessary active volume (at stator winding radius) to produce 10 MW of power is around 24.6 m³ which is slightly higher than the volume calculated in [116] for a 3 MW DDPM WTG (23.56 m³). Therefore potentially the generator can be very compact.

An issue that arises from the high K_s is the strong armature reaction on the field coils. Since in this design no EM shield is adopted a lower value for K_s should be assumed in order to reduce losses and avoid local field peaks in the rotor pole coils. As a consequence a larger stator winding diameter is assumed. The active length is set to 1m.

The mean stator winding radius and the inner and outer radii are given by:

$$R_{asheet} = 2.8 \text{ m}$$

$$R_{ai} = 2.785 \text{ m}$$

$$R_{ae} = 2.815 \text{ m}$$

Chapter 4 Rough Design of a 10 MW HTS wind turbine generator

The airgap thickness is 1/1000 of the diameter [117] and this yields an airgap thickness of $g \approx 5.6$ mm. The stator and rotor windings are enclosed in a single cryostat. This greatly reduces the effective airgap, enhances the coupling and minimizes the amount of ampere turns required for the same flux density at stator winding mean radius. However, in between the rotor and stator coils there is not only the mechanical airgap. In the stator there are cooling tubes passing through a cage type support structure. Over the rotor coils there is also some support structure necessary due to the large Lorentz forces acting on the coils. As a consequence the effective magnetic airgap of the generator increases. A proper dimensioning of that support structure is not done in this thesis. It is assumed that overall the space occupied by this support structure including the airgap is 300 mm. As a consequence the field coil radii are:

$$R_{fe} = 2.568\text{m}$$

$$R_{fsheet} = 2.5 \text{ m}$$

$$R_{fi} = 2.432 \text{ m}$$

From the stator winding external radius to the location of the ferromagnetic shield there is a considerable amount of support structure sustaining the stator winding and the cryostat walls. In a similar approach as for the effective airgap assumption it is assumed that the thickness of these layers amounts to 700mm. The thickness of the shield is set to be $t_{Fshield} = 100$ mm (calculated in following section). As a consequence the internal and external radii of the shield are given by:

$$R_{si} = 3.51$$

$$R_{se} = 3.61$$

Table 2 summarizes the geometrical characteristics of the proposed design.

Armature outer radius R_{ae} [m]	2.815
Armature inner radius R_{ai} [m]	2.785
Armature current sheet radius R_{asheet} [m]	2.8
Airgap length g [mm]	3
Effective airgap [mm]	300
Field winding outer radius R_{fe} [m]	2.568
Field winding inner radius R_{fi} [m]	2.432
Field winding current sheet radius R_{fsheet} [m]	2.5
Stator back iron internal radius R_{si} [m]	3.51
Stator back iron external radius R_{se} [m]	3.61
Active length l [m]	1

Table 2 Geometrical parameters

With the proposed dimensions from formula (44) the required K_s is calculated resulting in $K_s = 142.37$ kA/m. This corresponds in 1392 series turns per phase. These turns are distributed in 10 coils over the periphery of the generator which means approximately 140 turns per coil. These turns are arranged in 28 layers with 5 turns per layer. For the wire length estimation each turn has been assumed to have 2 straight sections and 2 semicircular

Chapter 4 Rough Design of a 10 MW HTS wind turbine generator

end sections. Successively the wire length for each layer is calculated. The total wire consumption for each phase has been estimated to amount around 4.8 km. The synchronous inductance of the machine is calculated with formulas (28) and (29) and multiplying with 1.5 to account for the other phases: $L_s = 0.127$ H.

The targeted peak radial flux density is set to $B_{so} = 2$ T. In order to achieve this value the required rotor electric loading amplitude is calculated to be $K_r = 10.9$ MA/m. The total field turns are 16962 turns which means 848 turns approximately per pole. These turns are arranged in 25 layers with 34 turns per layer. The wire length per pole is around 3.2 km. Also accounting for the stator the total wire length is estimated to be 80 km. The field coil self-inductance is calculated with formulas (28) and (29): $L_f = 18.6$ H. The maximum value of the mutual inductance is: $M_f = 0.5$ H. The self-inductance of the rotor pole is very high due to the very large number of turns.

The per unit synchronous reactance of the generator is 0.093 which is very low and a common characteristic with all superconducting machines. The short circuit ratio is given by the inverse of the per unit synchronous reactance and is 10.7. The proposed generator has a coupling coefficient of 0.3235. A conventional machine with the same dimensions would have 0.5835 and an aircore machine 0.3220. For the conventional machine caution should be paid in evaluating this value because the correct formula was applied but the dimensions do not match the restriction for a small airgap. This value is only given for comparison. The 300 mm of effective airgap is significant. Optimization of the support structure could decrease this value significantly and make the coupling tighter and thus having a better exploitation of the superconductor and higher transient reactance. Low synchronous reactance also means a low load angle (δ). The stator current is provided from a converter. This means that the $\cos\phi$ is controlled. Setting the terminal voltage as a reference and varying the $\cos\phi$ the load angle variation can be calculated. From the mentioned parameters active and reactive power can be calculated. These graphs are illustrated in the next page together with the armature reaction flux density at rotor field sheet radius.

Harmonic analysis is not carried out in this thesis. The number of pole pairs as already mentioned was chosen upon reported results from studies on space harmonics and wire consumption. Without going into deeper analysis by simply observing the last graphs it can be concluded that with a higher number of pole pairs the waveforms resemble better the actual loading in space and thus have a lower harmonic content, but at the same time the electric loading increases significantly.

Table 3 Design parameters

K_r	10.9 MA/m
K_s	142.37 kA/m
N_r	16962
N_s	1393
c	0.3235
scr	10.7
Total wire length	80 km

Chapter 4 Rough Design of a 10 MW HTS wind turbine generator

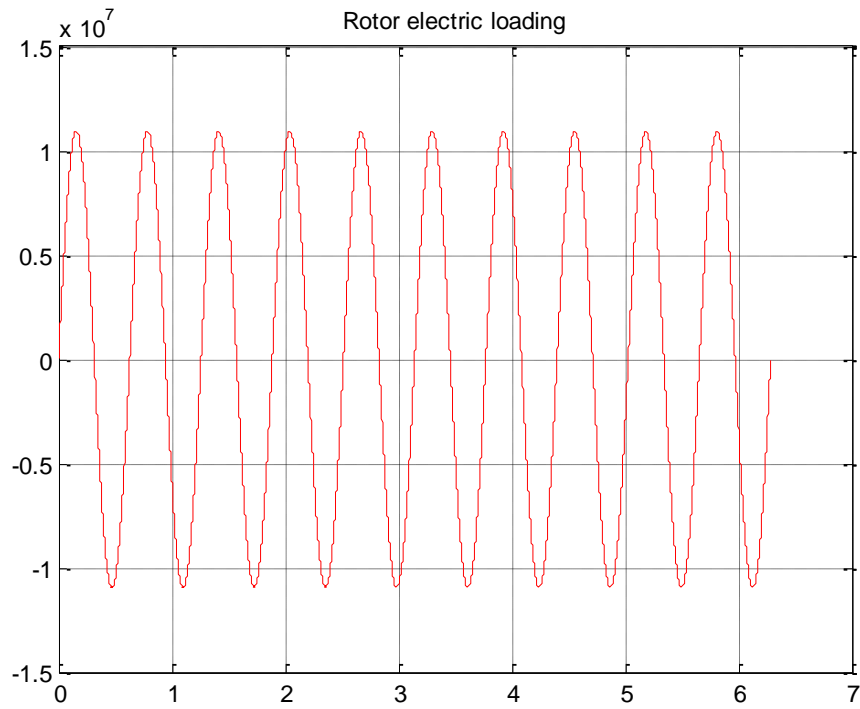


Figure 78 Rotor electric loading

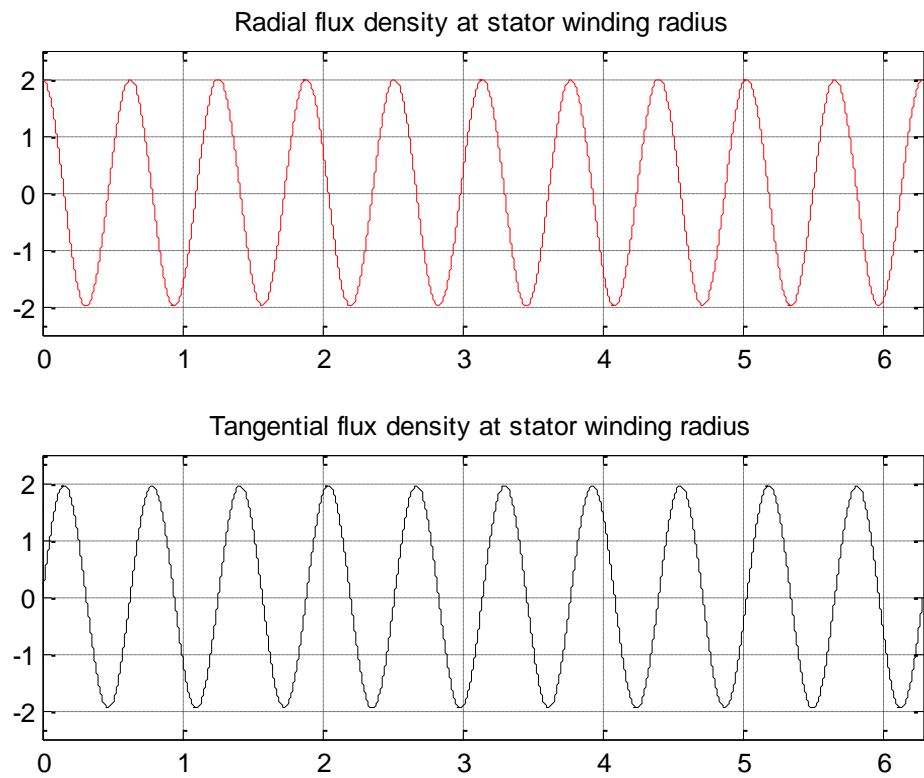


Figure 79 Flux density at stator winding radius

Chapter 4 Rough Design of a 10 MW HTS wind turbine generator

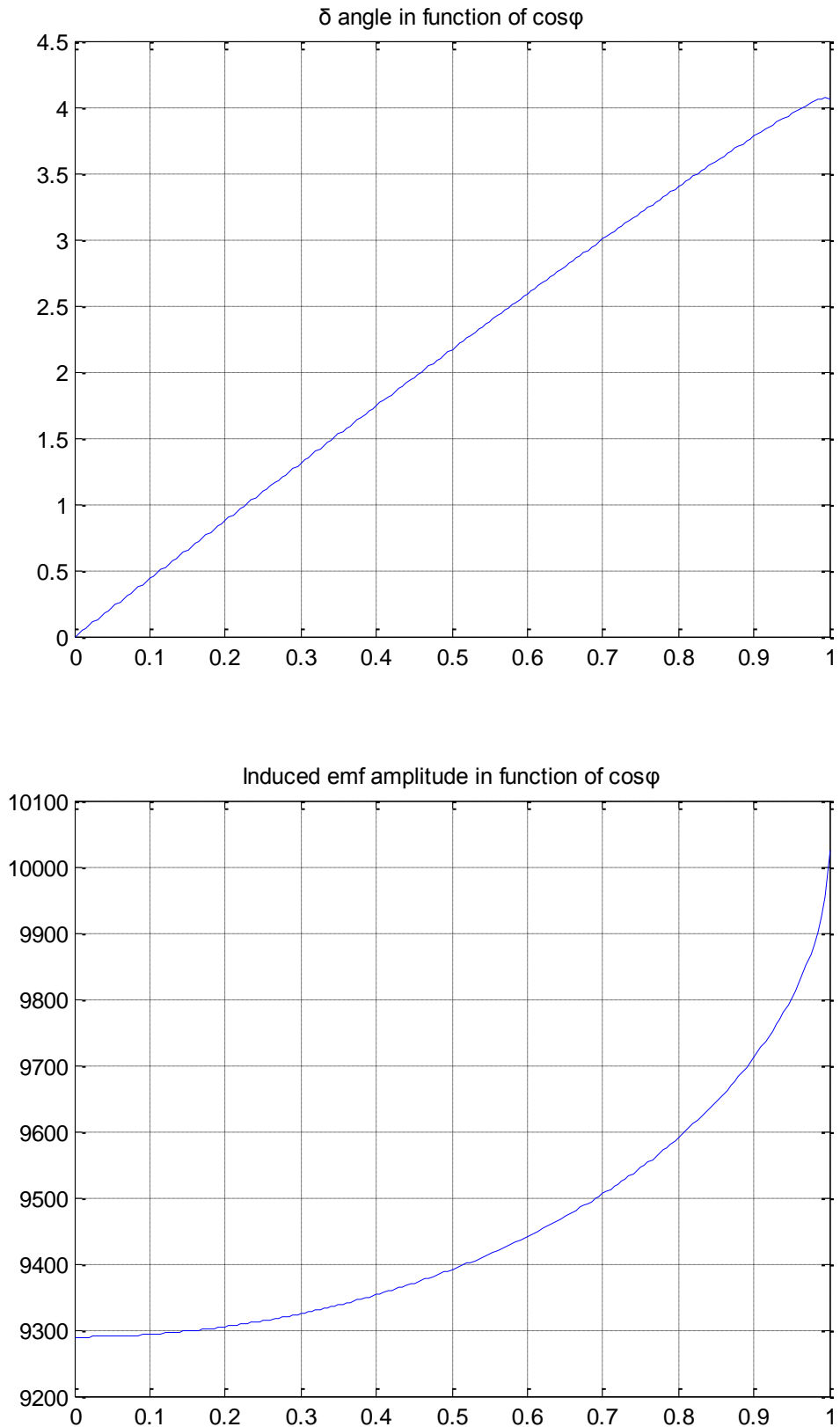


Figure 80 Emf variation with $\cos\phi$

Chapter 4 Rough Design of a 10 MW HTS wind turbine generator

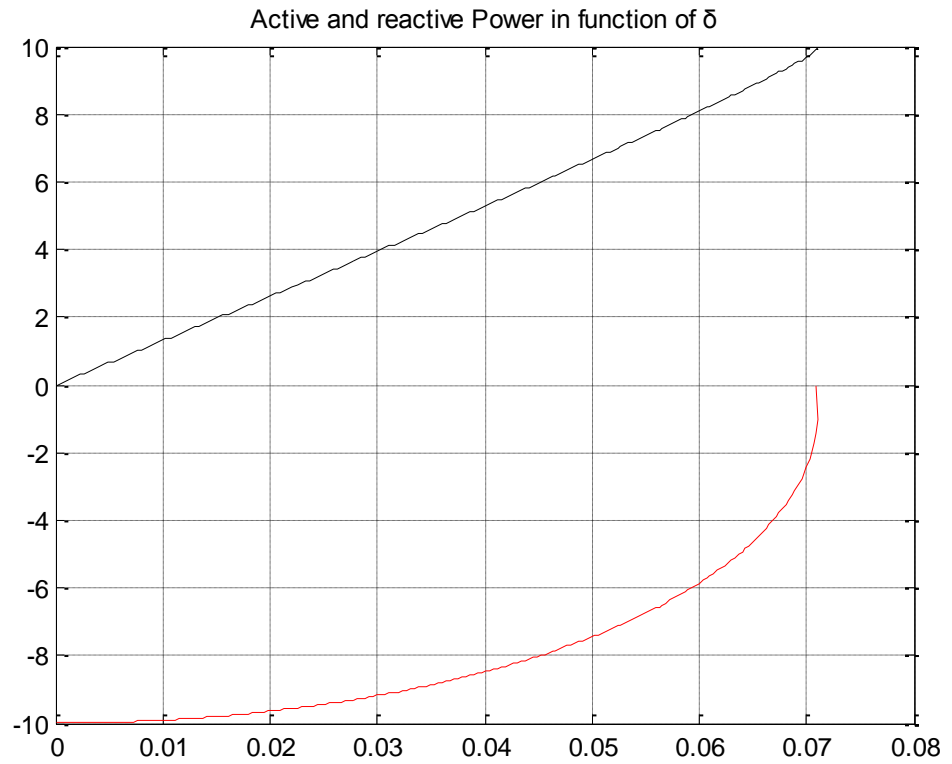


Figure 81 P and Q in function of δ

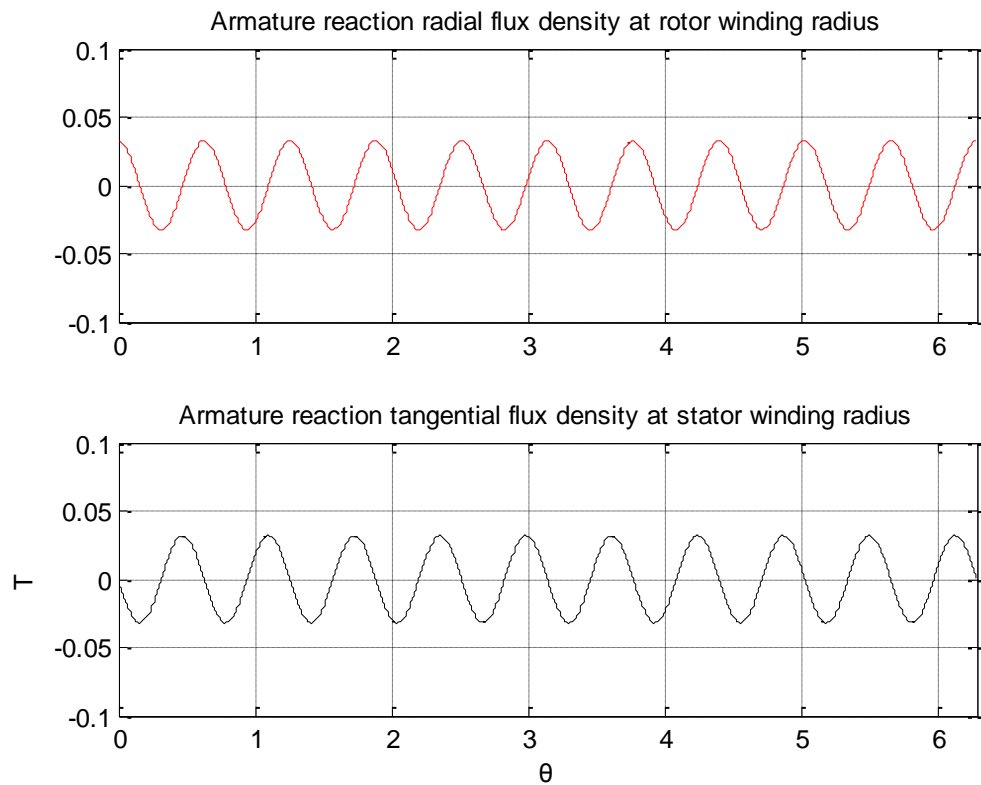


Figure 82 Armature reaction flux density at the field winding sheet radius

Chapter 4 Rough Design of a 10 MW HTS wind turbine generator

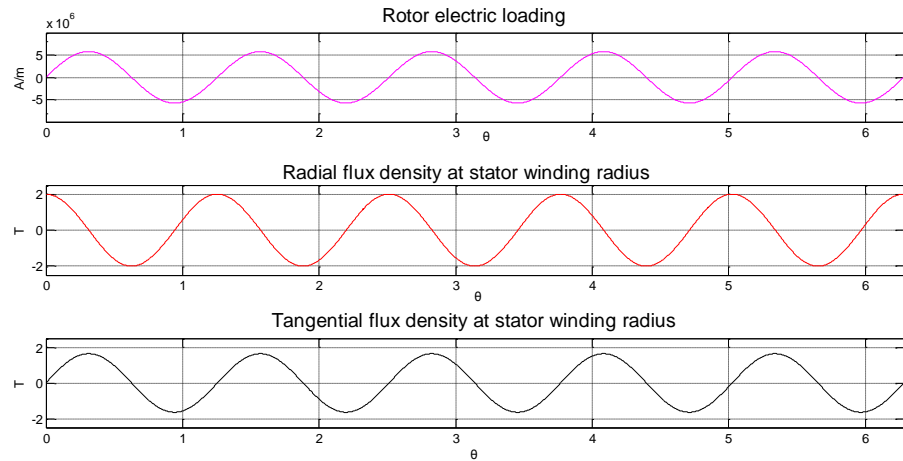


Figure 83 K_r, B_r, B_θ for $p=5$

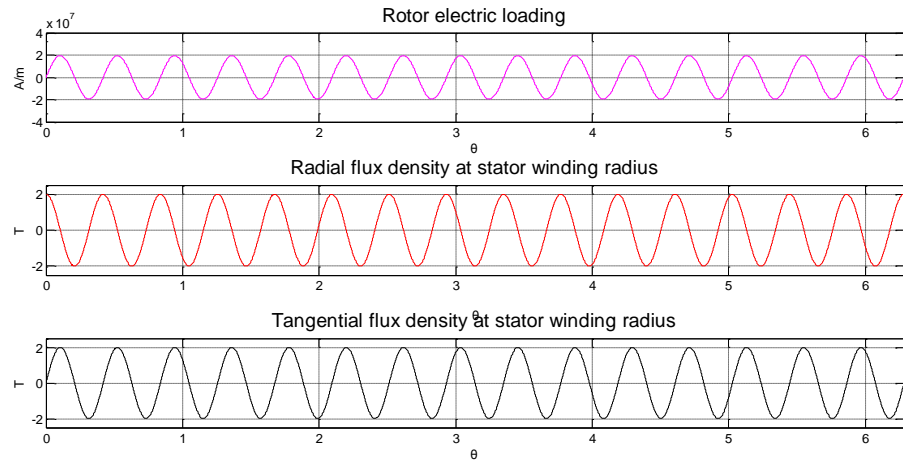


Figure 84 K_r, B_r, B_θ for $p=15$

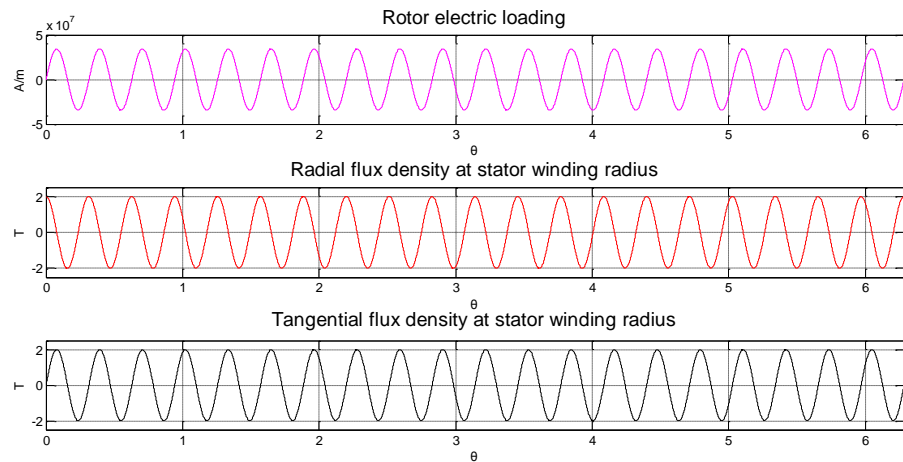


Figure 85 K_r, B_r, B_θ for $p=20$

Chapter 4 Rough Design of a 10 MW HTS wind turbine generator

4.5.4. Environmental shield calculation

The environmental shield is necessary for the attenuation of the fields outside the machine. Moreover, it provides a stiff support to the winding. The ferromagnetic environmental shield is assumed to operate at room temperature in order to reduce the cold mass and avoid the use of more expensive material. The thickness of the shield can be determined by considering that the shield has to carry all the flux outside its inner radius when the field winding is excited to generate the rated open circuit voltage [7]. Under load conditions due to the armature reaction this flux changes. However, at first approximation it can be assumed to be approximately equal to the total flux on the open circuit. The permeability of iron is assumed infinite. The verification of the shield's attenuation is done using the already given field formulas for the flux density.

For the calculation of the flux the following relation is used:

$$\Phi_f = \int_0^{\pi/2p} B_r(R_{si}, \theta) * l * R_{si} d\theta \quad (45)$$

By fixing an operating flux density in the yoke B_{yoke} the thickness of the shield is given by:

$$t_{Fshield} = \frac{\Phi_f}{l * B_{yoke}} \quad (46)$$

Assuming $B_{yoke} = 1$ T and plugging in the numbers yields $t_{Fshield} = 0.3$ m.

The verification of the field outside the machine yields for the calculated thickness a radial field amplitude of 0.071 mT. By setting the thickness of the shield at 0.1 m then the outside field becomes 20 mT which already is an acceptable value. As a consequence the thickness of the shield is set to $t_{Fshield} = 0.1$ m with a corresponding volume of 2.23 m³.

The material of the shield is a non-oriented iron silicon aluminum alloy. This particular alloy is lighter than silicon iron alloys and has reduced losses. As a reference a product of Thyssen Krupp Stahl AG was chosen. In particular the Powercore A grade alloy was chosen with product code M 235 35. This alloy has a density of 7600 kg/m³.

The loss in the shield has two components, namely hysteresis and eddy currents with both having a frequency dependence. Hysteretic losses can be assumed to have a linear dependence with the frequency, while eddy currents vary with the square of the frequency [117]. For the normal operating frequency of the proposed generator (1.8 Hz) it can be assumed that eddy current losses are negligible. The loss figures for non-oriented electrical steels are given for 50 or 60 Hz cycles. At that frequency the losses are predominately hysteretic. As a consequence it can be assumed that 80% of the loss figure is due to hysteresis. Successively this value is interpolated assuming a linear variation to 1.8 Hz in order to estimate the shield losses.

The loss factor for M 235 35 is 2.35 W/kg for 50 Hz and 1.5 T flux density. Assuming 80% of hysteretic losses results in 1.88 W/kg. Interpolating to 1.8 Hz yields 0.0376 W/kg. The volume of the shield is 2.23 m³ and for the particular alloy this translates to a weight of 16948 kg. As a consequence, the losses on the shield are estimated to be around 640 W.

Chapter 4 Rough Design of a 10 MW HTS wind turbine generator

Table 4 Environmental shield characteristics

Material	Aluminum iron silicon alloy
Shield thickness	100 mm
Lamination thickness	0.35 mm
Density	7600 kg m ⁻³
weight	16.9 tons
Hysteresis losses	640 W

4.6 Losses in the generator

For the calculation of the losses in superconductors detailed numerical codes are required. With the analytical formulas used in this section only a rough estimation is possible. The magnetization of the material and the current sharing between filaments in the wire's cross section are of utmost importance in AC loss calculation and in this thesis are not considered. There is an analogy between the magnetization of ferromagnetic materials and superconductors where also M-H loops are formed and therefore the loss can be computed from the area of the loop. AC losses in superconductors also suggest the fundamental difference that they have with normal conductors. Superconducting materials may be regarded as having their "skin effect" amplitude dependent whereas as it is known normal conductors have a frequency dependent skin effect.

In principle there are 2 ways to calculate AC losses and this is or via the integration of $E * J$ in the wire volume or via the surface integral of the poynting vector. The first approach is adopted and this implies that knowledge about the magnetization of the superconductor is required. The calculation is conducted adopting the critical state model which assumes that the current density in the superconductor or is equal to the critical value or is zero. The common practice in AC loss calculation is to calculate singularly the various contribution and sum up for the total losses. The following formulas given below are based on [119], but also on [120],[121],[122],[123] that basically adopt the same approach of this thesis.

The AC losses mainly consist in Hysteresis and eddy current losses in case of a DC transport current (DC loss is very small) while additional losses appear in case of an AC transport current. AC fields generate an emf within the superconductor which drives the current density beyond the critical value and thus driving the conductor is into the resistive operating region. Therefore, the loss mechanism can be considered resistive with the characteristic that this resistance is highly nonlinear resulting in an independent loss per cycle in respect to the cycle time and for this reason are called Hysteresis losses.

Hysteresis is a dominant portion of the total losses and is connected to the flux pinning: due to this mechanism the magnetic flux does not change reversibly in a superconductor. Flux creep and flux flow are also causing AC losses: In the first case there is a limited pinning force caused by the thermal activation of the lattice and in the second case is the circulation of a very large current that causes a Lorentz force on the flux line greater than the pinning force producing a flux flow. In multifilamentary wires the presence of applied field induces screening currents in the superconductor shielding it from the external field. The changing

Chapter 4 Rough Design of a 10 MW HTS wind turbine generator

magnetic field couples the filament making the screening current to circulate across the metal matrix.

The AC losses generally depend on:

- Operating temperature,
- Magnitude and direction of the magnetic field,
- Transport current
- Frequency
- Wire characteristics: filament diameter, twist pitch and matrix transverse resistivity

For the loss estimation the following assumptions are made:

- Twist pitch $l_p = 10$ mm (MgB₂ wires do not have any particular constraint but going lower might be risky)
- 61 filaments (maximum number declared by the company)
- Filament radius 64 μ m
- Transverse matrix resistivity $\rho_e = 8 * 10^{-8} \Omega\text{m}^{-1}$ [124]
- Total stator wire length 14.6 km
- Total rotor wire length 64.5 km
- Field direction perpendicular to the wire axis (transverse field)

Firstly the DC loss of the field coils is calculated. The electromagnetic behavior of superconductors is described by the power law:

$$E(L) = E_0 \left(\frac{I_T}{I_C} \right)^n \quad (47)$$

This relation reflects the industrial practice to consider the critical current of the superconductor as the current that produces a voltage drop of $E_0 = 1 \mu\text{V}/\text{cm}$. The value of n is an indication of the quality of the superconductor and for Hypertech MgB₂ wires is around 15. A higher value means that the superconductor has lower DC losses. In order to calculate the DC loss of the field coils, first the voltage drop of the entire cable is calculated by integrating (47) over the length of the cable and consequently the power loss can be computed by multiplying the current of the wire with the corresponding voltage drop. The total DC loss for the field coils amounts 630 W.

For the estimation of the AC losses the first step is to evaluate the penetration field B_p which is defined as (r : radius filament):

$$B_p = \frac{1}{\pi} 4 * \mu_0 * J_C * r \text{ T} \quad (51)$$

Defining β as:

$$\beta = \frac{B_{max}}{B_p} \quad (52)$$

Where B_{max} is the amplitude of the applied field oscillation. The formula for the estimation of the hysteresis loss differs depending on whether the penetration field is higher the

Chapter 4 Rough Design of a 10 MW HTS wind turbine generator

applied field which means evaluate if $\beta > 1$ or $\beta < 1$. For the stator wire with $B_{max} = 2$ T it results $\beta = 1.1952$ and the formula used for the calculation is:

$$Q_h = \frac{B_{max}^2}{2\mu_0} * \left(\frac{4}{3\beta} - \frac{0.71}{\beta^2} \right) \text{ [J/cycle m}^3\text{]}(53)$$

For the rotor wire $B_{max} = 0.03$ T and $\beta = 0.046$. As a consequence the formula used for the calculation is

$$Q_h = \frac{B_{max}^2}{2\mu_0} * 2 * \left(\frac{2*6}{3} - \frac{6^2}{3} \right) \text{ [J/cycle m}^3\text{]}(54)$$

In order to calculate the power loss the results of these formulas are multiplied with the frequency and the superconducting volume in the wire. This yield the following hysteresis loss for the stator and rotor wires:

$$P_{hstator} = 20.4 \text{ kW}$$

$$P_{hrotor} = 2 \text{ W}$$

The stator wire suffers grate hysteresis losses and this is due to the relatively large filament diameter and low filament number. Low AC loss LTS wires have a much higher filament number i.e. 200 filaments. Figure illustrates how the hysteresis losses vary in correspondence to the number of filaments. The rotor wire does not suffer considerable losses due to the very low armature reaction. The large effective airgap and the low K_s have yielded an acceptable hysteresis loss in the rotor coil even without EM shield.

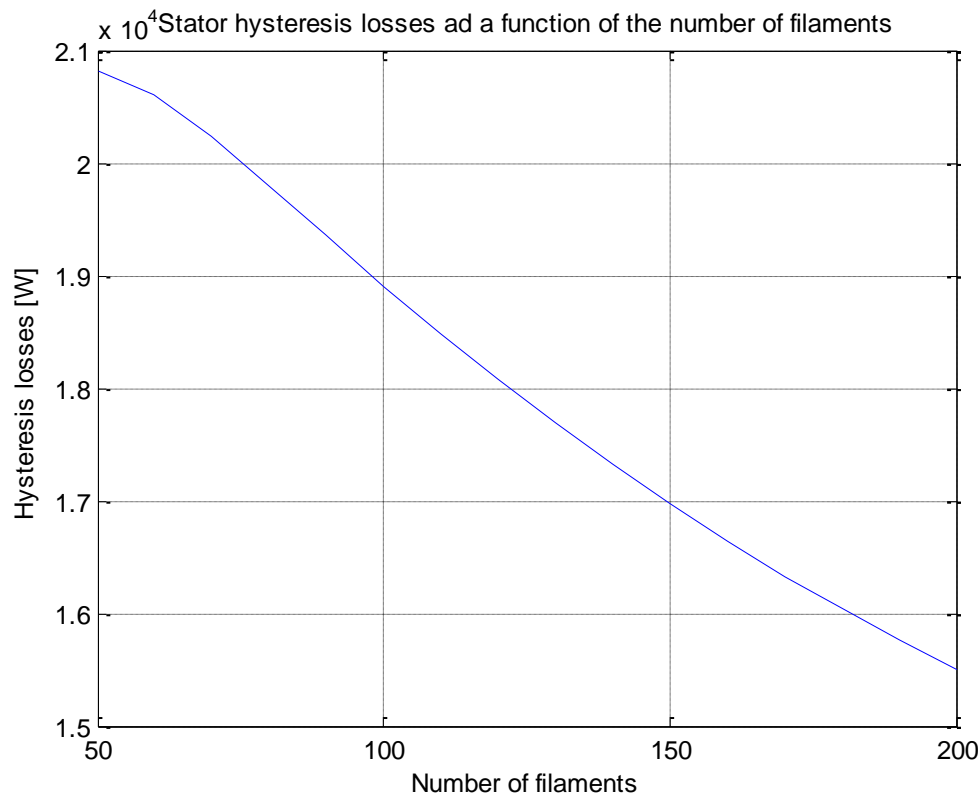


Figure 86 Stator hysteresis losses as a function of the number of filaments in the wire

Chapter 4 Rough Design of a 10 MW HTS wind turbine generator

For the calculation of the eddy current losses the time constant of the wire is defined as:

$$\tau = \frac{\mu_0}{2\rho_e} * \left(\frac{l_p}{2\pi}\right)^2 (54)$$

For the estimation of the coupling losses between filaments the following formula valid for sinusoidal field variation has been used:

$$Q_{cou} = \frac{B_{max}^2}{2\mu_0} * \frac{\pi\omega\tau}{(\omega\tau)^2+1} [\text{J/cycle m}^3] (55)$$

In order to calculate the power loss the result of this formula is multiplied with the frequency and in this case with the entire wire volume. This yields the following eddy current filament coupling loss for the stator and rotor wires:

$$P_{cou\ stator} = 186 \text{ W}$$

$$P_{cou\ rotor} = 0.42 \text{ W}$$

The last loss contribution that has been considered is the stator self field loss due to the AC transport current. The following formula is used:

$$P_{self\ field} = \frac{1}{\pi} * \mu_0 * f * I_c^2 * f(i) \text{ W/m} (56)$$

With i defined as the ratio of the maximum value of the transport current to the critical coil current and $f(i) = (1 - i) \ln(1 - i) + (2 - i) * \frac{i}{2}$. The total self field stator loss amounts to 51 W. It is kept very low due to the low utilization factor of the stator wire in terms of carried current versus critical current (almost 11%).

It should be once again stated that this is a very rough estimation of the losses. In this calculation the normal eddy current loss in the sheath of the superconductor was not taken into account. Moreover, phenomena concerning the influence of the current distribution on each superconductor strand due to the presence of the other coils with its consequences on the variation of the current density in the cross section have not been studied. These two mechanisms could attribute majorly. It is however, a conservative estimation due to the contrasting effects among the various mechanisms which results for example in the reduction of the hysteresis losses due to the coupling losses.

From the calculated parameters it clearly emerges that the dominant loss contribution come from the stator hysteresis loss.

Table 5 Summary of calculated losses in the superconductor

Rotor DC loss	630 W
Stator self field loss	51 W
Stator hysteresis loss	20.4 kW
Stator filament coupling loss	186 W
Rotor hysteresis loss	2 W
Rotor filament coupling loss	0.42 W
Total power loss	21.25 kW

4.7 Mechanical and thermal rough design

4.7.1. Morphological chart and design choices

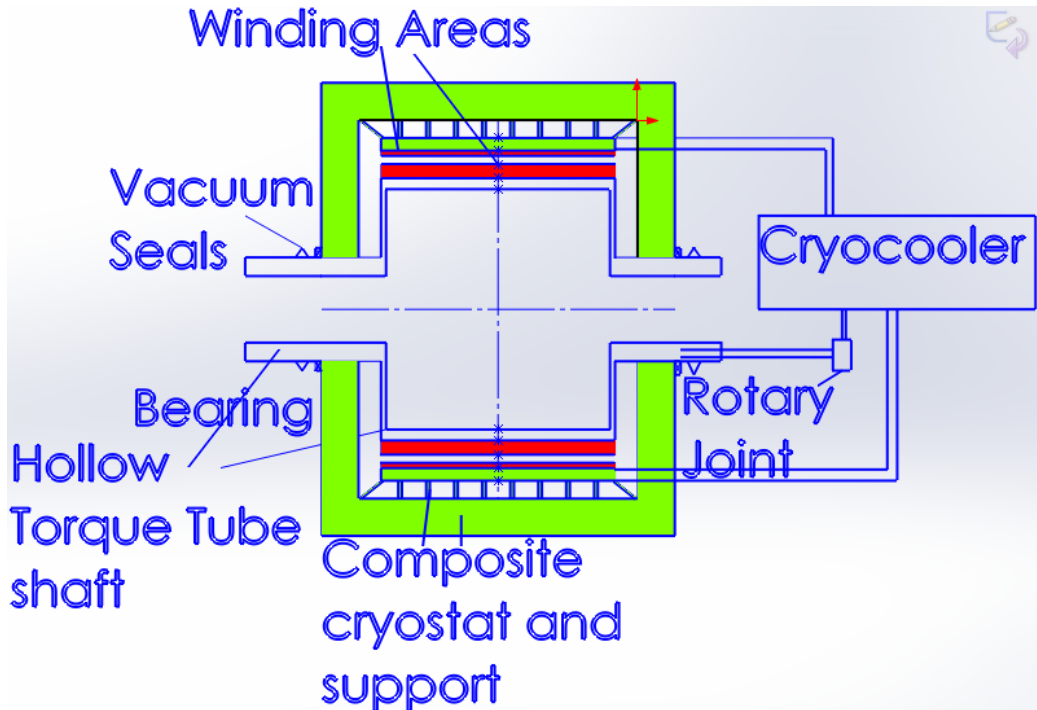


Figure 87 Cryostat lateral view and cooling concept

The mechanical and thermal design of fully superconducting machines are two closely linked and complex disciplines. A detailed design is well beyond the scope of this thesis and the capability of the author. In this section the main design choices are discussed. In the next two sections estimations are given regarding weight and cooling power.

Thermosyphon and bath cooling were not considered. Bath cooling seemed impractical for the power rating of the generator. Thermosyphon cooling can be very efficient and is adopted in prototypes (Siemens), but with modest heat loads. Due to the lack of expertise of the author in this field it seemed a risky option to expand the concept into large scale cooling. A safer option is the controlled closed loop system with circulation of a cryogen in pipes which are in contact with a metal surface that acts as a heat sink. The coils are wound on this metal surface and are globally conduction cooled. The windings operate under high quality vacuum and are impregnated with Stycast to enhance thermal conductivity. The cryostat is made of composite materials as most of the mechanical parts of the generator for weight reduction and heat leakage suppression. However, this choice implies that cool down times can be very long which in turn means that the machine should be kept cool at all times during operation in order not to restrict the turbine operation. The cryostat wall thickness is around 100 mm for the operating temperature range.

Table 6 depicts the morphological chart of the cooling system. This way of representation is one of the possible tools adopted for the conceptual design phase of any

Chapter 4 Rough Design of a 10 MW HTS wind turbine generator

device/product/system. The device is divided in subassemblies that have a specific function and these are illustrated in the first 2 columns of the table. Successively for each subassembly various solutions are identified and are registered in the other columns of the table. This way of representation is very practical and can give a quick overview of the available options in order to achieve a certain functionality. As a consequence the many equivalent ways of achieving a certain performance can be visualized through this chart by combining the various options for each subsystem.

Table 6 Morphological chart

System	Function	Means of achieving functions			
Cryogenic system	System type	Open loop	Closed loop	Cryogen free	
	Coolant type	H ₂	O ₂	He	Ne
	Cryocooler type	Stirling	GM	Pulse tube	
	Cryostat configuration	single	2 cryostats	Multiple cryostats	
	Cooling mode	Bath	Forced cooling in channels in thermal contact with wire	Thermo syphon cooling	Cable in conduit (assembly of wire + cooling channels)
Cryostat/ TT/support structure	Material	Steel	composites		
	Torque transmitting capability	Hollow cylinder	Shaft		
	Coil support structure	Slot type structure (windings inserted)	Cage type structure (over winding assembly)		
	Heat leakage	Support cross section minimization	Low λ construction material		
	Irradiative heat transfer	MLI	Radiation shield at intermediate temperature		
	Convective heat transfer	Vacuum			
	Thermal contraction	Choose compatible materials	Allow tolerances		
	Rotor cooling	Rotary joint	Rotating cryocooler		
	Convective heat transfer	Vacuum			

Chapter 4 Rough Design of a 10 MW HTS wind turbine generator

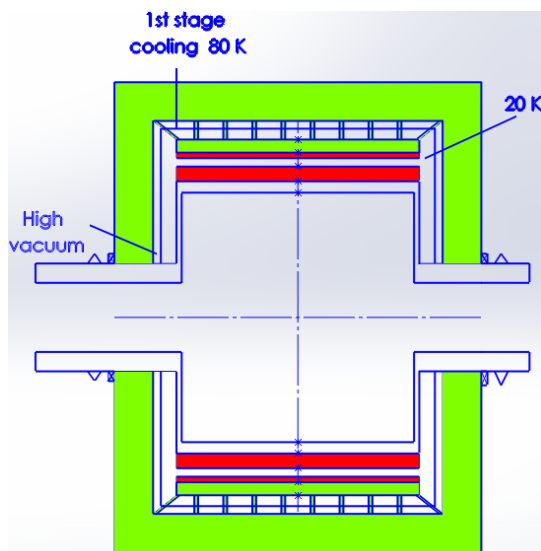


Figure 88 Temperatures in the cryostat

The stator is the location with major dissipation due to the higher AC losses. In order to avoid hot spots and temperature gradients that affect the performance of the superconductor cooling pipes are distributed in both sides of the winding. This means that there is a cage type composite structure with cooling pipes in both sides and wires embedded in “slots” in between.

The cooling pipes reach the rotor coils through a rotating coupling. Although this is a rather complex and costly option it is the only suitable for the required cooling power. Rotating cryocoolers currently available seem to provide a limited cooling power at 20 K in the range of few Watts. For reference two products were chosen. A Stirling cryocooler from Stirling cryogenics (320 W at 20 K 1000 kg 8 m² installation space) and a Cryomech GM cryocooler (70 W at 20 K 220 kg).

The operation at cryogenic temperatures has the consequence that radiative heat transfer plays an important role. Since the heat transfer scales with the 4th power of the temperature difference, breaking out the process with the use of intermediate temperature thermal shields protects the coils more effectively. This can be done with the use of a metallic surface anchored at that intermediate temperature. Usually cryocoolers operating at 20 K have a 1st stage around 80 K. At this stage the losses through the structure and part of the current leads can be removed. Multi-layer insulation (MLI) is also deployed to lower radiation. The MLI usually consists of 0.5 μm thick aluminum coated Mylar or Kapton sheets in the vacuum space. The evacuation and the initial cool down are time consuming: there are gases absorbed from the surface of MLI blankets and the blankets require a lot of time to reach thermal equilibrium. In the next section the number of layers and the radiative heat transfer load are calculated.

Compared to permanent magnet generators the largest stress contributor which is the attractive force between stator and rotor is not present. Eccentricity can be expected to play a smaller role (if the phenomenon is not very severe) due to the already large effective magnetic airgap of the machine. On the other hand with the omission of iron the stator

Chapter 4 Rough Design of a 10 MW HTS wind turbine generator

winding directly experiences forces and due to the simultaneously large currents and magnetic field the coils experience large Lorentz forces. As a consequence a detailed design of the coil is required in order to estimate the amount of support needed. This goes beyond this thesis and only some conceptual aspects of the mechanical design are treated.

Aiming at a low weight machine the material selection is restricted to composite materials. Composites have anisotropic properties depending on the direction of the beams and at the volumetric content of beams and matrix. Generally speaking comparing them to steel they can be 3 to 5 times stronger, 2 to 3 times stiffer and 3 to 4 times lighter [125]. Moreover the heat conductivity of these materials is several orders of magnitude lower compared to pure metals and aluminum alloys and an order of magnitude lower compared to Nickel and Titanium alloys.

From the mentioned general principles it can be deduced that the application of composites is a must in fully superconducting machines. However, this introduces more difficulty in the design due to the mentioned anisotropy of the material, but at the same time gives the chance to construct a material with the desired properties at the desired stress direction after a thorough study of the deformation of the structure. Figure 90 gives the structural properties of some materials as proposed in [112]. In order to make a rough assessment of the structure the values corresponding to the quasi isentropic materials are assumed.

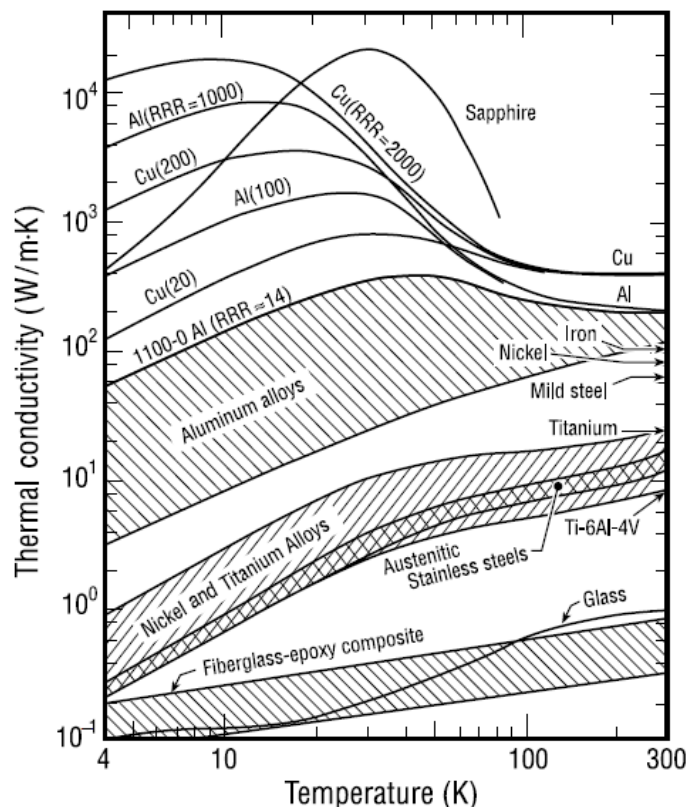


Figure 89 Thermal conductivity of some materials [102]

Chapter 4 Rough Design of a 10 MW HTS wind turbine generator

Material	Thermal expansion [K ⁻¹]	Thermal conductivity [W/m ·K]	Stiffens (E) [Pa]
SS316L	1,30E-05	7.60E+00	2,00E+10
G.fib.-Q 0°	1,17E-05	6,59E-01	2,46E+10
G.fib.-Q 90°	1,17E-05	6,59E-01	2,46E+10
C.fib.-Q 0°	2,82E-06	2,94E+00	5,36E+10
C.fib.-Q 90°	2,82E-06	2,94E+00	5,36E+10
G.fib.-B 0°	1,17E-05	6,59E-01	3,06E+10
G.fib.-B 90°	1,17E-05	6,59E-01	3,06E+10
C.fib.-B 0°	2,82E-06	2,94E+00	7,44E+10
C.fib.-B 90°	2,82E-06	2,94E+00	7,44E+10
AS4 C.fib -0°	-3,60E-07	8,65E+00	2,28E+11
AS4 C.fib -90°	1,80E-05	5,19E+00	1,66E+10
E-Glass fibers	5,40E-06	1,28E+00	7,24E+10
E-Glass fibers	5,40E-06	1,28E+00	7,24E+10
Epoxy	-4,09E-05	1,88E-01	4,28E+09

Figure 90 Thermal and mechanical properties of composites and steel at 77 K [112]

The torque tube (TT) is a sensible part of a superconducting machine and there is very little detailed information available. The TT design should have the following characteristics [126]:

- Strong in torsion to transmit the torque
- Rigid to avoid vibrations
- Minimize the heat leakage
- Accommodate for the thermal expansion/contraction of the material

The first 2 properties are achieved through a large cross sectional moment of inertia and short length and are in conflict with the 3rd property that requires small cross sectional to length ratio. In many HTS prototypes composite torque tubes are used (i.e. the Southampton University machine has a G 10 TT and the Siemens machine has a GFRP TT) which achieve very small heat leakage and very robust behavior (Siemens TT is able to carry 15 times the nominal torque). In [112] an investigation is carried out on the preferable shape of the TT comparing a hollow cylinder and a shaft. For the same torque capability the hollow cylinder is the one with lower heat leakage and this shape is assumed further on. The rotor pole coils are mounted on the surface of the TT cylinder embedded in a “cage” type structure.

The stator support structure has to transmit the reaction torque to the wind turbine frame and at the same time support the coils in experiencing Lorentz forces. In order to fulfill the second function a “cage” type structure is assumed were the windings are embedded into composite slots. Cylinder geometry is assumed on the back of the stator winding supporting it and transmitting the reaction torque. The stator is successively

Chapter 4 Rough Design of a 10 MW HTS wind turbine generator

mechanically connected to the cryostat walls through composite rods cantilevered to the cryostat wall. It is roughly assumed that these rods have a total area fill factor of the inside wall of 0.1. It is very likely that with a detailed design this value can be significantly different (probably lower since the properties of composite materials may be customized and yield high performance and cross sections for the rods can be used with favorable strength to surface area ratio).

4.7.2. Heat loads and cooling power estimation

There are five principal heat sources:

1 Conduction through support structure

The conduction loss through the support structure rods can be calculated by considering the conduction loss through solids and thus Fourier heat law:

$$\frac{dq}{dt} = \lambda(T)A \frac{dT}{dx} \quad (57)$$

Where $\frac{dq}{dt}$ is the rate of heat transferred, $\lambda(T)$ is the thermal conductivity of the material as a function of temperature, A is the area and $\frac{dT}{dx}$ is the temperature gradient in the material. Solving out the equation yields the formula for the conduction heat loss:

$$\dot{q} = \frac{A}{L} \bar{\lambda} \Delta T \quad (58)$$

Where L is the length and $\bar{\lambda}$ is the mean thermal conductivity given by

$$\bar{\lambda} = \frac{1}{\Delta T} \int_{T_1}^{T_2} \lambda(T) dT. \quad (59)$$

Material	\bar{k} [W/m K]			σ_U [MPa]	\bar{k}/σ_U [m ² /K s]†
	4–80 K	4–300 K	80–300 K	295 K	(80–300 K)
G-10	0.25	0.50	0.56	280	2×10^{-9}
Stainless Steel 304	4.5	11	13	1300	10×10^{-9}
Brass	24	55	65	400	2×10^{-7}
Copper	1300	660	460	250	2×10^{-6}

Figure 91 Characteristics of structural materials

The composite rods have a total area of 10% of the lateral surface area of the inside cryostat wall (cylinder). The overall length is assumed 300 mm with 100 mm in the higher temperature range 80-300 K and 200 mm in the lower temperature range 20-80 K. With these assumptions using formula (58) the total conduction loss amounts to 2.4 kW.

There is also a conduction loss through the ends of the torque tube. By using a hollow cylinder profile and ceramic coating outside of the cryostat [113] this contribution can be made negligible and it is not further considered.

2 Losses in superconductors

Chapter 4 Rough Design of a 10 MW HTS wind turbine generator

This voice represents the internal heat source of the generator. The losses in the superconductors have been calculated in the previous section. The total loss amounts to 21.25 kW. Naturally, since this heat is generated at the windings it should be removed at 20 K.

3 Radiation

The radiative heat flux transferred between 2 surfaces can be evaluated for the Stefan-Boltzmann equation:

$$q = \varepsilon\sigma(T_w^4 - T_c^4) \quad (59) \text{ W/m}^2$$

Where ε is the total emissivity, σ the Stefan-Boltzmann constant and T_w, T_c are the temperatures of the warm and cold surface respectively. For the common cryostat configurations it is sufficient to consider the parallel plate configuration for calculating the total emissivity

$$\varepsilon = \frac{\varepsilon_1 * \varepsilon_2}{\varepsilon_2 + \varepsilon_1 - \varepsilon_1 * \varepsilon_2} \quad (60)$$

The value of the emissivity depends on the surface condition of the materials and on the electrical resistivity (scales with the square root). This is the reason why highly conductive polished metals at cryogenic temperature have very low emissivity. However, surface degradation from each sort of residual (gas/oil even a fingerprint) can alter the value. As mentioned the construction material is G-10 (or another composite even if that particular material is discarded from some reason). In [102] a list of material emissivity is given. Polished metals i.e. Al have 0.03 whereas nonmetallic materials have 0.9. Thermal stress is not considered, but it usually occurs at interfaces of different materials. Therefore to the knowledge of the author using a composite as construction material and Al surfaces to reduce radiative heat transfer, might be a risky option.

It has been chosen to reduce the radiative heat transfer through the use of an intermediate thermal shield at 80 K and through the adoption of MLI insulation. As it can be seen in figure there is a thin cylindrical metal surface anchored at the 1st stage of the cryocooler. Therefore equation (59) is applied in 2 cases and that is from the outer wall of the cryostat (300 K) to the 1st stage metal surface (80 K) and from the later to the winding areas (20 K). MLI is also adopted. The presence of N layers modifies the heat transfer equation as follows:

$$q = \frac{\varepsilon}{N+1}\sigma(T_w^4 - T_c^4) \quad (61) \text{ W/m}^2$$

As a rule of thumb 10-20 layers are placed for each cm of spacing with thin insulating spacers between adjacent layers to minimize conductive heat transfer [102]. The spacing layers could be silk or a Nylon net. Assuming that there are 300 mm available for placing the MLI 60 layers are adopted. With these assumptions the results of the calculated radiative heat transferred are reassumed in table. For comparison it is also reported the value of the heat transferred in case of aluminum surfaces without intermediate thermal shield. As it can be seen the 2 cases are comparable.

Chapter 4 Rough Design of a 10 MW HTS wind turbine generator

Table 7 Radiative heat load estimation

Emissivity	0.9
MLI layers	60
Radiative heat at 1 st stage	117.5
Radiative heat at 2 nd stage	34.5
Total radiative heat	152 W
Radiative heat with polished metal	132 W

4 Convection in the evacuated space (imperfect vacuum)

Assuming a good vacuum quality this contribution is neglected.

5 Dissipation in current leads

The design of the current leads is a sensible subject that should be optimized in terms of performance and additional heat load that introduces. HTS current leads have become a viable alternative to conventional conductor current leads (usually copper or brass). The heat loss of optimized current leads can be assumed to be 1 W kA^{-1} [113]. The current leads have to transmit 2820 A to the field pole coils (20 coils overall) and 340 A to the armature coils (30 coils overall). This amounts to compressively 56.4 kA to the rotor and 10.2 kA to the stator. As a consequence the total loss from the current leads amounts to 66.6 W with the given loss ratio.

Table 8 Generator's heat budget

Total conduction heat load	2.4 kW
Total radiative heat load	152 W
Internal heat generation	21.25 kW
Current lead dissipation	66 W
Total external heat load	2.6 kW
Total heat budget	23.85 kW

The total heat budget estimation amounts to 23.85 kW. In the required temperature range to the author's knowledge there is no commercial off the self product that can deliver this cooling power. Two commercial products have emerged but both are far from delivering the requested performance. Figures 92 and 93 depict the performance of state of the art commercial cryocoolers depending on the temperature that the losses need to be removed. A stirling cryogenics stirring type cryocooler delivers at 20 K 320 W. The system is mounted with a cryogenic pump (Cryofan) which ensures the transfer of fluid from the cryocooler to the generator and is located outside the cryostat. The disadvantage of this system is that requires 8m^2 of installation space. A more light and compact GM cryocooler has been evaluated and is capable of delivering 70 W of cooling power at 20 K. It can be easily deduced that for the needs of this design both options result in a huge number of components. Stirling would require 75 cryocoolers with a total installation space of 600 m^2

Chapter 4 Rough Design of a 10 MW HTS wind turbine generator

absolutely impractical for a wind turbine. Analogously 340 GM cryocoolers are required which is also a result of questionable applicability.

In the author's view the only systems that could supply the required cooling power are the ones applied in H₂ liquefaction technology. These systems can provide several kW of cooling power. These are custom designed components and it turned out to be out of reach for the author to find a reference product.

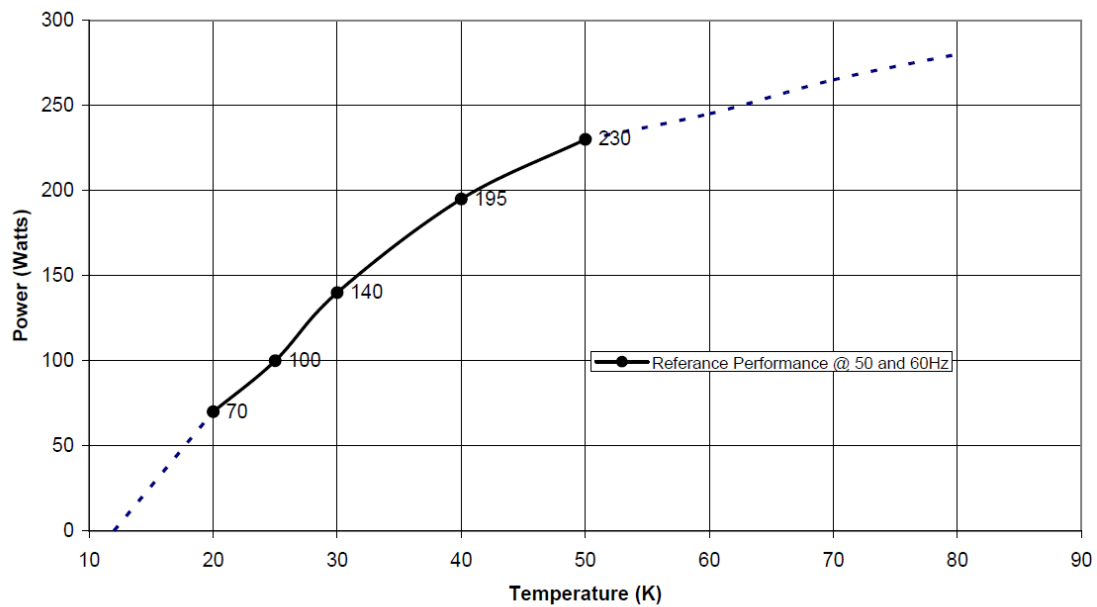


Figure 92 Cryomech cryocooler capacity curve

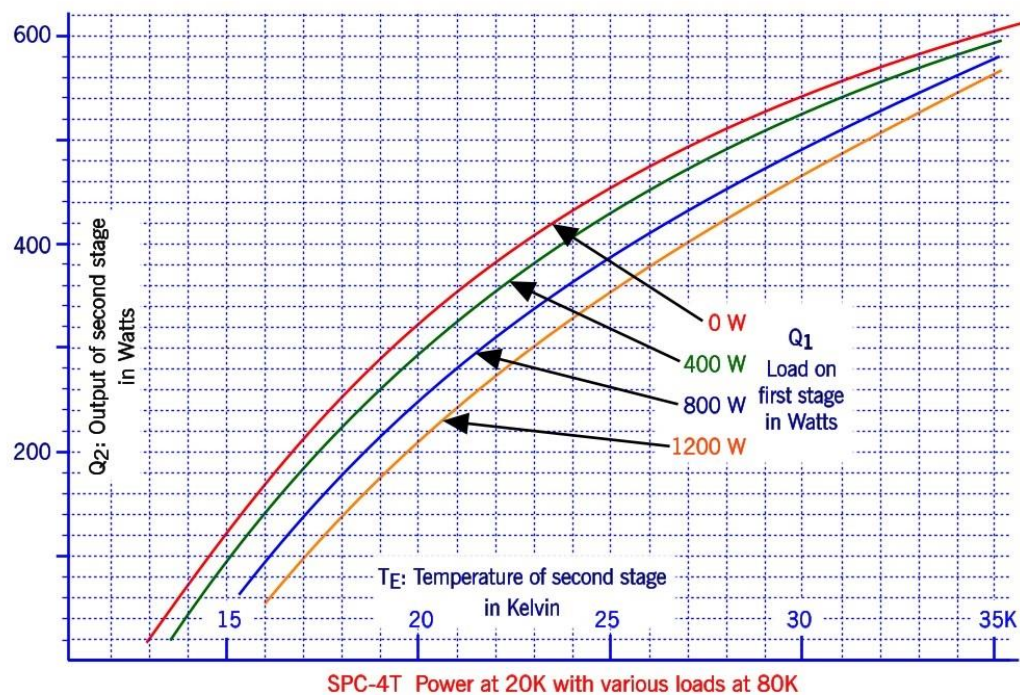


Figure 93 Stirling cryogenics cryocooler capacity curve

Chapter 4 Rough Design of a 10 MW HTS wind turbine generator

As it emerges for the required room temperature power to action the cooling system only some rough calculations can be done. The Carnot efficiency of a cryocooler is defined as:

$$\eta_{carnot} = \frac{T_c}{T_w - T_c} \quad (62)$$

The coefficient of performance (COP) is the inverse of the efficiency and represents the ratio of power that should be given at room temperature to provide 1 W of cooling at cryogenic temperatures. For the operating temperature and assuming a cryocooler efficiency of 30% of Carnot (value almost impossible to reach at 20 K with the current state of the art) we have a COP of 46.6 and a corresponding room temperature cooling power of 1.11 MW. The efficiency is 88.9 % which is disappointing thinking that the machine only produces less than 22 kW of electrical losses. Cryogenic technology is penalizing the proposed design in terms of efficiency.

4.7.3. Weight estimation

Not taking into account thermal stresses, in order to estimate the thickness of the TT the following equation is used [112]:

$$T = J_c \frac{\tau_{max}}{R_{out}} \quad (63)$$

With T the required transmitted torque, J_c is the polar moment of inertia given by $J_c = \frac{\pi * (R_{out}^4 - R_{in}^4)}{2 * R_{out}}$, τ_{max} the maximal shear stress in the material (material property) and R_{out} the outer radius of the cylinder. Analogously as for the TT, equation (63) may be used to estimate the stator support thickness by using the appropriate radii.

For the calculation due to the lack of specific data for the operating temperature (20 K) the values for 77 K are assumed as given in figure. In most materials (excluding the materials that become brittle at low temperatures like iron alloys) the yield strength increments at lower temperatures and therefore this should not be a very risky assumption. E-Glass fibers (G10) have superior properties and that is the assumed material.

Plugging in the numbers it results that very thin disks (less than 1mm disks) are able to bear the torque. Naturally, in the mechanical design safety and other factors influence and change the end result. Since the cage structure will also contain space of the cooling it is assumed that for the stator 200 mm of thickness for the cage structure while for the rotor this value is assumed to be 100 mm. Therefore for the weight estimation the stator and rotor support structures are assumed to be G-10 disks of 200 mm and 100 mm thickness respectively. The density of G-10 is around 1860 kg/m³[123]. As a consequence the rotor and stator support structures weigh 2.7 tons and 6.7 tons respectively.

In order to estimate the weight of the cryogenic system (excluding cryocoolers) it is assumed that overall 800 m of transfer lines are sufficient. It is very likely that this number will change after exact calculations. The specific weight of a large cross section transfer line [128] is 11.5 kg/m. This yields a weight of 9.2 tons. The cryostat is assumed as a cylinder disk of 100 mm wall thickness. This yields a weight of 3.5 tons.

Chapter 4 Rough Design of a 10 MW HTS wind turbine generator

Finally MgB_2 wires in average weigh 2600 kg/m^3 . Calculating the volume of the rotor wire multiplying with the total rotor length gives the volume and multiplied with the density gives the weight. Analogously is done for the stator. This yields a total weight of 1.3 tons.

4.8 Summary

General design parameters	
Rated power	10 MW
Speed range	3.6-10.7 RPM
Phase voltage	10 kV
Phase current	340 A
Field pole current	2820 A
K_r	10.9 MA/m
K_s	142.37 kA/m
N_r	16962 total series turns
N_s	1393 total series turns/phase
c	0.3235
scr	10.7
Total wire length	80 km
Geometrical parameters	
Armature outer radius R_{ae} [m]	2.815
Armature inner radius R_{ai} [m]	2.785
Armature current sheet radius R_{asheet} [m]	2.8
Airgap length g [mm]	3
Effective airgap [mm]	300
Field winding outer radius R_{fe} [m]	2.568
Field winding inner radius R_{fi} [m]	2.432
Field current sheet radius R_{fsheet} [m]	2.5
Stator back iron internal radius R_{si} [m]	3.51
Stator back iron external radius R_{se} [m]	3.61
Active length l [m]	1
Ferromagnetic shield	
Material	Aluminum iron silicon alloy
Shield thickness	100 mm
Lamination thickness	0.35 mm
Density	7600 kg m^{-3}
Hysteresis losses	640 W
Wire adopted	
Wire type	round Nb/Cu/Monel MgB_2
Impregnation	Stycast 2850
Filaments	61
Superconductor fraction	25%
Filament diameter	$64 \mu\text{m}$
Wire diameter	2-3 mm
Insulation thickness and material	0.5 mm Kapton
Total cross section diameter	3-4 mm
Strain	0.55%

Chapter 4 Rough Design of a 10 MW HTS wind turbine generator

Minimum bending radius	18-27 cm
Losses/heat loads	
Rotor DC loss	630 W
Stator self field loss	51 W
Stator hysteresis loss	20.4 kW
Stator filament coupling loss	186 W
Rotor hysteresis loss	2 W
Rotor filament coupling loss	0.42 W
Total internal power loss	21.25 kW
Total conduction heat load	2.4 kW
Total radiative heat load	152 W
Current lead dissipation	66 W
Total external heat load	2.6 kW
Total heat budget	23.85 kW
Room temperature power for cooling	1.11 MW
Efficiency	88.9 %
Weight estimation	
Rotor support	2.7 tons
Stator support	6.7 tons
Ferromagnetic shield weight	16.9 tons
Cryogenic tubes weight	9.2 tons
MgB ₂ wire weight	1.3 tons
Cryostat	3.5 tons
Total weight	40.3 tons

Chapter 5 Conclusion

In the final chapter of this thesis an evaluation of the proposed generator is presented and an attempt is made to extract more general conclusions regarding the feasibility of the application of superconducting technology in wind turbines.

It is evident that the proposed design is not feasible due to its poor performance in two (connected) topics:

- cryogenic budget
- relatively low efficiency accounting for the required cooling power

To the knowledge of the author a device capable of delivering almost 24 kW of cooling power at 20 K does not exist. At most an attempt could be made to design a system of multiple devices connected together. However, a very high number of the known commercial devices mentioned in the previous chapter is needed: 66 Sterling cryocoolers or 300 Cryomech. As a consequence, this seems unfeasible. Moreover, with 89% efficiency at full load (thus similar figure in partial loading since superconducting generators have rather flat efficiency curves), the proposed design cannot compete with the AMSC model of 94% (including converter) and performs slightly worse than the other drive train concepts compared in [30].

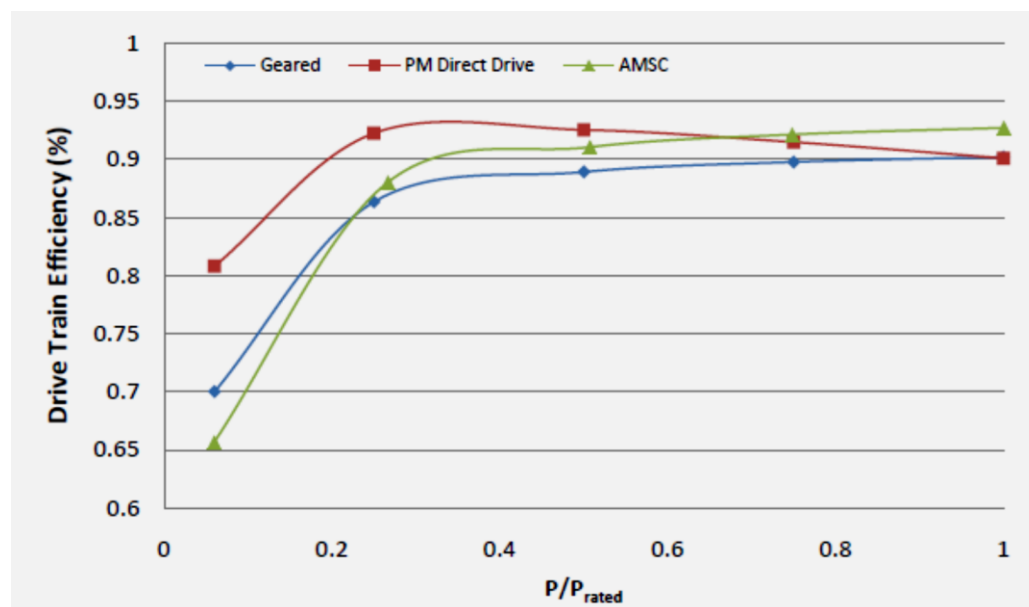


Figure 94 Efficiency comparison between geared, PM DD, AMSC [30]

In addition to this the weight of the generator has not been fully assessed due to the non-consideration of the cooling system. Therefore it is certain that the proposed design hardly incorporates any of the expected advantages of superconducting technology.

Chapter 5 Conclusion

This chapter is structured as follows. Firstly a brief analysis on the generator losses and the corresponding required cooling power is done. The objective is to identify the most penalizing factor and give recommendations in order to reach feasibility. Successively the capital cost of the generator is presented in order to compare it with the cost of the model proposed by AMSC. In the final section the conclusion of this thesis is given with the recommendations of the author for future development.

From table 5 in chapter 4 it clearly emerges that the major contributor to the AC losses of the proposed generator is the hysteresis loss of the stator winding with 20.4 kW to remove at 20 K. The corresponding rotor loss only amounts to 2 W due to the very low armature reaction “felt” by the rotor coils. This is mainly due to two design choices:

- to have a very large effective magnetic airgap due to the cage type composite support structure (300 mm)
- low armature winding current loading (142 kA/m)

This has not influenced negatively the overall wire consumption keeping it fairly low (80 km) and this is mainly due to the higher flux density achieved at stator winding radius.

The filament coupling losses in both stator and rotor are low and this is due to the twist pitch and transverse resistivity values that have been assumed. In case the assumptions are proved to be significantly different this loss figure can change dramatically. With the assumptions made this loss is not significant and is not considered further. In the generator windage losses are not accounted because the bearing losses are not considered and the friction losses in the airgap should not be present if a high vacuum quality is assumed.

As already mentioned the hysteresis loss is the main cause of the unfeasibility of the design. The hysteresis loss mainly depends on the filament diameter. As a consequence the state of the art MgB₂ wires with 61 μm filament radius are not suitable for the armature winding of a superconducting generator. State of the art NbTa wires have filaments with radii in the order of 7.5 μm. Assuming this result is also achieved with MgB₂ wires the number of filaments for the stator wire is around 4000 and the losses amount to 4 kW and thus a decrease by a factor of 5. This however represents a very significant progress to the current status of around 9 times bigger filaments being possible.

In case it would be possible to produce this wire the overall losses at cryogenic temperature would amount to almost 5 kW and with 30% Carnot efficiency assumed to 24 kW of room temperature cooling power. Still for this value currently does not exist a device capable to deliver such power. With the current commercial systems it would be required to deploy 16 Stirling or 71 Cryomech cryocoolers and thus far from practical to the opinion of the author. As a consequence progress in the wire development alone is not sufficient to enhance the applicability of the proposed design. In case better wires become available and significant advances in cryogenics make commercially available devices that provide significantly larger cooling power than the current ones this technology could become feasible.

The cryogenic technology is currently far from being available for the required cooling power range. It can be anticipated that in case hydrogen technology further expands and diffuses in

the future higher power and more efficient cryocoolers could be available. In any case the wire development should provide wires that approach the state of the NbTa wire characteristics. This is the only possible way to make a fully wind turbine superconducting generator feasible. This is however not at reach at this moment neither seems possible in the near future.

The application of superconducting technology in wind turbines is still a very promising technology. However, the technology is not mature yet for a superconducting generator at least with the approach adopted in this thesis. It could be that different winding arrangements like helical windings or cable in conduit wire structures reverse this trend and enhance feasibility. What is certain is that in case the overall losses at cryogenic temperature where the losses at room temperature this topology would have a major impact in wind turbines. In that case if its reliability could be demonstrated this would represent a major breakthrough in offshore wind turbines. The conclusion of this thesis is that in order to see further diffusion of superconducting technology major technological challenges are still not met and innovations at wire architecture and cryogenics are required.

In the meantime partially superconducting machines could be feasible under the condition to keep the cryogenic budget low. The next step of development should be the construction of a demonstrator that will help to assess the real potential of this technology.

References

References

1. "The European Wind Initiative", A European Wind Energy Association briefing June EWEA 2010
2. "The Economics of Wind Energy", A report by the European Wind Energy Association EWEA March 2009
3. "EWEA – Energy Mix In Europe to 2050 Wind stands at the center of future energy generation" Make consultancy presentation in EWEA 2013 in Vienna, Austria
4. "Renewable energy technologies: Cost analysis series, Volume 1: Power Sector Issue 5/5 Wind Power", IRENA working paper June 2012
5. "Offshore Wind Cost Reduction Pathways Study" The crown estate May 2012
6. Feng, Y. and Tavner, P.J. and Long, H. 'Early experiences with UK Round 1 offshore wind farms.', Proceedings of the Institution of Civil Engineers : energy., 163 (4). pp. 167-181,2010
7. F. Spinato, P.J. Tavner, G.J.W. van Bussel, E. Koutoulakos, "Reliability of wind turbine subassemblies", IET Proceedings – Renewable Power Generation, 2009, vol. 3, pp. 387–401.
8. S. Faulstich, B. Hahn, P. Lyding, P. Tavner "Reliability of offshore turbines – identifying risks by onshore Experience", presented in European Offshore Wind 2009, Conference and Exhibition, 14-16 Sept 2009, Stockholm, Sweden
9. "UpWind Design limits and solutions for very large wind turbines. A 20 MW turbine is feasible" Research report March 2011
10. H. Polinder, S.W.H. de Haan, J.G. Slootweg, M.R. Dubois, "Basic operation principles and electrical conversion systems of wind turbines," EPE Journal, vol. 15, no. 4, pp. 43–50, Dec. 2005.
11. C. Lewis, J. Muller, "A direct drive wind turbine HTS generator", IEEE Power Engineering Society General Meeting, 24-28 June 2007, Florida, pp. 1-8.
12. "Wind in power 2011" European statistics, published in February 2012 from EWEA
13. GWEC "Global Wind Report 2011"
14. Richard Green, Nicholas Vasilakos "The economics of offshore wind", Energy Policy, Volume 39, Issue 2, February 2011, Pages 496-502, ISSN 0301-4215
15. "The European offshore wind industry key 2011 trends and statistics" EWEA 2012
16. Antonio García-Olivares, Joaquim Ballabrera-Poy, Emili García-Ladona, Antonio Turiel, A global renewable mix with proven technologies and common materials, Energy Policy, Volume 41, February 2012, Pages 561-574, ISSN 0301-4215
17. H. Polinder, "Overview of and trends in wind turbine generator systems", IEEE Power and Energy Society General Meeting, 24-29 July 2011, pp.1-8.
18. Li, H.; Chen, Z.; , "Overview of different wind generator systems and their comparisons," Renewable Power Generation, IET , vol.2, no.2, pp.123-138, June 2008
19. Asger Bech Abrahamsen, Bogi Bech Jensen "Superconducting Direct Drive Wind Turbine Generators: Advantages and Challenges" part of: "Wind Energy Conversion Systems. Technology and trends "(ISBN: 978-1-4471-2200-5), pages: 53-80, 2012, Springer Publishing Company

References

20. Hui Li; Zhe Chen; Polinder, H.; , "Optimization of Multibrid Permanent-Magnet Wind Generator Systems," Energy Conversion, IEEE Transactions on , vol.24, no.1, pp.82-92, March 2009
21. Peter Tavner, Ehsan Abdi, Mark Tatlow, Richard McMahon "Design and Performance Analysis of a 5 MW Medium-Speed Brushless DFIG Drivetrain" presented in EWEA 2013 in Austria
22. Henk Polinder, Deok-Je Bang, H. Li, Z. Chen "Upwind Concept report on generator topologies, mechanical & electromagnetic optimization Part1" 2007
23. A. Jarquin Laguna, N.F.B. Diepeveen "Dynamic Analysis of Fluid Power Drive-trains for Variable Speed Wind Turbines: a Parameter Study" presented in EWEA 2013 in Austria
24. "Offshore wind cost reduction pathways: Technology work stream" BVG associates may 2012
25. "Value breakdown for the offshore wind sector" A report commissioned by the Renewables Advisory Board February 2010
26. Emre Uraz "Offshore Wind Turbine Transportation & Installation Analyses. Planning Optimal Marine Operations for Offshore Wind Projects" Master Thesis written at Gotland University Department of Wind Energy, June 2011
27. Dan Ancona, Jim McVeigh "Wind Turbine - Materials and Manufacturing Fact Sheet" Prepared for the Office of Industrial Technologies, US Department of Energy By Princeton Energy Resources International, LLC.. August 2001
28. Marc Humphries "Rare earth elements: the global supply chain", Congressional Research Service September 2011
29. Peter C. Dent "Rare earth elements and permanent magnets" Journal of applied physics 2012
30. B. Maples, M. Hand, and W. Musial "Comparative Assessment of Direct Drive High Temperature Superconducting Generators in Multi-Megawatt Class Wind Turbines", NREL 2010
31. <http://www.rsc.org/>, Royal society of chemicals last accessed 6/10/2012
32. Nesrin Horzum "SYNTHESIS AND CHARACTERIZATION OF MgB₂ SUPERCONDUCTING WIRES" Msc Thesis Submitted to the Graduate School of Engineering and Sciences of Izmir Institute of Technology
33. E. I Leyarovski "A method for obtaining neon and helium from air on an industrial scale", cryogenics 1970
34. <http://www.thermopedia.com>, last accessed on 6/10/2012
35. "Superconductivity: Present and Future Applications", Coalition for the Commercial Application of Superconductors, IEEE Council on Superconductivity (IEEE CSC)
36. Y. Iwasa "Case Studies in Superconducting Magnets: Design and Operational Issues" Springer 2009
37. <http://www.magnet.fsu.edu>, National High Magnetic Field Laboratory last accessed 15/1/2013
38. S.S. Kalsi, "Applications of high temperature superconductors to electric power equipment", John Wiley & Sons, April 2011

References

39. "Applications of high-temperature superconductors in power technology" Reports on Progress in Physics Volume 66 Number 11 John R Hull 2003 Rep. Prog. Phys. 66 1865
40. <http://hoffman.physics.harvard.edu/materials/Cuprates.php>, last accessed on 13/9/2011
41. David Larbalestier, Alex Gurevich, D. Matthew Feldmann and Anatoly Polyanski "High-Tc superconducting materials for electric power applications" Nature 414, 368-377(15 November 2001)
42. J. F. Gieras, "Advancements in Electric Machines" Springer, 2010
43. Kagiya, T., Yamazaki, K., Kikuchi, K., Yamade, S., Nakashima, T., Kobayashi, S., Hayashi, "Recent Progress in High Performance Ag-Sheathed Bi2223 Wire (DI-BSCCO)" IOP Publishing. IOP Conf. Series: Materials Science and Engineering 18 (2011)
44. Vinod, K., Kumar, R. G., & Syamaprasad, U. (2006) "Prospects for MgB₂ superconductors for magnet application" Trivandrum, India: Regional Research Laboratory (CSIR)
45. Ginley D. S., Cardwell D.A. (2002) "HANDBOOK OF SUPERCONDUCTING MATERIALS"
46. M. Tomsic, M. Rindfleisch, J. Yue, K. McFadden, J. Phillips 2007 "OVERVIEW OF MgB₂ SUPERCONDUCTOR APPLICATIONS"
47. Personal communication with M. Tomsic president of Hypertech on 30/10/2012
48. Herman ten Kate "Superconducting Magnets Quench propagation and Protection" Lecture material TU Twente, Twente School of Superconductivity
49. N. Tuovinen "Application of magnet quench analysis" Msc thesis Tampere University of Technology
50. Antti Stenvall "An Electrical Engineering Approach to the Stability of MgB₂ Superconductor" Phd thesis Tampere University of Technology
51. A. Stenvall, A. Korpela, R. Mikkonen and G. Grasso "Stability considerations of multifilamentary MgB₂ tape" Superconductor Science and Technology Volume 19 Number 2 IOP Science
52. Minyi Fu, Xiaofeng Xu, Zhengkuan Jiao, H. Kumakura, K. Togano, Liren Ding, Futang Wang, Jinglin Chen "Minimum quench energy and normal zone propagation velocity in MgB₂ superconducting tape," Physica C: Superconductivity, Volume 402, Issue 3, 15 February 2004, Pages 234-238
53. M. Marchevsky, Y-Y Xie and V Selvamani "Quench detection method for 2G HTS wire" Supercond. Sci. Technol. 23 (2010) 034016 (6pp) IOP Science
54. Umans, S.D.; Shoykhet, B.A. "Quench in high-temperature superconducting motor field coils: experimental results," Industry Applications, IEEE Transactions on , vol.42, no.4, pp.983-989, July-Aug. 2006
55. www.hypertechresearch.com, MgB₂ applications brochure
56. M. Miki, B. Felder, Y. Kimura, K. Tsuzuki, R. Taguchi, Y. Shiliang, Y. Xu, T. Ida, M. Izumi, "Applied HTS Bulks and Wires in machines for marine propulsion", Transactions of the Cryogenic engineering conference 28 June–2 July 2009 Tucson (Arizona, USA)
57. G. Klaus, M. Wilke, J. Fraunhofer, W. Nick, H.-W. Neumuller, "Design challenges and benefits of HTS synchronous machines", IEEE Power Engineering Society General Meeting, 24-28 June 2007, pp.1-8

References

58. K.F. Goddard, B. Lukasik, J. Sykulski, "Alternative designs of a superconducting synchronous generator: the Southampton approach", 18th International Conference on Electrical Machines ICEM, 6-9 Sept. 2008, pp.1-6
59. B. Gamble, G. Snitchler, S.S. Kalsi, "HTS generator topologies", IEEE Power Engineering Society General Meeting 2006, IEEE
60. M. Wilke, K. Schleicher, G. Klaus, W. Nick, H.-W. Neumuller, J. Fraunhofer, K. Kahlen, R. Hartig, "Numerical calculations for high-temperature superconducting electrical machines" 18th International Conference on Electrical Machines, ICEM 2008.
61. N Mijatovic, A B Abrahamsen, C Træholt, E Seiler, M Henriksen, V M Rodriguez-Zermeno, N F Pedersen "Superconducting generators for wind turbines: design considerations", 9th European Conference on Applied Superconductivity (EUCAS 09), Journal of Physics: Conference Series 234 (2010)
62. R. Radebaugh, "Refrigeration for superconductors", Proceedings of the IEEE, 2004, vol. 92, pp. 1719 – 1734.
63. R. Radebaugh, "Cryocoolers: the state of the art and recent developments", Journal of Physics-Condensed Matter, 2009, Vol. 21, pp. 1-9
64. A.T.A.M. de Waele 2011 "Basic Operation of Cryocoolers and Related Thermal Machines" JOURNAL OF LOW TEMPERATURE PHYSICS Volume 164, Numbers 5-6, 179-236
65. Handbook of Superconducting Materials Edited by David S Ginley and David A Cardwell Taylor & Francis 2002 Pages 1879–1896
66. Steven W. Van Sciver, Cryogenic systems for superconducting devices, Physica C: Superconductivity, Volume 354, Issues 1–4, May 2001, Pages 129-135
67. S.S. Kalsi, K. Weeber, H. Takesue, C. Lewis, H.W. Neumuller, R. D. Blaugher, "Development status of rotating machines employing superconductor field windings", Proceedings of the IEEE, 2004, pp. 1688-1704.
68. J. Fraunhofer, M. Kaufhold, P. Kummeth, G. Nerowski, W. Nick "High temperature superconductor machines - A high step for large rotating electric machines", International Symposium on Power Electronics, Electrical Drives, Automation and Motion, 23-26 May 2006, pp.379-383.
69. W. Nick, M. Frank, G. Klaus, J. Fraunhofer, H.-W. Neumüller, "Operational experience with the world's first 3600 rpm 4 MVA generator at Siemens", IEEE Transactions on Applied Superconductivity, 2007, vol.17, pp. 2030-2033
70. R. Fair, C. Lewis, J. Eugene, M. Ingles, "Development of an HTS hydroelectric power generator for the Hirschaid power station" 9th European Conference on Applied Superconductivity 2010 Journal of Physics: Conference Series, Volume 234, Issue 3, pp. 032008 (2010)
71. www.atg.ga.com, last accessed on 17 March 2012
72. Miki, M., Tokura, S., Hayakawa, H., Inami, H., Kitano, M., Matsuzaki, H., et al. (2006). Development of a synchronous motor with Gd–Ba–Cu–O bulk superconductors as pole-field magnets for propulsion system. IOP PUBLISHING
73. Matsuzaki, H., Kimura, Y., Morita, E., Ogata, H., Ida, T., Izumi, M., et al. (2007). HTS Bulk Pole-Field Magnets Motor With a Multiple Rotor Cooled by Liquid Nitrogen. IEEE Transactions on Applied Superconductivity vol 17 no 2 June 2007, (pp. 1553-1556)

References

74. Al-Mosawi, M.K., Beduz C. and Yang, (2005) "Construction of a 100 kVA high temperature superconducting synchronous generator" IEEE Transactions on Applied Superconductivity, 15, (2, Part 2), 2182-2185
75. Goddard, K.F.; Lukasik, B.; Sykulski, J.K.; , "Alternative designs of a superconducting synchronous generator: the Southampton approach," Electrical Machines, 2008. ICEM 2008. 18th International Conference on , vol., no., pp.1-6, 6-9 Sept. 2008
76. B Lukasik "DESIGN AND OPTIMISATION OF A CORELESS SUPERCONDUCTING SYNCHRONOUS GENERATOR" PhD thesis School of electronics and computer science, Faculty of engineering and applied science, University of Shouthampton
77. Al-Mosawi, M.K.; Goddard, K.; Beduz, C.; Yang, Y.; , "Coreless HTS Synchronous Generator Operating at Liquid Nitrogen Temperatures," Applied Superconductivity, IEEE Transactions on , vol.17, no.2, pp.1599-1602, June 2007
78. <http://www.oswald.de>, last accessed on 17 March 2012
79. Sim, M, Park, H. Lim, G. Cha, J. Ji, J. Lee "TEST OF AN INDUCTION MOTOR WITH HTS WIRE AT END RING AND BARS" IEEE Transactions on Applied Superconductivity 2003.
80. Nakamura, T.; Miyake, H.; Ogama, Y.; Morita, G.; Muta, I.; Hoshino, T. "Fabrication and Characteristics of HTS Induction Motor by the Use of Bi-2223/Ag Squirrel-Cage Rotor" IEEE Transactions on Applied Superconductivity 2006
81. Quddes, M.R.; Sekino, M.; Ohsaki, H.; , "Electromagnetic design study of 10 MW-class wind turbine generators using circular superconducting field coils," Electrical Machines and Systems (ICEMS), 2011 International Conference on , vol., no., pp.1-6, 20-23 Aug. 2011
82. Terao, Y.; Sekino, M.; Ohsaki, H.; , "Electromagnetic Design of 10 MW class Fully Superconducting Wind Turbine Generators," Applied Superconductivity, IEEE Transactions on , vol.PP, no.99, pp.1, 0
83. Keysan, O.; Mueller, M.A.; , "A Homopolar HTSG Topology for Large Direct-Drive Wind Turbines," Applied Superconductivity, IEEE Transactions on , vol.21, no.5, pp.3523-3531, Oct. 2011
84. A. Wolf "Design of SeaTitan™ Wind Turbine with HTS generator" EWEA 2010 poster presentation 7
85. "HIGH TEMPERATURE SUPERCONDUCTING WIND TURBINE GENERATORS", W. Cao 2011
86. Lewis, J. Müller, "A DIRECT DRIVE WIND TURBINE HTS GENERATOR" Power Engineering Society General Meeting, 2007, IEEE
87. C. Bannigan Convertteam UK Limited "SUPERCONDUCTOR GENERATOR: ONE SMALL STEP?" www.powerengineeringint.com, last accessed on 16 March 2012
88. Ohsaki, H., Sekino, M., Suzuki, T., & Terao, Y. (2009). Design Study of Wind Turbine Generators using Superconducting Coils and Bulks. IEEE, (pp. 479-484).
89. Ohsaki, H.; Terao, Y.; Quddes, R.M.; Sekino, M.; , "Electromagnetic characteristics of 10 MW class superconducting wind turbine generators," Electrical Machines and Systems (ICEMS), 2010 International Conference on , vol., no., pp.1303-1306, 10-13 Oct. 2010
90. "Wind Power Generation and Wind Turbine Design" Edited by Wei Tong WIT press Southampton Boston 2010

References

91. Ke Ma, Blaabjerg, F. Dehong Xu, "Power devices loading in multilevel converters for 10 MW wind turbines," *Industrial Electronics (ISIE), 2011 IEEE International Symposium on*, vol., no., pp.340,346, 27-30 June 2011
92. Course on superconductors MIT open course ware downloaded from <http://ocw.mit.edu>
93. N Mijatovic, A B Abrahamsen, C Træholt, E Seiler, M Henriksen, V M Rodriguez-Zermeno and N F Pedersen "Superconducting generators for wind turbines: Design considerations" *Journal of Physics Conference Series Volume 234 Part 3*
94. N.Maki "Design study of high-temperature superconducting generators for wind power systems" *IOP Science Journal of Physics: Conference Series 97 2008*
95. M. Tomsic, M. Rindfleisch, J. Yue, K. McFadden, J. Phillips, M. D. Sumption, M. Bhatia, S. Bohnenstiehl, E. W. Collings "Overview of MgB₂ Superconductor Applications" *International Journal of Applied Ceramic Technology Volume 4, Issue 3, pages 250–259, July 2007*
96. M Wilson presentation from CERN Technical Training April 2005
97. M.D. Sumption, M. Bhatia, F. Buta, S. Bohnenstiehl, M. Tomsic, M. Rindfleisch, J. Yue, J. Phillips, S. Kawabata, E.W. Collings, Multifilamentary MgB₂-based solenoidal and racetrack coils, *Physica C: Superconductivity, Volume 458, Issues 1–2, 1 July 2007, Pages 12-20*
98. D Evans "Turn, layer and ground insulation for superconducting magnets", *Physica C: Superconductivity, Volume 354, Issues 1–4, May 2001, Pages 136-142*
99. Sunderland A.G.; Heggarty J.W.; Noble C.J.; Scott N.S.; Morris M.J.; Hara M.; Gerhold J. "Electrical insulation specification and design method for superconducting power equipment *Cryogenics*, Vol. 38, Num. 11, November 1998, pp. 1053-1061 Elsevier
100. Seungyong Hahn; Dong-Keun Park; Bascunan, J.; Iwasa, Y., "HTS Pancake Coils Without Turn-to-Turn Insulation," *Applied Superconductivity, IEEE Transactions on*, vol.21, no.3, pp.1592,1595, June 2011
101. Young-Gyun Kim; Seungyong Hahn; Kwang Lok Kim; Oh Jun Kwon; Haigun Lee, "Investigation of HTS Racetrack Coil Without Turn-to-Turn Insulation for Superconducting Rotating Machines," *Applied Superconductivity, IEEE Transactions on*, vol.22, no.3, pp.5200604,5200604, June 2012
102. Jack W. Ekin "Experimental Techniques for Low-Temperature Measurements *Cryostat Design, Material Properties, and Superconductor Critical-Current Testing*" Oxford university press
103. Kapton brochure downloaded from http://www2.dupont.com/Kapton/en_US/ last accessed in 28/11/2012
104. Sumption, M.D.; Bohnenstiehl, S.; Buta, F.; Majoros, M.; Kawabata, S.; Tomsic, M.; Rindfleisch, M.; Phillips, J.; Yue, J.; Collings, E.W., "Wind and React and React and Wind MgB₂ Solenoid, Racetrack and Pancake Coils," *Applied Superconductivity, IEEE Transactions on*, vol.17, no.2, pp.2286,2290, June 2007
105. M Runde, A Stenvall, N Magnusson, G Grasso and R Mikkonen "MgB₂ coils for a DC superconducting induction heater" *Journal of Physics: Conference Series Volume 97 conference 1*
106. J. L. Kirtley Jr. (1995) "Air-core armature shape: A comparison of helical and straight with-end-turns windings" *Electric Machines & Power Systems*, 23:3, 263-278

References

107. J. L. Kirtley , “ Basic Formulas for Air Core Synchronous Machines , ” Paper 71 CP 155 - PWR, Winter Power Meeting, IEEE, New York, 1971.
108. TJE Miller and A. Hughes: “Analysis of fields and inductances in air-cored and iron-cored synchronous machines”, Proc. IEE, 1977,124, (2), pp. 121-126.
109. TJE Miller and A. Hughes: “Comparative design and performance analysis of air-cored and iron-cored synchronous machines” Proc. IEE, 124(2):127{132, 1977.
110. Abrahamsen, A.B.; Mijatovic, N.; Seiler, E.; Sorensen, M.P.; Koch, M.; Norgard, P.B.; Pedersen, N.F.; Traeholt, C.; Andersen, N.H.; Ostergard, J.; , "Design Study of 10 kW Superconducting Generator for Wind Turbine Applications," *Applied Superconductivity, IEEE Transactions on* , vol.19, no.3, pp.1678-1682, June 2009
111. N Mijatovic, A B Abrahamsen, C Træholt, E Seiler, M Henriksen1, V M Rodriguez-Zermeno and N F Pedersen "Superconducting generators for wind turbines: Design considerations" Journal of Physics Conference Series Volume 234 Part 3
112. N Mijatovic "Superconducting Wind Turbine Generators" PhD thesis DTU 2012
113. P. Tixador "Fully superconducting generators" Handbook of Applied Superconductivity, Volume 2 Edited by Bernd Seeber Taylor & Francis 1998 Pages 1553–1577
114. S. K. Baik, Y. K. Kwon, H. M. Kim, J. D. Lee ,Y. C. Kim, H. J. Park, W. S. Kwon and G. S. Park "Loss analysis of a 1 MW class HTS synchronous motor", Journal of Physics: Conference Series Volume 153 Number 1 IOP Science 2003
115. "Superconductivity for Large Scale Wind Turbines" General Electric Global Research, Scientific Report submitted to DOE EERE – Wind & Water Power Program, April 2012
116. Polinder, H.; Van der Pijl, F.F.A.; de Vilder, G.-J.; Tavner, P., "Comparison of direct-drive and geared generator concepts for wind turbines," Electric Machines and Drives, 2005 IEEE International Conference on , vol., no., pp.543,550, 15-15 May 2005
117. Juha Pyrhonen, Tapani Jokinen, Valeria Hrabovcova "Design of rotating electrical machines", Wiley editions 2008
118. Ronghai Qu; Yingzhen Liu; Jin Wang, "Review of Superconducting Generator Topologies for Direct-Drive Wind Turbines," *Applied Superconductivity, IEEE Transactions on* , vol.23, no.3, pp.5201108,5201108, June 2013
119. Wilson 1983. SUPERCONDUCTING MAGNETS Oxford Science publications
120. A. Wolfbrandt, “AC losses in HTS as a function of magnetic fields with arbitrary directions,” Ph. D. thesis, Dept. El. Eng. Royal Inst. Tech. Stockholm Sweden, 2004
121. M.S E. Lee “AC loss in superconducting composites: Continuous and discrete models for round and rectangular cross sections and comparisons to experiments”, PhD dissertation, School of The Ohio State University 2004
122. S.A. Giljarhus “AC losses in MgB₂ superconductors” Master of science thesis, Norwegian university of Science and Technology 2007
123. H. Daffix, P. Tixador 1997 “Design of a fully superconducting synchronous motor”, *Electric Machines & Power Systems*, 25:3, 227-245

References

124. R. A. Matula "Electrical resistivity of copper, gold palladium and silver"
125. V.S. GangaRao, P.V. Vijay, "Feasibility review of FRP materials for structural applications" West Virginia University 2010
126. " A. Bejan "Improved thermal design of the cryogenic cooling system for a superconducting synchronous generator PhD dissertation, Massachusetts Institute of Technology 1974
127. <http://www.matweb.com>, last visited on 17/4/2013
128. <http://www.technifab.com>, last visited on 17/4/2013